

Functional Analysis of the *Dictyostelium discoideum* Rho GTPases RacH and RacA

Inaugural-Dissertation

zur Erlangung des Doktorgrades
der Mathematisch-Naturwissenschaftlichen Fakultät
der Universität zu Köln



vorgelegt von
Carola Neffgen
aus Köln
2005

Referees/Berichterstatter:

**Prof. Dr. Angelika A. Noegel
Prof. Dr. Helmut W. Klein**

**Date of oral examination/
Tag der mündlichen Prüfung:**

07.02.2006

The present research work was carried out under the supervision of Prof. Dr. Angelika A. Noegel and the direction of Dr. Francisco Rivero at the Institute of Biochemistry I, Medical Faculty, University of Cologne, Cologne, Germany, from January 2003 to December 2005.

Diese Arbeit wurde von Januar 2003 bis Dezember 2005 am Institut für Biochemie I der Medizinischen Fakultät der Universität zu Köln unter der Leitung von Prof. Dr. Angelika A. Noegel und der Betreuung von PD Dr. Francisco Rivero durchgeführt.

Acknowledgements

At first I want to thank my supervisor, Dr. Francisco Rivero, for his guidance throughout the course of this investigation.

I thank Prof. Dr. Angelika A. Noegel, Institute of Biochemistry I, Medical Faculty, University of Cologne, Germany for giving me the opportunity to perform this work at her institute.

Thanks also to Prof. Dr. Helmut W. Klein and Prof. Dr. Jürgen Dohmen for readily being examiners of this thesis.

I want to express my special thanks to Rolf for his very valuable technical suggestions and his help.

I thank Somesh for the nice introduction into the work.

Moreover I want to thank Miho Iijima and Dr. Peter Devreotes for kindly providing the RacH-KO strain and Dr. Markus Maniak for useful discussions and providing many important antibodies.

I also owe my thanks Kathrin Meyer and Alexandra Ley for rendering technical assistance. I am also thankful to Martina, Maria, Rosi and Berthold for their help and cooperation. Thanks also to Bärbel, Brigitte and Sonja for providing the materials that made work in the lab possible and efficient.

My special thanks are also due to Budi and Gudrun for their help in all computer matters. I thank the secretaries Bettina Laus and Dörte Püsche for their help in administration issues.

I also thank the whole department "Biochemie I" for the nice atmosphere, I appreciated the presence of all colleagues and friends very much- thank you Yogi, Hafi, Martina, Rolf, Akis, Vasily, Rja, Deen, Damu, Hua, Georgia, Eva-Maria, Marion, Maria, Rosi, e, Christorph, Andreas,, Jörg .

My heartfelt thanks go to Jessica for her help and support whenever I needed it. And also to Soraya- thank you for the great time we spent together and your encouragement.

I also highly acknowledge the financial support received from the DFG.

Last but not at all at least, I would like to thank my parents for their support during my studies and my aunt for always understanding and supporting me.

Table of Contents

Acknowledgements	3
Table of Contents	4
Abbreviations.....	8
I INTRODUCTION.....	10
1 <i>Dictyostelium discoideum</i> as a model organism	10
2 Small GTPases of the Rho family.....	11
3 Regulation of small GTPases and the elicited cellular responses	14
4 The endocytic pathway in <i>Dictyostelium discoideum</i>	16
5 Post-translational modification of Rho GTPases	17
6 RhoBTB proteins	19
7 RacA – the representative of RhoBTB proteins in <i>Dictyostelium discoideum</i>	20
8 Cullins – known interaction partners of RhoBTB proteins.....	21
9 Aim of the work.....	23
II MATERIALS AND METHODS	24
1 Materials.....	24
1.1 Laboratory materials	24
1.2 Instruments and equipments.....	25
1.3 Kits.....	26
1.4 Enzymes, antibodies, substrates, inhibitors and antibiotics.....	26
1.5 Chemicals and reagents	27
1.6 Media and buffers	28
1.6 Biological materials	29
1.7 Plasmids.....	29
1.8 Synthetic oligonucleotides	29
1.9 Generated vectors.....	30
2 Methods.....	31
2.1 <i>Dictyostelium discoideum</i> cell culture	31
2.1.1 Growth of <i>Dictyostelium</i>	31
2.1.1.1 Growth in liquid nutrient medium (Claviez 1982)	31
2.1.1.2 Growth on SM agar plates	31
2.1.2 Development of <i>Dictyostelium</i>	31
2.1.3 Preservation of <i>Dictyostelium</i>	32
2.1.4 Transformation of <i>Dictyostelium</i> cells by electroporation.....	32
2.2 <i>Dictyostelium discoideum</i> molecular biological and biochemical methods.....	33
2.2.1 Preparation of total protein from <i>Dictyostelium</i>	33
2.2.2 Subcellular fractionation.....	34
2.2.3 Isolation of <i>Dictyostelium</i> genomic DNA.....	34
2.2.4 Fast isolation of <i>Dictyostelium</i> genomic DNA for PCR.....	35

2.2.5 Isolation of total RNA from <i>Dictyostelium</i> cells.....	35
2.2.6 Expression and purification of a C-terminal peptide of RacA without tag.....	35
2.2.7 Immunoprecipitation from <i>Dictyostelium</i> cell lysate	36
2.2.8 Actin polymerisation assay	37
2.3 Methods for studying the endo- and exocytic pathway of <i>Dictyostelium discoideum</i>	38
2.3.1 Endocytosis and exocytosis assays	38
2.3.2 TRITC-labelling of yeast	38
2.3.3 Phagocytosis	39
2.3.4 FITC-labelling of bacteria.....	39
2.3.5 Determination of endosomal pH	40
2.3.6 Visualisation of pH changes during endosomal traffic in vivo	40
2.3.7 Secretion of lysosomal enzymes	41
2.4 Immunological methods	42
2.4.1 Generation of polyclonal antibodies against RacA.....	42
2.4.2 Affinity purification of polyclonal antibodies by the blot method.....	42
2.4.3 Indirect immunofluorescence of <i>Dictyostelium</i> cells.....	42
2.4.3.1 Preparation of <i>Dictyostelium</i> cells	42
2.4.3.2 Methanol fixation	43
2.4.3.3 Picric acid-paraformaldehyde fixation.....	43
2.4.3.4 Immunolabelling of fixed cells	44
2.4.3.5 Mounting of coverslips	44
2.4.3.6 DAPI and phalloidin staining of fixed cells.....	45
2.5 Tandem affinity purification of RacA	45
2.5.1 Preparation of the <i>Dictyostelium</i> lysate	46
2.5.2 Beads preparation.....	47
2.5.3 Binding to IgG beads	47
2.5.4 TEV protease cleavage.....	47
2.5.5 Binding to, and elution from, Calmodulin beads.....	47
2.6 Microscopy	49
2.6.1 Live cell imaging of <i>Dictyostelium</i> cells expressing GFP-RacA and GFP-RacH	49
2.6.2 Microscopy of fixed preparations	49
2.6.3 Microscopy of agar plates	50
2.7 Video imaging and chemotaxis assay	50
2.8 Computer analysis	50
III RESULTS.....	51
1 Functional characterisation of RacA.....	51
1.1 Generation of RacA polyclonal antibody and verification of RacA expression throughout development	51

1.1.1	Expression of RacA C-terminal peptide for polyclonal antibody production	51
1.1.2	Expression of RacA throughout development	52
1.2	Generation and functional analysis of a RacA deficient strain	53
1.2.1	Generation of a RacA deficient strain	53
1.2.2	Screening for a RacA deficient strain	53
1.2.3	<i>racA</i> transcript is still synthesised	56
1.2.4	Confirmation of RacA knock out by Western blot	57
1.2.5	Characterisation of the RacA deficient strain	57
1.2.5.1	Growth in axenic medium	57
1.2.5.2	Endo- and exocytosis	60
1.2.5.3	Cytokinesis and F-actin organisation of RacA-KO cells	60
1.2.5.4	Chemotaxis and F-actin polymerisation responses upon cAMP stimulation	61
1.2.5.5	RacA deficient cells spread faster on bacterial lawn	66
1.2.5.6	Development of RacA deficient cells	66
1.2.6	Identification of potential binding partners of RacA	66
1.2.6.1	Tandem affinity purification	67
1.2.6.2	Immunoprecipitation of RacA	67
1.2.6.3	Identification of <i>Dictyostelium discoideum</i> cullins	68
1.2.6.4	Interaction of RacA with cullins analysed by yeast-two-hybrid	73
1.3	Overexpression of RacA, its mutant variants and single domains	73
2	Functional analysis of RacH	75
2.1	Confirmation of RacH knock out and overexpressor strains	75
2.2	Growth and endo/exocytosis of RacH mutants	76
2.2.1	Detailed analysis of endocytosis in RacH deficient cells	79
2.2.1.1	RacH-KO cells show deficient acidification of early endosomes	79
2.2.1.2	Visualisation of pH changes during endosomal traffic in vivo	80
2.2.1.3	Secretion of lysosomal enzymes	80
2.2.1.4	Subcellular distribution of vacuolin is affected in RacH deficient cells	82
2.2.1.5	Co-localisation of RacH with early and late endosomes and lysosomes was noticeable but not pronounced	85
2.3	Cytokinesis and development of RacH mutants	86
2.4	Chemotaxis, cell motility and F-actin polymerisation	88
3	Determinants of RacH subcellular localisation	90
IV	DISCUSSION	93

1 RacA potential binding partners and RacA-KO conditional defect indicate a signal transduction pathway downstream of RacA	93
1.1 Putative RacA-binding partners	93
1.1.1 Previously described RacA binding partners.....	93
1.1.2 Analysis of cullin-RacA interaction by means of the yeast-two-hybrid system	94
1.1.3 Potential RacA binding partners detected by immunoprecipitation	95
1.2 Conditional defects in growth, cytokinesis and F-actin organisation of RacA deficient cells correspond to phenotypes of myosin II and PAKa null cells	96
2 RacH is a regulator of endocytosis and depends in this function on its subcellular localisation.....	100
2.1 Role of RacH in endocytosis.....	100
2.1.1 Observations leading to a detailed analysis of endocytosis.....	100
2.1.2 Impact of RacH on early endocytosis	101
2.1.3 Disturbance of the post-lysosomal system in RacH deficient cells.....	102
2.1.4 RacH might affect endocytosis by regulating the actin cytoskeleton	104
2.1.5 RacH localisation points to its function in endocytosis and its effectors.....	105
2.1.6 RacH function is restricted to endocytosis	106
2.2 Determinants of RacH targeting	106
2.3 Proper targeting of RacH is required for function	107
Summary / Zusammenfassung	109
Appendix.....	111
Bibliography.....	113
Erklärung	123
Curriculum vitae	124
Lebenslauf.....	125

Abbreviations

APS	ammonium persulphate
ATP	adenosine 5'-triphosphate
bp	base pair(s)
BCIP	5-bromo-4-chloro-3-indolylphosphate
BSA	bovine serum albumin
Bsr	blasticidin resistance cassette
BTB	Broad-Complex, Tramtrack and Bric à brac
cAMP	cyclic adenosine monophosphate
cDNA	complementary DNA
CIAP	calf intestinal alkaline phosphatase
Cul	cullin
dNTP	deoxyribonucleotide triphosphate
DABCO	diazobicyclooctane
DEPC	diethylpyrocarbonate
DMSO	dimethylsulphoxide
DNA d	deoxyribonucleic acid
DNase	deoxyribonuclease
DTT	1,4-dithiothreitol
ECL	enzymatic chemiluminescence
EDTA	ethylenediaminetetraacetic acid
EGTA	ethyleneglycol-bis (2-amino-ethylene) N,N,N,N-tetraacetic acid
ELISA	enzyme linked immunosorbent assay
FITC	fluorescein isothiocyanate
G418	geneticin
GFP	green fluorescent protein
GST	glutathione S-transferase
HRP	horse radish peroxidase
IgG	immunoglobulin G
IPTG	isopropyl- β -D-thiogalactopyranoside
kb	kilo base pairs
Luminol	5-amino-2,3-dihydro-1,4-phtalazindion
MES	morpholinoethansulphonic acid
β -ME	β -mercaptoethanol
MOPS	Morpholinopropanesulphonic acid
MW	molecular weight
NP-40	nonylphenylpolyethyleneglycol
pNPP	para-nitrophenyl phosphate
OD	optical density
ORF	open reading frame
PAGE	polyacrylamide gel electrophoresis
PCR	polymerase chain reaction
PMSF	phenylmethylsulphonylfluoride
RT-PCR	reverse transcript polymerase chain reaction
RNA	ribonucleic acid
RNase	ribonuclease
rpm	rotations per minute
SAP	shrimp alkaline phosphatase
SDS	sodium dodecyl sulphate
TEMED	N,N,N',N'-tetramethyl-ethylendiamine

TRITC	tetramethylrhodamine isothiocyanate
U	unit
UV	ultra violet
w/v	weight by volume
v/v	volume by volume
w/v	weight by volume
WT	wild-type
X-gal	5-bromo-4-chloro-3-indolyl- β -D-galactopyranoside

Units of Measure and Prefixes	Unit Name
°C	degree Celsius
kDa	kiloDalton
g	gram
h	hours
ml	millilitre
m	metre
min	minute
sec	second
V	volt
mol	mole

Symbol	Prefix (Factor)
k	kilo (10^3)
c	centi (10^{-2})
m	milli (10^{-3})
μ	micro (10^{-6})
n	nano (10^{-9})
p	pico (10^{-12})

I INTRODUCTION

1 *Dictyostelium discoideum* as a model organism

Dictyostelium discoideum is a eukaryote whose natural habitat is the deciduous forest soil where free-living amoebae feed on bacteria and multiply by equal mitotic division. From an evolutionary point of view it is located before the branching of metazoa and fungi but after the divergence of plants (Eichinger et al., 2005).

Especially its lifecycle is peculiar (Figure 1). Upon exhaustion of the bacterial food source more than 100,000 free-living cells aggregate by chemotaxis towards cAMP to form a multicellular structure. Differentiation and sorting out of spore and stalk cells takes place in the multicellular structure.

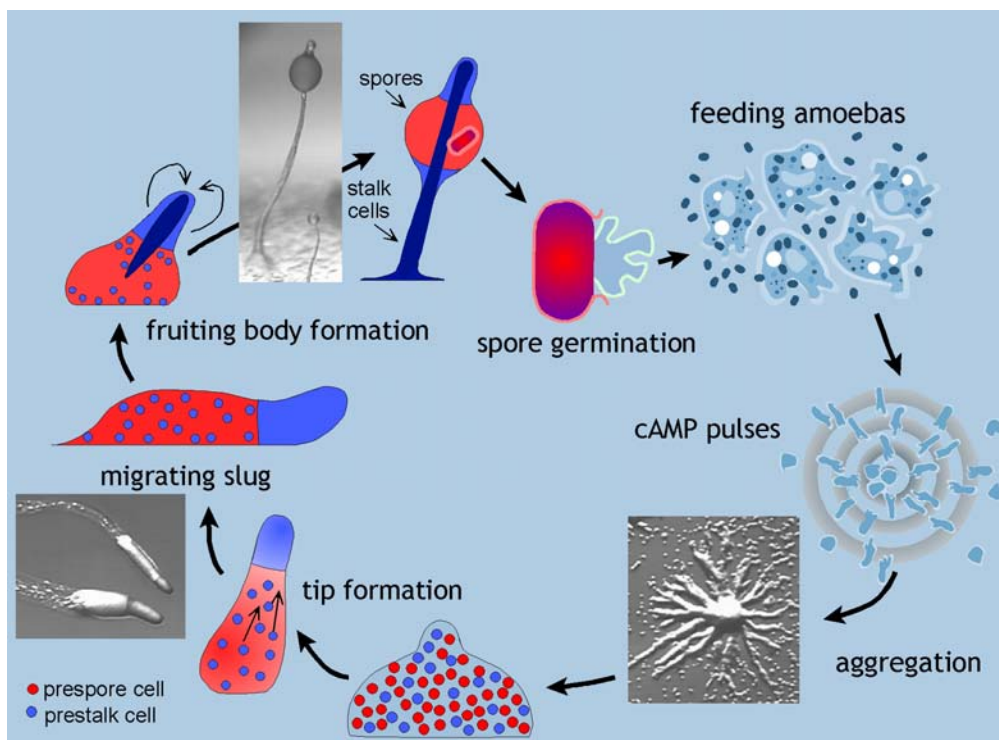


Figure 1: Lifecycle of *Dictyostelium discoideum*. During growth phase *Dictyostelium* exists as single cell amoeba. Upon starvation *Dictyostelium* undergoes chemotaxis towards a pulsatile cAMP wave yielded by the cells emanating from the aggregation centre to its periphery. More than 100,000 cells stream to the centre where they form the mound, which is the first stage in the multicellular development. It forms a tip, which coordinates further development. Next a finger like structure emerges which either immediately culminates into a fruiting body or a motile slug that migrates to a favourable environment before transforming into the fruiting body. The fruiting body is composed of a mass of spores supported by a stalk. Under suitable conditions spores will hatch out and yield amoebae again, thus closing the cycle. Under standard laboratory conditions fruiting bodies form within 24 h (picture is taken from the homepage of P. Schaap's group, University of Dundee).

D. discoideum is amenable to a variety of biochemical, molecular genetic and cell biological techniques. In particular the ease of cultivation facilitates the isolation of proteins associated with the actin network. The molecular genetic techniques available include gene inactivation by homologous recombination, gene replacement, antisense strategies, restriction enzyme-mediated integration (REMI), library complementation and expression of green fluorescent protein (GFP) fusion proteins. Since the organism is haploid, mutants can be immediately obtained by homologous recombination. The genome consists of 6 chromosomes with sizes ranging from 4 to 8 Mb (Cox et al., 1997; Kuspa and Loomis, 1996) resulting in a total of about 34 Mb of DNA; a multicopy 90 kb extrachromosomal element that harbours the rRNA genes, and the 55 kb mitochondrial genome (Eichinger et al. 2005).

Another important contribution to support the state of *Dictyostelium discoideum* as a powerful model organism is the recently completed genome and cDNA sequencing projects (Eichinger et al., 2005). The estimated number of genes is ~12,500. Despite their apparent simplicity, many of the known genes show a high degree of sequence similarity to homologues in vertebrate species (Eichinger et al., 2005). *Dictyostelium* amoebae are equipped with a complex actin cytoskeleton that endows the cells with motile behaviour comparable to that of leukocytes (Noegel and Schleicher., 2000). This implies that many signal transduction pathways regulated by Rho GTPases in animal cells are also present in *Dictyostelium*. In particular, components like PI3K, PAK, WASP, Scar, diverse RhoGAPs and RhoGEFs as well as RhoGDI have been identified in this organism (Eichinger et al., 2005; Rivero and Somesh, 2002).

Thus all these advantages of *Dictyostelium* offer a unique opportunity to characterise the interplay of Rho GTPases with the actin cytoskeleton and the implicated signal transduction pathways.

2 Small GTPases of the Rho family

The Ras superfamily of small GTPases contains over 80 members. Although the function of many of these remains obscure, they can be grouped into six broad families – Ras, Ran, Rad, Rab, Arf and Rho – according to a combination of protein homology and function. Members within each family share 40% or more amino acid sequence identity and exhibit conserved motifs required for interaction with specific classes of downstream effectors (Bourne et al., 1991; Takai and Ono, 2001).

The Rho family of small GTPases are key regulators of the actin/myosin cytoskeleton during chemotaxis (Raftopoulou and Hall, 2004). But besides mediating cellular movement, Rho

GTPases are involved in a wide diversity of cellular processes, like vesicle trafficking, morphogenesis, microtubule organisation, cytokinesis, gene expression, cell cycle progression, apoptosis and tumorigenesis, all processes depending on the re-organisation of the cytoskeleton (VanAelst and D'Souza-Schorey, 1997). In mammals about 20 proteins of the Rho family have been described. According to their effects on actin organisation, the family of RhoGTPases has been further subclassified into at least three subfamilies Rho, Rac and Cdc42: Rac proteins elicit the formation of lamellipodia and membrane ruffles, Rho members coordinate stress fibre and adhesion plaque formation, and Cdc42 stimulates the formation of filopods.

Analysis of the completed *Dictyostelium* genome has revealed a total of 119 genes encoding small GTPases, encompassing all five families mentioned above. The family of RhoGTPases is represented by 19 members, constituted of representatives of the Rac family, but lacking Rho and Cdc42 proteins. The first seven Rho-related genes (*rac1a*, *rac1b*, *rac1c* and *racA* to *racD*) were identified by Bush et al. (1993) using degenerated oligodeoxynucleotide probes corresponding to conserved domains of the GTPases to screen a cDNA library. *RacE* was identified as the gene disrupted in a cytokinesis mutant generated by REMI (Larochelle et al., 1996). *RacF1* was isolated using a PCR approach with degenerated primers corresponding to two highly conserved GTP-binding sites (Rivero et al., 1998). Bioinformatics tools were used to detect further Rho-related proteins in *Dictyostelium*: *racF2*, *racG* to *racJ* and *racL* and one pseudogene (ψ *rack*) (Rivero et al., 2001). Finally the availability of the completed *Dictyostelium* genome sequence has allowed the detection of three additional *rho/rac* genes, *racO*, *racN* and *racM*, making a total of 19 (Weeks et al., 2004).

The phylogenetic analysis (Figure 2) of the Rho GTPases produced a significant cluster of the *Rac1A*, *Rac1B* and *Rac1C* proteins with the metazoan Rac group of proteins. In addition, it shows clustering of *RacF1*, *RacF2* and *RacA* and the failure of *RacA* to group with the metazoan RhoBTB proteins. The other Rho GTPase besides *RacA*, being subject of this work, *RacH*, although not a true Rac protein is closer to Rac and Cdc42 (up to 74% similarity) than to other subfamilies like Rho, Rif or Rnd (51-63% similarity) (Rivero et al., 2001). With few exceptions (*RacA*, *RacD* and *RacE*), *Dictyostelium* Rho proteins are around 200 residues long, which is in the range of almost all small GTPases. *RacD* and *RacE* possess serine-rich insertions of different lengths close to the C-terminal membrane association domain, and *RacA* belongs to the novel subfamily of RhoBTB proteins (Ramos et al., 2002). The Rho insert, an insertion of usually 13 residues with high sequence variability, is a signature characteristic of Rho GTPases and determines in part the specificity of functions of Rho against GTPases of other families. All *Dictyostelium* Rac proteins present a Rho insert rich in charged residues,

although shorter than 13 amino acids in some of them (RacA, RacE, RacH and RacJ) (Rivero et al., 2001).

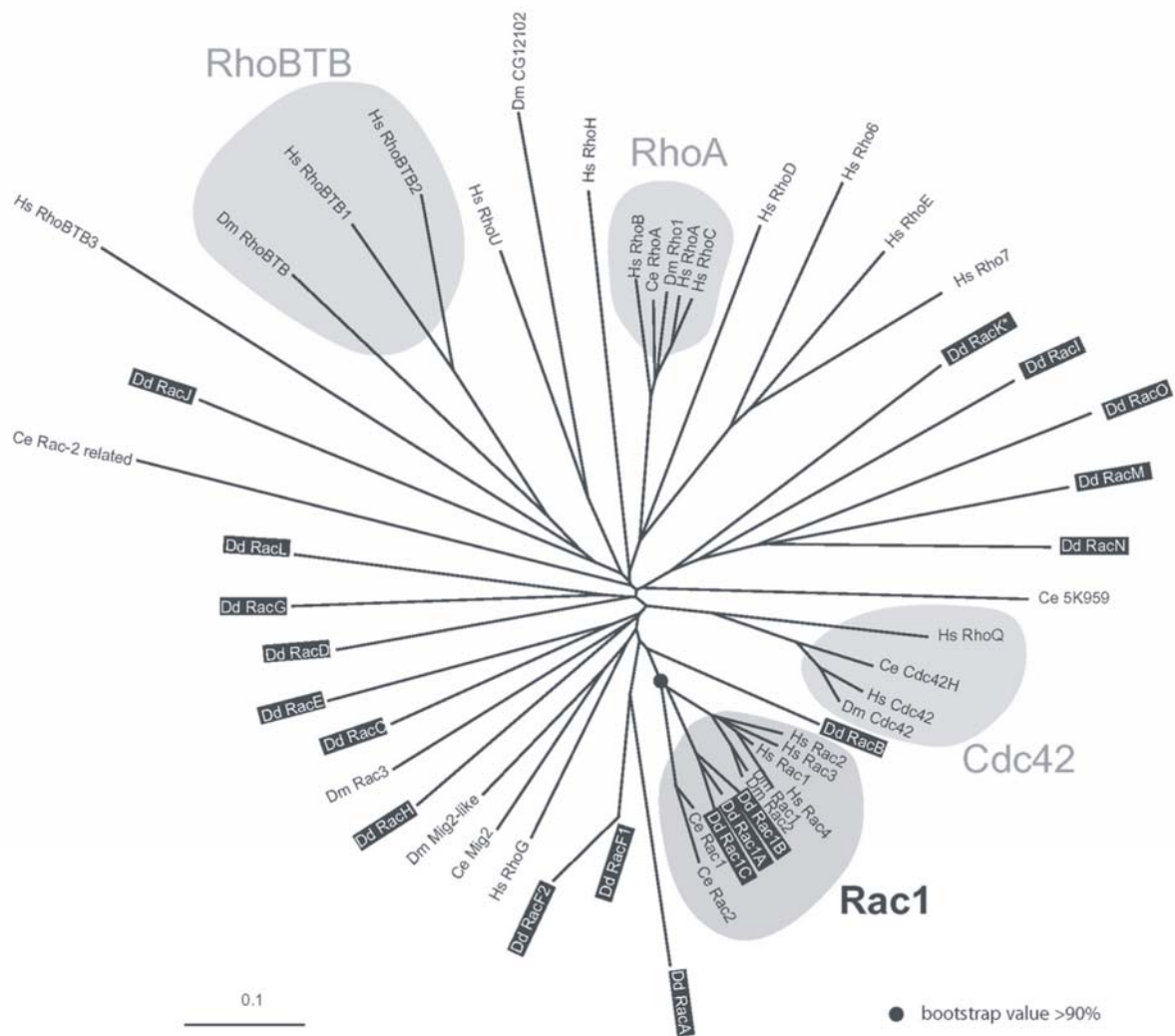


Figure2: Phylogenetic analysis of the Rho/Rac GTPases. Representative species for which fairly complete sets of Rho proteins are available have been selected: *Dictyostelium discoideum* (Dd), *Saccharomyces cerevisiae* (Sc), *Arabidopsis thaliana* (At), *Caenorhabditis elegans* (Ce), *Drosophila melanogaster* (Dm) and *Homo sapiens* (Hs). The phylogenetic tree was constructed using the neighbor-joining method with correction for multiple substitutions. Only the GTPase core devoid of hypervariable regions and additional domains was used. The Rho-related proteins of *D. discoideum* are highlighted. Well-defined subfamilies have been labelled. *D. discoideum*, like animals, has representatives of the Rac subfamily, but lacks Rho and Cdc42 proteins. Note that the GTPase domain of DdRacA/RhoBTB is more closely related to Rac proteins than to RhoBTB proteins. The scale bar indicates 10% divergence (the picture is taken from: Weeks 2004).

3 Regulation of small GTPases and the elicited cellular responses

The small GTPases act as molecular switches, cycling between an active GTP-bound state and an inactive GDP-bound state, a process that is regulated by **GEFs** (guanine nucleotide exchange factors) and **GAPs** (GTPase activating proteins) (Figure 3). GEFs catalyze the conversion to the GTP-bound state and GAPs accelerate the intrinsic rate of hydrolysis of bound GTP to GDP. Additionally, **GDIs** (GDP-dissociation inhibitors) have been described that capture Rho in both GTP and GDP-bound states and allow it to cycle between cytosol and membranes.

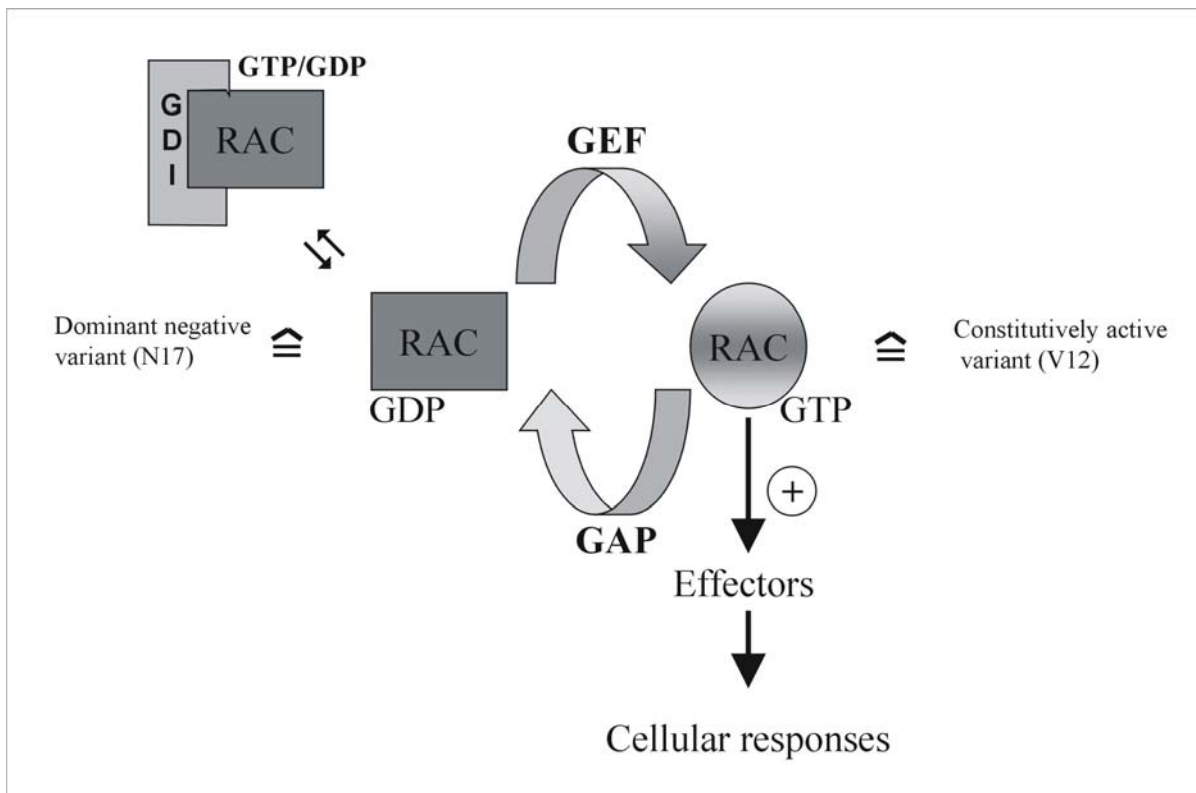


Figure 3: Regulation of Rho family proteins. Most Rho proteins are active when bound to GTP and inactive when bound to GDP. Activation is catalysed by exchange factors (GEFs) and inactivation by GTPase activating proteins (GAPs). Several Rho family proteins also bind to guanine-nucleotide dissociation inhibitors (GDIs) in the cytoplasm and are inactive in this complex. When bound to GTP, Rho proteins interact with target proteins to induce downstream responses. Point mutations that result in constitutively active or dominant negative forms of the GTPase are indicated.

In its active state Rho GTPases interact with a multitude of effectors that relay upstream signals to cytoskeletal components. Point mutations that result in constitutively active (V12, L61) or dominant negative forms (N17) of the GTPases allow to elucidate the influence of either state in appropriate experimental conditions/model organisms. The number of effectors in most of the cases only bound to the active form of the GTPase is as numerous as the number of cellular

responses elicited by the Rho GTPases. They channel Rho GTPase activity into the particular processes.

The pivotal process regulated by Rho GTPases is the rearrangement of the actin cytoskeleton (Raftopoulou and Hall, 2004). However, there is an increasing body of evidence implying members of this family in many aspects of endocytic traffic (Chimini, 2000; Ellis and Mellor, 2000). Although some of these processes might involve actin rearrangement - for instance it was shown that Rac and Cdc42 are required for the accumulation of Wiskott–Aldrich syndrome protein (WASP) and the Arp2/3 complex at the nascent phagosome, promoting actin polymerisation necessary for progression of phagocytosis (Ellis and Mellor, 2000) - others might not. Studies with actin-depolymerising agents have shown that minor depolymerisation of the actin cytoskeleton can stimulate vesicle budding, thereby supporting this idea. Greater depolymerisation of actin was found to prevent budding of clathrin-coated vesicles, suggesting that local remodelling of the actin cytoskeleton (i.e. a combination of polymerisation and depolymerisation) is required (Lamaze, 1997).

In *Dictyostelium discoideum* Rac1a/b/c seem to regulate the basal level of F-actin, its dynamic reorganisation in response to chemoattractants, and cellular polarity during chemotaxis (Chung et al., 2000; Dumontier et al., 2000). This was demonstrated by overexpression of constitutively active mutants of Rac1A, Rac1B and Rac1C. All had identical phenotypes resulting in an increase in the assembly of F-actin, while dominant negative forms had the opposite effect (Palmieri et al., 2000). Additionally the overexpression of the mutated Rac1 proteins resulted in a slight defect in cytokinesis, when cells were grown in suspension. Furthermore, activated Rac1 inhibited both phago- and pinocytosis (Dumontier et al., 2000; Palmieri et al., 2000). RacB seems to play in particular a role in the regulation of phago- and pinocytosis (Lee et al., 2003). Recently RacB null cells gave the hint that it also affects chemotaxis (Park et al., 2004). RacC overexpression led to the formation of irregular actin-rich structures (Seastone et al., 1998) as RacG-overexpressing cells did, giving rise to abundant actin-driven filopods at the plasma membrane (Somesh, 2002). They share another common phenotype: both exhibit increased phagocytosis rates. The pinocytosis rate of RacG is unaltered whereas fluid phase uptake in RacC overexpressors is impaired. These data indicate that diverse Rho proteins have an impact on endocytosis processes by acting through different pathways. This fits to studies on other GTPases and signaling components (PI3-kinases in particular, (Buczynski et al., 1997), indicating that in *Dictyostelium* phagocytosis and pinocytosis are regulated through distinct mechanisms (Rupper and Cardelli, 2001). Also RacF1 seems to control endocytosis as it is located to phago- and pinosomes although a phenotype in endocytosis in the RacF1 knock out was not detectable (Rivero et al., 1998). The highly similar RacF2 protein might functionally

compensate the lack of RacF1. The first Rho GTPase shown to be apparently essential for cytokinesis was RacE as demonstrated in RacE null cells that formed large multi-nucleate cells when grown in suspension (Laroche et al., 1996).

4 The endocytic pathway in *Dictyostelium discoideum*

In *Dictyostelium* the endocytic pathway (Figure 4) has been operationally divided into four steps: uptake at the plasma membrane, transit through early acidic endosomes followed by a late neutral compartment and finally exocytosis (Maniak, 2003). The freshly formed endosome is surrounded by an F-actin shell and other cytoskeletal components (Insall et al., 2001; Peracino et al., 1998) as well as proteins involved in signal transduction. It becomes uncoated one minute after endocytosis. The uncoated vesicle is available for fusion processes, its lumen becomes acidified within seconds (Maniak, 1999), indicating that vesicles have fused with other vesicles which contain the vacuolar H⁺-ATPase (Maniak, 2001). In the following the vesicles are supplied with two succeeding sets of lysosomal enzymes (Souza et al., 1997). As the first set of enzymes, comprising phosphatases and proteinases that are modified by the addition of GlcNAc-1-P, and the second set of lysosomal enzymes, bearing Man-6-P-OCH₃ modified residues, do not coexist in the same vesicles, it is assumed that these steps are intervened by lysosomal retrieval dependent on myosin Ib and Rab7 (Souza et al., 1997). The endosomes of the following stages are characterised by a neutral luminal pH. This change is brought about by the budding of transport intermediates that remove the vacuolar H⁺-ATPase from the membrane of late and possibly recycle it for use in the acidification of early endosomes (Nolta et al., 1994; Rauchenberger et al., 1997). Late endosomes recruit the cytoskeletal proteins coronin (Rauchenberger et al., 1997), Scar (Seastone et al., 2001), and Arp2/3 (Insall et al., 2001), which act together to provide the endosome with a coat of filamentous actin (Rauchenberger et al., 1997). Additionally it is assumed that any time, when the vesicle is neutralised, vacuolin can associate with the vesicle membrane to prevent further cycling and homotypic fusion. The duration of this stable neutral phase could be determined by Rab7 or one of the other Rab proteins, which are known to act as molecular timers (Rybin et al., 1996). If during the neutral phase the vesicle contacts the plasma membrane, exocytosis follows. The contents of late endosomes are released into the surrounding medium, which include indigestible particulate material and soluble components as well as lysosomal enzymes like α -mannosidase and β -glucosidase (Dimond et al., 1981).

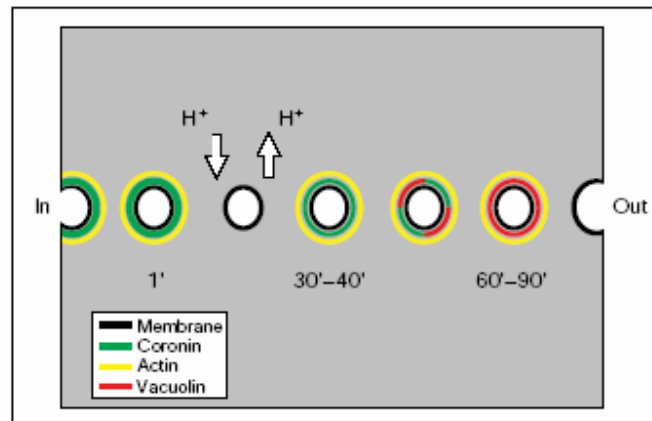


Figure 4: Composition of the vesicle coat during endo- and exocytosis. At the beginning of endocytosis both, particle- and fluid-containing vacuoles, are transiently surrounded by a cytoskeletal coat. When this coat has dissociated, acidification and digestion of the vesicle contents occur, followed by exocytosis of the indigestible remnants after 60–90 minutes. The neutral compartment, vesicles observed after 40 to 90 minutes after internalisation, consists of a few vacuoles of 2-3 μm in diameter which sequentially acquire coronin and vacuolin. Approximate times are given in minutes. H^+ , in conjunction with the inward and outward pointing arrows, represents the beginning and end of the acidic phase, respectively (picture taken from Rauchenberger et al., 1997).

5 Post-translational modification of Rho GTPases

Like Ras, Rho GTPases are synthesised as cytosolic proteins but have the capacity to associate with membranes by virtue of a series of posttranslational modifications of a C-terminal CAAX sequence motif (where C is cysteine, A represents aliphatic amino acids and X is any amino acid) (Figure 5). This motif signals for covalent attachment of an isoprenoid lipid unit to the cysteine residue. Two distinct soluble CAAX prenyltransferases have been described in eukaryotic cells: farnesyl transferase (FTase) and geranylgeranyl transferase (GGTase). The FTase catalyzes the addition of a C15 farnesyl unit to CAAX sequences where X is serine, methionine, cysteine, alanine or glutamine. Whereas the GGTase catalyzes the addition of a C20 geranylgeranyl unit to CAAX sequences where X is leucine or isoleucine. The prenyl-CAAX motif is substrate for a specific protease that cleaves the AAX tripeptide. The modified prenyl cysteine is then recognized by a specific carboxyl methyl transferase that methylesterifies the α -carboxyl group. These two enzymes are membrane proteins localised in the ER (Zhang and Casey, 1996). The CAAX motif alone targets proteins to the ER and Golgi (Choy et al., 1999). Thus CAAX processing alone is necessary but not sufficient to target CAAX proteins to the plasma membrane. Transfer of processed CAAX proteins from the endomembrane to the plasma membrane requires a second C-terminal signal within the hypervariable region upstream of the CAAX motif - either a series of basic amino acids (K-ras4B) or cysteine residues that are

sites of palmitoylation (N-ras and H-ras) (Choy et al., 1999; Hancock et al., 1990; Hancock et al., 1991; Michaelson et al., 2001). Unlike Ras proteins, many Rho proteins are constitutively sequestered in the cytosol through interaction with RhoGDI. Targeting of these molecules to the plasma membrane or other cellular compartments requires release from this cytosolic chaperone as well as an appropriate second signal (Michaelson et al., 2001). Mutation of the second signal of Ras and Rho proteins leads to retention of the GTPase at the endomembrane (Choy et al., 1999). Some Rho family GTPases that lack second signals, such as Cdc42, reside on the endomembrane when dissociated from RhoGDI (Michaelson et al., 2001). Thus, the inherent membrane destination for any CAAX protein is determined by the nature of the second signal.

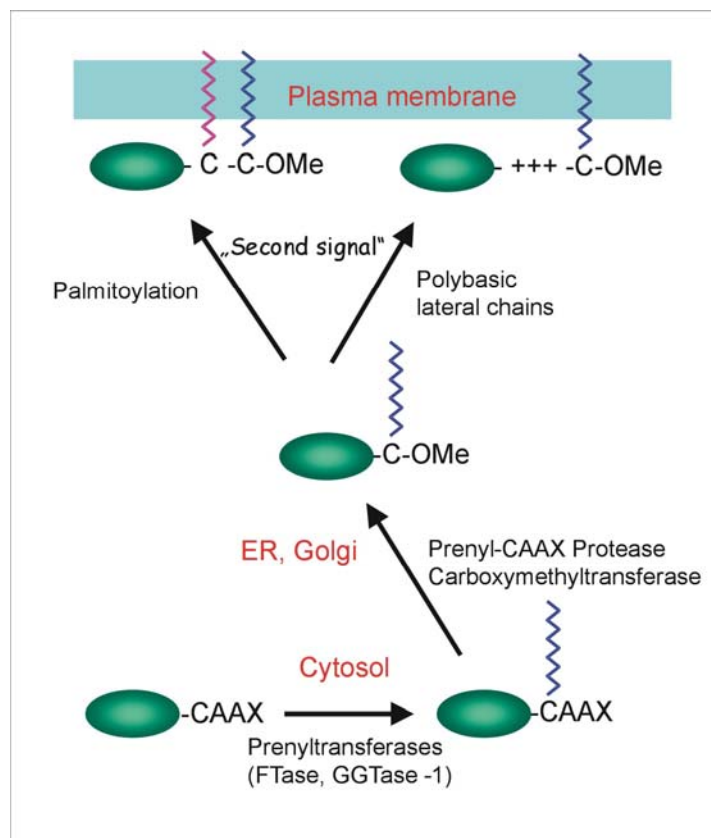


Figure 5: Post-translational modification of Rho GTPases. Prenylation of the CAAX motif targets proteins specifically to the endomembrane where they are proteolysed and methylated. The second signal mediating plasma membrane targeting may be one or two cysteines upstream of the CAAX motif that are modified by palmitoylation or a polybasic stretch.

Posttranslational modification by isoprenoid lipids not only is essential for targeting, but appears to be critical for GTPase function as well. This was initially investigated in Ras proteins, where mutation of the CAAX motif or treatment with farnesyltransferase inhibitors abolishes plasma membrane association and causes a complete loss of oncogenic transforming activity

(Hancock et al., 1990). The functional relevance of protein prenylation for Rho GTPases has been studied in RhoA and RhoB: nonprenylated versions of activated RhoA or RhoB displayed a loss of transforming activity (Lebowitz et al., 1997), and the type of prenylation in part determines the function of RhoB: farnesylated RhoB is a growth promoting protein, whereas geranylgeranylated RhoB is an apoptosis-inducing protein (Lebowitz et al., 1997).

6 RhoBTB proteins

The RhoBTB subfamily of Rho GTPases (Figure 6) was identified during the study of Rho-related protein-encoding genes in *Dictyostelium discoideum* (Rivero et al., 2001). The BTB domain (Broad-Complex, Tramtrack, and Bric à brac, also called POZ domain, for pox virus and zink finger) is an evolutionary conserved domain involved in protein–protein interaction (Aravind and Koonin, 1999). The BTB domain is usually found in some C₂H₂-type zinc-finger transcription factors and in some actin-binding proteins carrying the KELCH domain. They participate in homomeric and heteromeric associations with other BTB domains (Aravind and Koonin, 1999). The crystal structure of some BTB domains has been solved. They constitute tightly intertwined dimers with an extensive hydrophobic interface. The folding consists of a cluster of α -helices flanked by short β -sheets at both, the top and bottom of the molecule (Ahmad et al., 1998). At present three proteins constitute the RhoBTB subfamily in vertebrates (RhoBTB1 to 3), and orthologues also exist in insects, but not in *C. elegans*, fungi or plants (Ramos et al., 2002). The remarkable modular architecture of RhoBTB proteins suggests that these proteins could play a pivotal role as scaffolds, functioning as docking points for molecules participating in diverse signal transduction cascades.

Proteins of this novel subfamily are composed of a GTPase domain, a proline-rich region, two BTB domains and a carboxyl-terminal domain of unknown function. The first BTB domain is interrupted by intervening sequences of variable length that are rich in charged amino acids. These sequences are unrelated among the different RhoBTB proteins, suggesting that they might confer different binding affinities for their specific interaction partners and thus, enabling the protein to operate in different signaling pathways. Of the known representatives only the vertebrate RhoBTB3 ends with a prenylation signal, indicating that targeting of the other RhoBTB proteins is mainly achieved by their regulators or effectors.

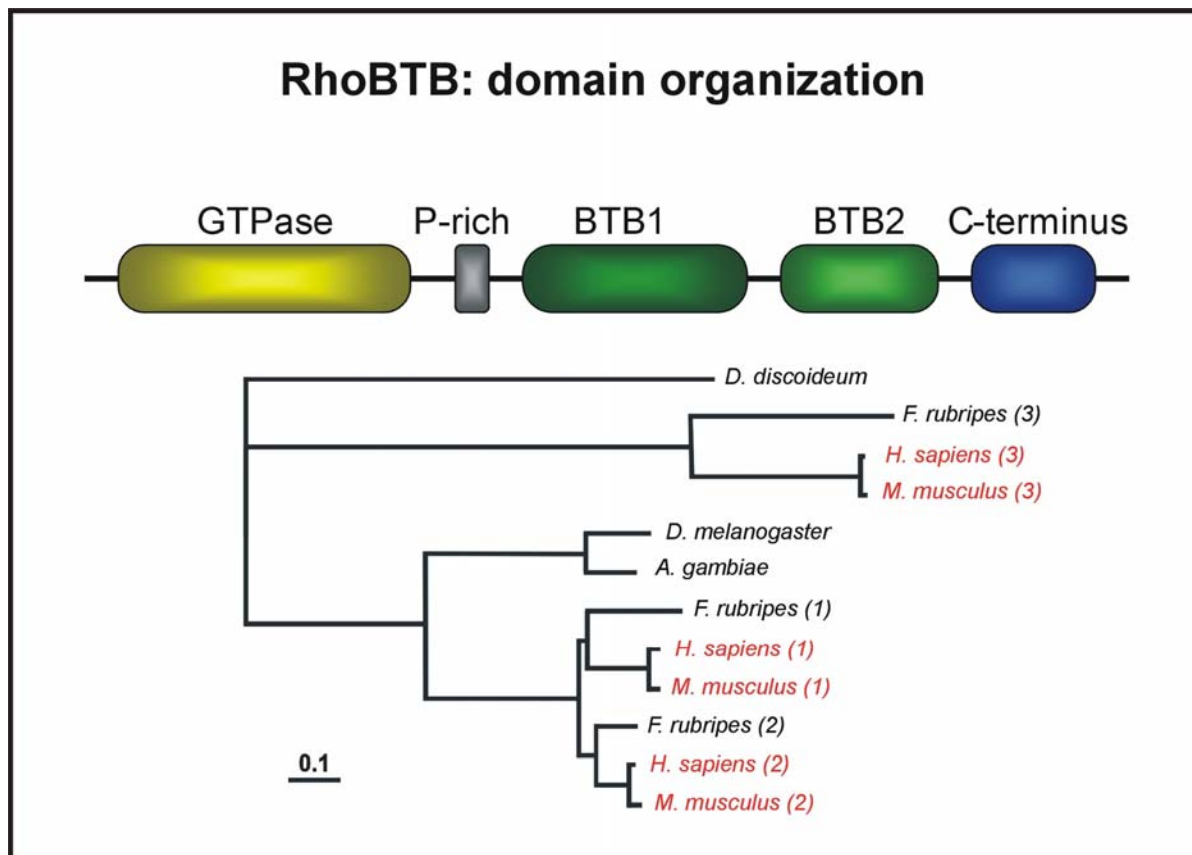


Figure 6: Domain architecture and phylogenetic tree of the RhoBTB family. Representative species for which complete sets of RhoBTB proteins are available have been selected. Besides the three *Homo sapiens* RhoBTB proteins, the sequences of the three RhoBTB proteins of *Mus musculus* and *Fugu rubripes* and of the RhoBTB orthologs from *Anopheles gambiae*, *Drosophila melanogaster* and *Dictyostelium discoideum* (RacA) are shown. The numbers in brackets correspond to the different RhoBTB isoforms in the species considered (The picture was taken from Ramos et al., 2002).

7 RacA – the representative of RhoBTB proteins in *Dictyostelium discoideum*

As the name of the *Dictyostelium discoideum* representative of the RhoBTB subfamily RacA already indicates, its GTPase domain is closer related to the Rac subfamily of Rho GTPases than to the Rho subfamily. But as it reveals the overall and so particular domain architecture of RhoBTB proteins, it has been attributed to the RhoBTB subfamily. As all Rac GTPases of *Dictyostelium* also RacA possesses a highly divergent Rho insert domain rich in charged residues that determines the specificity of Rac against GTPases of other families. RacA consists of 598 aa and the first of the two BTB domains is interrupted (as in all RhoBTB proteins) by intervening, highly charged sequences that are unrelated among the different RhoBTB proteins. Like the other members of the subfamily (with the exception of RhoBTB3), RacA does not possess a prenylation motif. Thus its subcellular localisation is assumed to be mediated by

interacting partners. This task might be carried out by members of the cullin family, that will be introduced in the next section.

8 Cullins – known interaction partners of RhoBTB proteins

The function of the RhoBTB proteins is at present unknown cullin 3 (Cul 3) has been revealed to be a prominent binding partner for BTB domain proteins in *S. pombe* (Furukawa et al., 2003; Xu et al., 2003) and *C. elegans* (Pintard et al., 2003). Geyer et al. (2003) proved that all three BTB domain-containing proteins encoded by the fission yeast genome bind to Cul3 (Geyer et al., 2003). In particular the binding of the mammalian RhoBTB2 protein to cullin 3 has been reported (Wilkins et al., 2004). So what is the nature of cullins, what are their functions and what role do BTB domain proteins play in the cullin context?

Cullin family members were identified in humans (Du et al., 1999; Michel and Xiong., 1998), mice (Singer et al., 1999), *C.elegans* (Kipreos et al., 1996), *D.melanogaster* (Ou et al., 2002), *S.pombe* (Kominami and Ueno., 1996) and budding yeast (Michel, 2003). Comparison of sets of cullins from these organisms allowed grouping them into four different classes, namely 1, 2 & 5, 3, 4, according to similarities of cullin N-termini belonging to the same class. The overall protein structure, except the first 50 amino acids of their N-termini, is very conservative within the cullin family. Moreover the nature of the cullin N-termini determines the composition of complexes they constitute, as cullins turned out to be components of multiprotein complexes, ubiquitin ligases (E3s) (reviewed in (Deshaies, 1999) (Figure 7). These complexes specifically recognise substrates and mediate their ubiquitin-dependent degradation.

First, a brief overview on protein ubiquitylation: ubiquitylation is the result of a highly specific multi-enzyme process, involving classes of enzymes known as E1s, E2s and E3s. There is a single known E1 (ubiquitin-activating enzyme) gene, several E2s (ubiquitin-conjugating enzymes) and a substantially greater number of potential E3s (ubiquitin protein ligases). Specificity in ubiquitylation is conferred primarily by E3s. The E3 ubiquitin ligases provide two distinct functions: catalysing isopeptide bond formation and targeting of the substrate. There are two major classes of E3: HECT domain E3s and RING finger E3s.

Cullins are subunits of the RING finger ubiquitin ligases, that show, as mentioned above, different compositions, depending on the class, the cullin belongs to and mediate ubiquitin-dependent degradation of a specific set of substrates (see Figure 7). The substrates of Cul1-associated SCF complexes and Cul2 ubiquitin ligases are well established, they are less well known for other cullin family members. Only a very limited number of in vivo ubiquitylation

targets, detected in Cul 3 knock outs have been identified (Kurz et al., 2002; Maeda et al., 2001; Pintard et al., 2003; Singer et al., 1999). Cullin ligases are regulated by neddylation and contain the RING finger factor HRT1/Rbx1/Roc1.

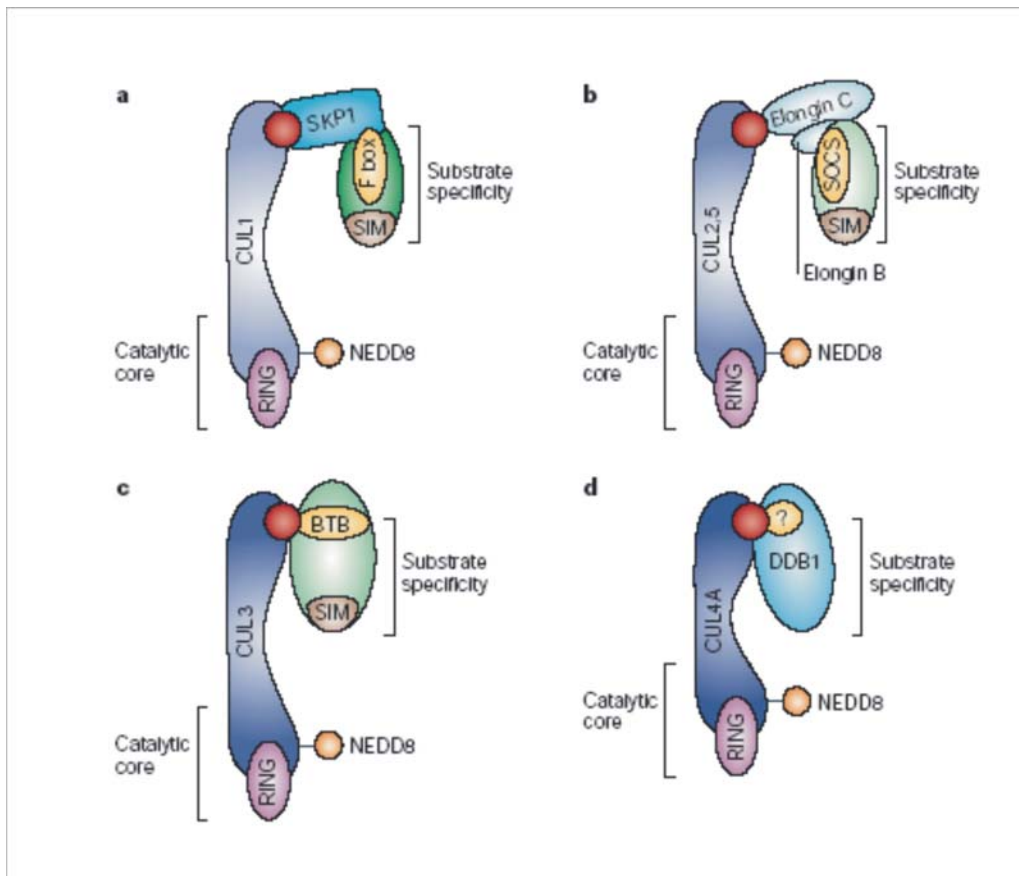


Figure 7: The common catalytic core of cullin–RING ligases (CRLs), which consists of a RING protein and a cullin family member, defines this modular class of ubiquitin ligases. (A) CUL1 CRLs, which are known commonly as SKP1, CUL1, F-box (SCF) proteins, recruit substrates through the adaptor protein SKP1 and an F-box-protein substrate receptor. **(B)** CUL2 and CUL5 CRLs recruit substrates through an elongin-BC adaptor and a suppressor of cytokine signalling/elongin BC (SOCS/BC)-box-protein substrate receptor (labelled SOCS in the figure). **(C)** CUL3 CRLs recruit substrates through BTB domain-containing substrate receptor proteins. **(D)** CUL4A CRLs might recruit substrates through the adaptor protein DNA damage-binding protein-1 (DDB1), which interacts with CUL4A using an unknown motif (highlighted by '?'), and through putative substrate-receptor complexes such as DET1–COP1 (Petroski and Deshaies., 2005).

In the Cul1-SCF and the Cul2, 5-ECS complexes Skp1 and Elongin C mediate between the cullin and the substrate-recognition protein (F-Box and SOCS-box proteins) (reviewed in Deshaies 1999). For Cul3 complexes the BTB proteins are proposed to define a recognition motif for the assembly of substrate-specific RING/Cul3/BTB ubiquitin ligase complexes (Geyer et al., 2003), thus BTB proteins are assumed to maintain the function of both, mediators as well as substrate specificity adaptors.

9 Aim of the work

The aim of the work is to define the role of the Rho GTPases RacA and RacH in cytoskeleton-dependent processes. The role of proteins of the Rho, Rac and Cdc42 subfamilies in actin organisation and other processes in mammalian cells has been widely studied. However, many other Rho GTPases remain largely uncharacterised. The presence of multiple *rac* genes in *Dictyostelium* and its advantages as a model organism offer a unique opportunity to unravel the processes regulated by Rho GTPases.

In this work we have undertaken the functional analysis of *Dictyostelium* RacA and RacH RhoGTPases mainly by studying the respective knock out strains. To identify processes depending on RacA or RacH, the performance of the knock outs in activities that require a rearrangement of the actin cytoskeleton (growth, cytokinesis, pinocytosis, phagocytosis, locomotion, F-actin polymerisation, aggregation) was analysed. Additionally, identification of RacA binding partners has been attempted as they may give further hints to RacA function.

As it was known that RacH was targeted to intracellular membranes of the nuclear envelope, the ER and Golgi apparatus (Somesh, 2002), it was investigated whether its function is mainly related to its subcellular localisation. This has been addressed by the analysis of mistargeted RacH mutants. Furthermore localisation determinants have been elucidated by means of chimeric constructs and alanine exchange mutants.

II MATERIALS AND METHODS

1 Materials

Common media, buffers and solutions used for cell culture, molecular biological and biological methods and not listed in this section are described elsewhere (Sambrook et al., 2001). Unless otherwise indicated, chemicals were purchased from SIGMA, Fluka, Merck or Roth.

1.1 Laboratory materials

Cellophane sheet, Dry ease	Novex
Centrifuge tubes, 15 ml,	Greiner
Coverslips (glass), Ø12 mm, Ø18 mm, Ø55 mm	Assistant
Corex tube, 15 ml, 50 ml	Corex
Cryo tube, 1 ml	Nunc
Electroporation cuvette, 2 mm electrode gap	Bio-Rad
Gel-drying frames	Novex
Hybridisation bag	Life Technologies
Microcentrifuge tube, 1.5 ml, 2.2 ml	Sarstedt
Micropipettes, 1-20 µl, 10-200 µl, 100-1,000 µl	Gilson
Micropipette tips	Greiner
Multi-channel pipette	Finnigan
Needles (sterile), 18G27G	Terumo, Microlance
Nitrocellulose membrane, BA85	Schleicher and Schuell
Nitrocellulose round filter, BA85, Ø82 mm	Schleicher and Schuell
Nylon membrane	Bodyne B Pall
Parafilm	American Nat Can
Pasteur pipettes, 145 mm, 230 mm	Volac
PCR soft tubes, 0.2 ml	Biozym
Petri dishes (35 mm, 60 mm, 100 mm)	Falcon
Petri dishes (90 mm)	Greiner
Plastic cuvette, semi-micro	Greiner
Plastic pipettes (sterile), 1 ml, 2 ml, 5 ml, 10 ml, 25 ml	Greiner
Quartz cuvette Infracil	Hellma
Quartz cuvette, semi-micro	Perkin Elmer
Saran wrap	Dow
Scalpels (disposable), Nr. 10, 11, 15, 21	Feather
Slides, 76 x 26 mm	Menzel
Syringes (sterile), 1 ml, 5 ml, 10 ml, 20 ml	Amefa, Omnifix
Syringe filters (Acrodisc), 0.2 µm, 0.45 µm	Gelman Sciences
Tissue culture flasks, 25 cm ² , 75 cm ² , 175 cm ²	Nunc
Tissue culture dishes, 6 wells, 24 wells, 96 wells	Nunc
Whatman 3MM filter paper	Whatman
X-ray film, X-Omat AR-5, 18 x 24 mm, 535 x 43 mm	Kodak

1.2 Instruments and equipments

Centrifuges (microcentrifuges):	
Centrifuge 5417 C	Eppendorf
Centrifuge Sigma B	Braun
Cold centrifuge Biofuge fresco	Heraeus instruments
Centrifuges (table-top, cooling, low speed):	
Centrifuge CS-6R	Beckman
Centrifuge RT7	Sorvall
Centrifuge Allegra 21R	Beckman
Centrifuges (cooling, high speed):	
Beckman Avanti J25	Beckman
Sorvall RC 5C plus	Sorvall
Centrifuge-rotors:	
JA-10	Beckman
JA-25.50	Beckman
SLA-1500	Sorvall
SLA-3000	Sorvall
SS-34	Sorvall
Dounce homogeniser, 10 ml B.	Braun
Electrophoresis power supply, Power-pac-200, -300	Bio-Rad
Electroporation unit Gene-Pulser, Xcell	Bio-Rad
Fluorimeter PTI	Photon Technology Int
Freezer (-80°C)	Nunc
Freezer (-20°C)	Siemens, Liebherr
Gel-documentation unit	MWG-Biotech
Heating block DIGI-Block JR	NeoLab
Heating block, Dry-Block DB x 20	Techne
Hood, Hera Safe (HS 12)	Heraeus
Hybridization oven	Hybaid
Ice machine	Ziegra
Incubators:	
CO ₂ -incubator, BBD 6220, BB 6220	Heraeus
CO ₂ -incubator WTC Binder	Biotran
Incubator, microbiological	Heraeus
Incubator with shaker Lab-Therm	Kuehner
Magnetic stirrer, MR 3001 K	Heidolph
Microcontroller	Luigs and Newmann
Microscopes:	
Light microscope, CH30	Olympus
Light microscope, DMIL	Leica
Light microscope, CK2	Olympus
Fluorescence microscope, DMR	Leica
Fluorescence microscope, 1X70	Olympus
Confocal laser scanning microscope, DM/IRBESP	Leica
Stereomicroscope, SZ4045TR	Olympus
Oven, conventional	Heraeus
PCR machine, PCR-DNA Engine PTC-200	MJ Research
pH-Meter	Knick
Refrigerator	Liebherr
Semi-dry blot apparatus, Trans-Blot SD	Bio-Rad
Shakers GFL	Kuehner

Sonicator, Ultra Turrax T25 basic	IKA Labortechnik
Speed-Vac concentrator, DNA 110	Savant
Spectrophotometer, Ultraspec 2000, UV/visible	Pharmacia Biotech
Ultracentrifuges:	
Optima TLX	Beckman
Optima L-70K	Beckman
Ultracentrifuge-rotors:	
TLA 45	Beckman
TLA 100.3	Beckman
SW 41	Beckman
UV crosslinker UVC 500	Hoefler
UV transilluminator TFS-35 M	Faust
Vortex, REAX top	Heidolph
Video cameras	
JAI CV-M10 CCD Camera	Stemmer Imaging
SensiCam	PCO Imaging
Water bath	GFL
X-ray film developing machine, FPM-100A	Fujifilm

1.3 Kits

Nucleobond AX	Macherey-Nagel
NucleoSpin Extract 2 in 1	Macherey-Nagel
Nucleotrap	Macherey-Nagel
Original TA Cloning	Invitrogen
pGEM-T Easy	Promega
Qiagen Midi- and Maxi-prep	Qiagen

1.4 Enzymes, antibodies, substrates, inhibitors and antibiotics

Calf Intestinal Alkaline Phosphatase (CIAP)	Roche
Deoxyribonuclease I (DNase I)	Roche
Klenow fragment (DNA polymerase)	Roche
Restriction endonucleases	Amersham
	New England Biolabs
Reverse transcriptase, Superscript II	Life Technologies
Ribonuclease H (RNase H)	Roche
S1-nuclease	Amersham
T4 DNA ligase	Roche
<i>Taq</i> -polymerase	Roche
<i>Pfu</i> -polymerase	Roche
Tev protease	Invitrogen

Primary antibodies:

Mouse anti-actin monoclonal antibody Act 1-7	(Simpson <i>et al.</i> , 1984)
Mouse anti-GFP monoclonal antibody K3-184-2	(Gloss <i>et al.</i> , 2003)
Mouse anti-interaptin monoclonal antibody 260-60-10	(Rivero <i>et al.</i> , 1998)
Mouse anti-PDI monoclonal antibody 221-135-1	(Monnat <i>et al.</i> , 1997)
Mouse anti-comitin monoclonal antibody 190-340-2	(Weiner <i>et al.</i> , 1993)
Mouse anti-lysosome monoclonal antibody 221-342-5	(Neuhaus <i>et al.</i> 1998)
Mouse anti-vatA monoclonal antibody 221-35-2	(Jenne <i>et al.</i>)

Mouse anti-Arp-3 monoclonal antibody	(Insall et al.)
Mouse anti-PAKb monoclonal antibody	(Côté et al.)
Mouse anti-vacuolin monoclonal antibody 221-1-1	(Rauchenberger et al.)

Secondary antibodies:

Goat anti-mouse IgG, peroxidase conjugated	Sigma
Goat anti-rabbit IgG, peroxidase conjugated	Sigma
Mouse anti-goat IgG, peroxidase conjugated	Sigma
Goat anti-mouse IgG, Cy3 conjugated	Sigma

Inhibitors:

Diethylpyrocarbonate (DEPC)	Sigma
Leupeptin	Sigma
Pepstatin	Sigma
Phenylmethylsulphonyl fluoride (PMSF)	Sigma
LY294002	Sigma
Protease inhibitor cocktail	Roche

Antibiotics:

Ampicillin	Gruenthal
Blasticidin S	ICN Biomedicals
Chloramphenicol	Sigma
Dihydrostreptomycinsulphate	Sigma
Geneticin (G418)	Life Technologies
Kanamycin	Sigma, Biochrom
Tetracyclin	Sigma

1.5 Chemicals and reagents

Acetic acid (98-100%)	Riedel-de-Haen
Acrylamide (Protogel: 30:0,8 AA/Bis-AA)	National Diagnostics
Agar-Agar (BRC-RG)	Biomatic
Agarose (Electrophoresis Grade)	Life Technologies
Calmodulin Affinity Resin	Stratagene
Chloroform	Riedel-de-Haen
Dimethylformamide	Riedel-de-Haen
Ethanol	Riedel-de-Haen
Glycerine	Riedel-de-Haen
Glycine	Riedel-de-Haen
IgG Sepharose	Pharmacia
Isopropyl-D-thiogalactopyranoside (IPTG)	Loewe Biochemica
Methanol	Riedel-de-Haen
Morpholino propane sulphonic acid (MOPS)	Gerbu
N- [2-Hydroxyethyl] piperazine-N-2- -ethanesulphonic acid (HEPES)	Biomol
Radiolabelled nucleotide: α - ³² P-deoxyadenosine triphosphate (10 mCi/ml)	Amersham
Sodium hydroxide	Riedel-de-Haen
Yeast Nitrogen Base	Difco
Yeast extract	Oxoid

1.6 Media and buffers

All media and buffers were prepared with deionised water filtered through an ion-exchange unit (Membra Pure). The media and buffers were sterilised by autoclaving at 120°C and antibiotics were added to the media after cooling to approx. 50°C. For making agar plates, a semi-automatic plate pouring machine (Technomat) was used.

Ax2 medium, pH 6.7: (Claviez *et al.*, 1982)

7.15 g yeast extract
14.3 g peptone (protease)
18.0 g maltose
0.486 g KH_2PO_4
0.616 g $\text{Na}_2\text{HPO}_4 \cdot 2\text{H}_2\text{O}$
add H_2O to make 1 litre

Phosphate agar plates, pH 6.0:

9 g agar
add Soerensen phosphate buffer, pH 6.0
to make 1 litre

Salt solution: (Bonner, 1947)

10 mM NaCl
10 mM KCl
2.7 mM CaCl_2

SM agar plates, pH 6.5: (Sussman, 1951)

9 g agar
10 g peptone
10 g glucose
1 g yeast extract
1 g $\text{MgSO}_4 \cdot 7 \text{H}_2\text{O}$
2.2 g KH_2PO_4
1 g K_2HPO_4
add H_2O to make 1 litre

Soerensen phosphate buffer, pH 6.0: (Malchow, 1972)

2 mM Na_2HPO_4
14.6 mM KH_2PO_4

MES buffer pH 6.5:

20 mM 2-[N-morpholino]ethane sulfonic acid
1 mM EDTA

250 mM sucrose

1.6 Biological materialsBacterial strains:

<i>E. coli</i> BL21 (DE)	(Studier, 1986)
<i>E. coli</i> DH5 α	(Hanahan, 1983)
<i>E. coli</i> MC1061 (with episomal pSCM)	(Wertman, 1986)
<i>E. coli</i> XL1 blue	(Bullock et al., 1987)
<i>E. coli</i> B/r	(Ward et al.)
<i>Klebsiella aerogenes</i>	(Williams and Newell., 1976)

Dictyostelium discoideum strain:

Ax2-214. An axenically growing derivative of wild strain, NC-4 (Raper, 1935). Commonly referred to as Ax2.

Yeast strains:

Y187	(Harper et al., 1993)
Y190	(Harper et al., 1993)
AH 109	(James et al., 1996)

1.7 Plasmids

Plasmid name	Reference
PDEX-RH	(Westphal et al., 1997)
pT7	Stan et al.
pGEM-T Easy	Promega
pBluescript	Stratagene
pUC bsr	(Sutoh, 1993)
pGADT7	Clontech
pGBKT7	Clontech
pACT2	Clontech
pAS2-1	Clontech
MB38	(Blaauw <i>et al.</i> , 2000)
TAP	Schaap and Gould, 2004

1.8 Synthetic oligonucleotides

All primers were ordered from Sigma and are listed in the appendix.

1.9 Generated vectors

Application	Insert	Vector	bp of cDNA sequence	
GFP-RacA overexpressors in Dd	Full-length	PDNeo		
	Full-length-V12	pDEX-RH		
	Full-length-N17	pDEX-RH		
	GTPase	pDEX-RH	1-547	
	GTPase-V12	pDEX-RH	1-547	
	GTPase-N17	pDEX-RH	1-547	
	PB1B2C	pDEX-RH	585-1797	
	B1B2C	pDEX-RH	670-1797	
	B2C	pDEX-RH	1143-1797	
	B1	pDEX-RH	670-1200	
	B2	pDEX-RH	1143-1545	
	C	pDEX-RH	1522-1797	
	GTPase-CAAX-WT	pDEX-RH	1-547	
	GTPase-CAAX-V12	pDEX-RH	1-547	
	GTPase-CAAX-N17	pDEX-RH	1-547	
	B1 Δ insert	pDEX-RH	670-1200, Δ 787-804	
	Inducible GFP-RacA overexpressors in Dd	B1	MB38	670-1200
		B2	MB38	1143-1545
		RacAFL N17	MB38	
RacAFLWT		MB38		
RacAFL V12		MB38		
RacA Yeast-2-Hybrid	B1B2C	pGBKT7	670-1797	
	B2	PACT	1143-1545	
	B1	PAS	670-1200	
	B1 Δ ins	pGBK	670-1200, Δ 787-804	
	B2	pGBKT7	1143-1545	
	GTPaseV12	pGBKT7	1-547	
	GTPase	PAS	1-547	
	GTPase-V12	PAS	1-547	
	GTPase-N17	PAS	1-547	
CullinYeast-2-Hybrid	Cul A	PACT		
	CulB	PACT		
	Cul III	PACT		
	Cul IV	pACT		
	CulV	pACT		
TAP system	RacAFL	NTAP		
	RacAFL	CTAP		
RacA peptide expression	B1	pT7-8	670-1200	
	B2C	pT7-8	1143-1797	
GFP-RacH mutant expression	RacH2xAla	pDEX	see Results 3	
	RacH4xAla	pDEX	see Results 3	
	RacH Δ ins	pDEX	RacH FL, Δ 375-392	

2 Methods

For common cell biological, molecular biological and biochemical methods the reader is referred to Sambrook and Russel 2001.

2.1 *Dictyostelium discoideum* cell culture

2.1.1 Growth of *Dictyostelium*

2.1.1.1 Growth in liquid nutrient medium (Claviez 1982)

Dictyostelium discoideum Ax2 and the derived transformants were grown in liquid AX2 medium containing dihydrostreptomycin (40 µg/ml) and other appropriate selective antibiotics at 21°C either in a shaking-suspension in Erlenmeyer flasks with shaking at 160 rpm or on petri dishes. For all the cell biological works, cultures were harvested at a density of 3-5 x 10⁶ cells/ml.

2.1.1.2 Growth on SM agar plates

Dictyostelium cells were plated onto SM agar plates overlaid with *Klebsiella aerogenes* and incubated at 21°C for 3-4 days until *Dictyostelium* plaques appeared on the bacterial lawns. To obtain single clones of *Dictyostelium*, 50-200 cells were suspended in 100 µl Soerensen phosphate buffer and plated onto *Klebsiella*-overlaid SM agar plates. Single plaques obtained after incubation at 21°C for 3-4 days were picked up with sterile tooth-picks, transferred either to new *Klebsiella*-overlaid SM agar plates or to separate Petri dishes with Ax2 medium supplemented with dihydrostreptomycin (40 µg/ml) and ampicillin (50 µg/ml) (to eliminate the bacteria) and any other appropriate selective antibiotic (depending upon mutant).

2.1.2 Development of *Dictyostelium*

Development of *Dictyostelium* is induced by starvation. Cells grown to a density of 2-3 x 10⁶ cells/ml were pelleted by centrifugation at 2,000 rpm (Sorvall RT7 centrifuge) for 2 min at 4°C and were washed two times in an equal volume of cold Soerensen phosphate buffer in order to remove all the nutrients present in the culture medium. 5 x 10⁷ cells/ml were then resuspended in 3 ml Soerensen phosphate buffer and evenly distributed onto phosphate-buffered agar plates (90 mm). The plates were air-dried and any excess liquid was carefully aspirated without

disturbing the cell layer. The plates were then incubated at 21°C. Different stages of development were observed and images were captured at selected time points. For development in suspension culture, the cells were resuspended in Soerensen phosphate buffer at a density of 1×10^7 cells/ml and were shaken at 160 rpm and 21°C for desired time periods. For development on nitrocellulose filters 0.5×10^8 cells were deposited on nitrocellulose filters (Millipore type HA, Millipore) and allowed to develop at 21°C as described (Newell, 1969).

2.1.3 Preservation of *Dictyostelium*

Dictyostelium cells were allowed to grow in Ax2 medium to a density of $4-5 \times 10^6$ cells/ml. 9 ml of the dense grown culture were collected in a 15 ml Falcon tube on ice and supplemented with 1 ml horse serum and 1 ml DMSO. The contents were mixed by gentle pipetting, and aliquoted in cryotubes (1 ml). The aliquots were incubated on ice for 30 min, followed by storage at -20°C for at least 2 h. Finally, the aliquots were transferred to -80°C for long-term storage. For reviving the frozen *Dictyostelium* cells, an aliquot was taken out from -80°C and thawed immediately at 37°C in a water bath. In order to remove DMSO, the cells were transferred to a Falcon tube containing 30 ml Ax2 medium and centrifuged at 2,000 rpm (Sorvall RT7 centrifuge) for 2 min at 4°C. The cell pellet was resuspended in 10 ml of Ax2 medium and 200 µl of the cell suspension was plated onto SM agar plates overlaid with *Klebsiella* while the remaining cell suspension was transferred into a 100-mm Petri dish and antibiotics were added when appropriate. Cells in the Petri dish were allowed to recover overnight at 21°C and the medium was changed the next day to remove the dead cells and the traces of DMSO, whereas, the SM agar plates coated with cell suspension and bacteria were incubated at 21°C until plaques of *Dictyostelium* cells started to appear.

2.1.4 Transformation of *Dictyostelium* cells by electroporation

The electroporation method for transformation of *Dictyostelium* cells described by de Hostos *et al.* (1993) was followed with little modifications. *Dictyostelium discoideum* cells were grown axenically in suspension culture to a density of $2-3 \times 10^6$ cells/ml. The cell suspension was incubated on ice for 20 min and centrifuged at 2,000 rpm (Sorvall RT7 centrifuge) for 2 min at 4°C to collect the cells. The cells were then washed with an equal volume of ice-cold Soerensen phosphate buffer and afterwards with an equal volume of ice-cold electroporation buffer. After washings, the cells were resuspended in electroporation buffer at a density of 1×10^8 cells/ml.

For electroporation, 20-25 µg of the plasmid DNA was added to 500 µl of the cell suspension and the cell-DNA mixture was transferred to a pre-chilled electroporation cuvette (2 mm electrode gap, Bio-Rad). Electroporation was performed with an electroporation unit (Gene Pulser, Bio-Rad) using a preset program for *Dictyostelium discoideum*. After electroporation, the cells were immediately spread onto a 100-mm Petri dish and were allowed to sit for 10 min at 21°C. Thereafter, 1 ml of healing-solution was added dropwise onto the cells and the Petri dish was incubated at 21°C on a shaking platform at 50 rpm for 15 min. 10 ml of Ax2 medium were added into the Petri dish and the cells were allowed to recover overnight. The next day, the medium was replaced by the selection medium containing appropriate antibiotic. To select for stable transformants, selection medium was replaced every 24-48 hr until the control plate (containing cells electroporated without any DNA) was clear of live cells.

Electroporation buffer:

100 ml 0.1 M potassium phosphate buffer
17.12 g sucrose
add distilled H₂O to make 1 litre
autoclave

0.1 M Potassium phosphate buffer:

170 ml 0.1 M KH₂PO₄
30 ml 0.1 M KH₂PO₄
adjust to pH 6.1

Healing-solution:

150 µl 0.1 MgCl₂
150 µl 0.1 CaCl₂
10 ml electroporation-buffer

2.2 *Dictyostelium discoideum* molecular biological and biochemical methods

2.2.1 Preparation of total protein from *Dictyostelium*

1×10^7 to 5×10^8 *Dictyostelium* cells either vegetative or at different stages of development were washed once in Soerensen phosphate buffer. Total protein was prepared by lysing the pellet of cells in 500µl of 1 x SDS sample buffer. Equal amounts of protein (equivalent to 2×10^5 to 1×10^7 cells/lane) were loaded onto discontinuous SDS-polyacrylamide gels.

2.2.2 Subcellular fractionation

Dictyostelium cells were collected by centrifugation (1000 x g for 5 min) and resuspended in MES buffer supplemented with a protease inhibitor mixture (50 µg/ml leupeptin, 10 µg/ml pepstatin A, 2 mM benzamidine, 1 mM PMSF). Cells were lysed on ice using a sonicator, and light microscopy was performed to ensure that at least 95% of the cells were broken. Membranes and supernatants were separated by centrifugation (100,000 x g for 30 min), and the samples were resuspended in SDS sample buffer (Laemmli 1970).

2.2.3 Isolation of *Dictyostelium* genomic DNA

Genomic DNA from *Dictyostelium* was prepared according to the method described by Nellen *et al.* (1987), with slight modifications. *Dictyostelium* cells were allowed to grow on *Klebsiella*-covered SM plates at 21°C. After 2-3 days, when the plates were covered with densely grown *Dictyostelium*, cells were collected in 15 ml ice-cold water, pelleted and washed twice with ice-cold water to get rid of *Klebsiella*. Alternatively, the pellet of 1×10^8 *Dictyostelium* cells grown in shaking suspension was washed twice with ice-cold Soerensen phosphate buffer. The pellet of *Dictyostelium* cells was finally resuspended in 5 ml cold Nucleolysis buffer. The nuclei fraction was obtained by centrifugation at 3,000 rpm (Sorvall RT7 centrifuge) for 10 min. The nuclear pellet obtained was carefully resuspended in 1 ml TE, pH 8.0, with 0.5% SDS and 0.1 mg/ml proteinase K and incubated at 37°C for 3-5 h. The genomic DNA was extracted twice with phenol/chloroform (1:1 v/v), precipitated by adding 2.5 vol. 96% ethanol and 1/10 vol. 3 M sodium acetate, pH 5.2. The DNA precipitate was carefully spooled with a Pasteur pipette, washed with 96% ethanol, air-dried and dissolved in the desired volume of TE, pH 8.0.

Nucleolysis buffer:

10 mM magnesium acetate
10 mM NaCl
30 mM HEPES, pH 7.5
10% sucrose
2% Nonidet P40

2.2.4 Fast isolation of *Dictyostelium* genomic DNA for PCR

1×10^6 cells were collected in 1 ml H₂O, pelleted again resuspended in 95 μ l of 1x PCR buffer supplemented with 2% NP40 and 0.1 mg/ml proteinase K and incubated at 56°C for 45 min. Then the mixture was kept at 95°C for 10 min and pelleted briefly. 15 μ l of the mixture are used as PCR template of a reaction with a total volume of 50 μ l.

2.2.5 Isolation of total RNA from *Dictyostelium* cells

The pellet of 1×10^8 cells (harvested at growth or different stages of development) was washed with ice-cold DEPC-H₂O and lysed in 1 ml of guanidine isothiocyanate. The lysate was centrifuged at 13,000 rpm for 10 min at 4°C to pellet the insoluble materials and the supernatant was transferred to a fresh eppendorf tube and incubated at room temperature for 5 min. This was followed by immediately adding 1 vol of chloroform (Tris or water saturated) to separate the aqueous and organic phase and again allowed to stand at room temperature for 5 min. Then the mixture was centrifuged at 13,000 rpm for 15 min at 4°C and the upper aqueous phase was collected carefully and extracted with an equal volume of phenol/chloroform (1:1 v/v), till no interphase was visible. This was followed by an extraction with an equal volume of chloroform and so that finally the RNA appeared in the upper aqueous phase. This phase was collected and the RNA was precipitated by adding an equal volume of isopropanol and incubating the samples overnight at -80°C. At the next day, the RNA was pelleted and washed with 70% ethanol, air-dried and dissolved in the desired volume of DEPC-H₂O. The concentration of RNA was determined by measuring the OD₂₆₀ of the RNA solution using a spectrophotometer. The RNA samples were stored at -80°C.

DEPC-H₂O:

0.1% DEPC in H₂O mixed by stirring for 5-6 h
autoclaved

2.2.6 Expression and purification of a C-terminal peptide of RacA without tag

The C-Terminal sequence of RacA from the second BTB domain onwards till the end (bp 1143-1797 of the RacA cDNA sequence) was cloned into the pT7 expression vector and transformed into the *E. coli* MC1061L strain. One litre of LB-medium containing ampicillin (100 μ g/ml) and

kanamycin (20 µg/ml) was inoculated and grown at 37°C until the OD₆₀₀ was 0.6. Isopropyl β-D-thiogalactoside was added to a final concentration of 500 µM and the cells were cultured for a further 3.5 h at 37°C. The cells were then harvested by centrifugation and resuspended in 25 ml of ice cold buffer A. The cells were incubated on ice for 10 min and pelleted by spinning at 6,000 x g for 5 min at 4°C. The pellet obtained was resuspended in buffer P. Lysis was done by one round of freeze thawing, the lysate was sonicated (6 pulses of 10 sec), keeping the tube on ice. Sonication was followed by homogenisation using a Dounce homogeniser for 2-3 min in order to ensure complete and efficient cell lysis. In order to get rid of the cytosolic components the lysate was centrifuged at 100,000 x g for 30 min. The supernatant was discarded and the pellet containing the B2C peptide was resuspended in 2 x SDS sample buffer. 4 ml of this sample were loaded on 12% SDS-PA gels. The separated proteins were stained with 0.3 M copper chloride solution and the band of interest excised and cut into small pieces. The peptide was eluted out of the gel using the Bio-Rad Model 422 Electro-Eluter according to the supplier manual.

Buffer A, pH 7.5:

50 mM TrisHCl
1 mM EGTA
1 mM EDTA
20% sucrose

Buffer P:

PBS
5 mM EDTA
50 µg/ml leupeptin
10 µg/ml pepstatin A
2 mM benzamidine
1 mM PMSF

2.2.7 Immunoprecipitation from *Dictyostelium* cell lysate

Dictyostelium cells grown axenically were harvested and washed twice with Soerensen phosphate buffer. Cells suspended in twice the volume of the homogenisation buffer were lysed by sonication followed by treatment with a Dounce homogeniser. The complete lysis of the cell was confirmed by visual inspection of a drop of lysate under a light microscope. The lysate was centrifuged at 10,000 x g for 25 min at 4°C. The supernatant was precleaned by incubating with protein A sepharose beads for 1 h at 4°C. 600 µl of cleared supernatant were incubated with 100 - 800 µl of antibody solution, 325 µl 5 x immunoprecipitation buffer, 0.1 % Triton X-100 and protein A sepharose beads at 4°C for 3 h. Beads were washed twice with 1 x IP buffer. Washed beads were then incubated with 5 x SDS-sample buffer for 5 min at 95°C. The released proteins were resolved by SDS-PAGE (10 %). The size fractionated proteins were stained with silver. The bands shown in Figure 24 were analysed by mass spectrometry.

Homogenisation buffer:

0.33 x PBS, pH 7.4

2 mM benzamidine

4 mM DTT

2mM EDTA

0.5 mM PMSF

(Triton X-100 was added after the sonication to a final concentration of 0.5 %)

5 x IP buffer:

0.5 m Potassium phosphate buffer

0.375 M NaCl

25 mM EDTA

5 mM Benzamidine

2.5 mM PMSF

Adjust the pH to 7.9, prepare fresh

2.2.8 Actin polymerisation assay

Chemoattractant-induced F-actin formation in aggregation competent cells was quantitated as described Hall *et al.* (1988). Cells were resuspended at 2×10^7 cells/ml in Soerensen buffer and starved for 6 to 8 h. 1 ml of cell suspension was transferred to a well of a 24- well plate on a shaker and stimulated with 1 μ M cAMP, 50 μ l samples were taken at various time points and transferred immediately to tubes containing 450 μ l of stop solution.

Stop solution, pH 6.8:

20 mM potassium phosphate

3.7% formaldehyde

0.1% Triton X-100

0.25 μ M TRITC-phalloidin

10 mM Pipes

5 mM EGTA

2 mM MgCl₂

Formaldehyde fixes the cells instantaneously while TRITC-phalloidin binds to F-actin. After staining for 1 hour, F-actin was pelleted by centrifugation for 5 minutes at 15,000 x g. Pellets were extracted with 1 ml methanol for 16 hours and fluorescence (540/565 nm) was read in a fluorimeter.

2.3 Methods for studying the endo- and exocytic pathway of *Dictyostelium discoideum*

2.3.1 Endocytosis and exocytosis assays

Fluid-phase endocytosis assays and exocytosis were performed according to the methods of Aubry *et al.* (1994) using either TRITC-dextran (76,000 Mr, Sigma T1162) or FITC-dextran (FD-70S, Sigma) (Buczynski 1997). In both cases *Dictyostelium* cells were grown to $< 5 \times 10^6$ cell/ml. The cells were centrifuged and resuspended at 5×10^6 cells /ml in fresh axenic medium at 21°C and incubated for 15 min on a shaker to allow cells to recuperate. Then either TRITC- or FITC-dextran was added to a final concentration of 2 mg/ml. Samples were withdrawn at different time intervals. When TRITC-dextran was used the cells of the 1 ml samples were pelleted after a period of 3 min of incubation with 100 µl of trypan blue (2 mg/ml) to quench nonspecifically bound marker. The pellet was resuspended in phosphate buffer and the fluorescence was immediately measured using a fluorimeter (544 nm excitation/ 574 nm emission). In the case of FITC-dextran 500 µl were collected and added to 2 ml microfuge tubes containing 1.5 ml of ice-cold Soerensen buffer. Samples were collected until the end of the experiment. Then cells were pelleted, washed once with ice-cold Soerensen buffer, pelleted again followed by resuspension in 1 ml of lysis buffer. Fluorescence was measured at 470 nm excitation/ 515 nm emission. For fluid-phase exocytosis assays, cells were pulsed with TRITC-dextran or FITC-dextran (2 g/ml) for 2 h, washed and resuspended in fresh axenic medium. Fluorescence from the marker remaining in the cells was measured every 15 minutes for 2 h.

Lysis buffer, pH 9.3:

50 mM Na₂HPO₄
0.2% Triton X-100

2.3.2 TRITC-labelling of yeast

Preparation of heat-killed yeast cells:

Five grams of dry yeast *Saccharomyces cerevisiae* (Sigma) were suspended in 50 ml of PBS in a 100 ml Erlenmeyer flask and incubated for 30 min in a boiling water bath with stirring. After boiling, the yeast cells were washed five times with PBS, followed by two washings with Soerensen phosphate buffer. The yeast cells were then finally resuspended in Soerensen phosphate buffer at a concentration of 1×10^9 yeast cells/ml. Aliquots of 1 ml and 20 ml were made and stored at -20°C.

TRITC-labelling of heat-killed yeast cells:

For labelling, the pellet of 2×10^{10} heat-killed yeast cells were resuspended in 20 ml of 50 mM Na_2HPO_4 , pH 9.2, containing 2 mg of TRITC (T5646, Sigma) and incubated for 30 min at 37°C on a rotary shaker. After washing twice with 50 mM Na_2HPO_4 , pH 9.2, and four times with Soerensen phosphate buffer, aliquots of 1×10^9 yeast cells/ml were frozen at -20°C.

2.3.3 Phagocytosis

Phagocytosis was performed according to Maniak *et al.* (1995). *Dictyostelium* cells were grown to $< 5 \times 10^6$ /ml over 5 generations in axenic medium. Cells were centrifuged and resuspended at 2×10^6 /ml in fresh axenic medium at 21°C. TRITC-labelled yeast cells prepared according to Materials and Methods 2.3.2 were added in a 5 fold excess (10^9 yeast cells/ml stock). Cells were incubated on a rotary shaker at 160 rpm. Samples were taken at different intervals and the fluorescence of non-internalised yeasts was quenched by incubating for 3 min with 100 μ l trypan blue (2 mg/ml). Cells were centrifuged again, resuspended in phosphate buffer and the fluorescence was measured using a fluorimeter (544 nm excitation/ 574 nm emission).

2.3.4 FITC-labelling of bacteria

300 ml LB medium were inoculated with *E. coli* B/r and grown overnight at 21°C. The bacteria were harvested at 5,000 x g for 10 min. The bacterial pellet was washed 2x with Soerensen buffer. The suspension was adjusted to 1×10^{10} bacteria/ml (achieved by measuring the OD_{600} of a diluted aliquot of the bacterial suspension: 1 OD = 1×10^9 /ml). For labelling the pellet of 50ml suspension was resuspended in 50 ml labelling buffer containing FITC and incubated 3 h at 37°C on a rotatory shaker (wrapped with aluminium foil to avoid bleaching). The bacteria were again pelleted, washed 4x with Soerensen buffer and the suspension was adjusted to 2×10^{10} bacteria/ml and stored at -20°C in 1- or 2 ml aliquots protected from the light.

Labelling buffer:

50 mM Na_2HPO_4 , pH 9.2

FITC (70,000 Mr, Sigma-Aldrich, freshly dissolved in DMSO to 0.1 mg/ml final concentration)

2.3.5 Determination of endosomal pH

Endosomal pH was measured by the dual excitation ratio method (Temesvari et al., 1996) with FITC-dextran as a pH probe. Cells were resuspended at 5×10^6 cells/ml in axenic medium and allowed to recover for 10 minutes. Basal endosomal pH was measured after loading for 3 h with FITC-dextran, the time period shown to be sufficient for the complete loading of all the endolysosomal compartments with a fluid phase marker (Aubry et al., 1994; Rodriguez-Paris et al., 1993). For measurement cells were resuspended in fresh medium, washed and resuspended in 50 mM MES buffer (pH 6.5) at a concentration of 5×10^6 cells/ml. The fluorescent excitation intensities (I) at 450 nm and 495 nm were determined. The emission wavelength was 520 nm in both cases. The fluorescence excitation ratio at 495 nm and 450 nm I_{495}/I_{450} was calculated, and endosomal pH determined from an *in vitro* standard curve of FITC-dextran in a pH range of 4-7.

Phagosomal pH was determined using FITC-labelled *E. coli* as a pH sensitive phagocytic probe. Cells were resuspended at 5×10^6 cells/ml in axenic medium and allowed to recover for 10 min. A pulse with FITC-labelled *E. coli* (5×10^9 *E. coli*/1 $\times 10^6$ *Dictyostelium* cells) for 10 minutes in shaking suspension followed. The cells were then diluted with ice-cold axenic medium. After 3 washes they were resuspended at 5×10^6 cells/ml in room temperature medium. At the indicated time points 2.5×10^6 cells were harvested, washed and resuspended in 50 mM MES (pH 6.5) buffer. Fluorescence was measured at 520 nm following excitation at 450 nm and 495 nm. The intraphagosomal pH was determined by extrapolation from an *in vitro* standard curve gained by measuring the fluorescence ratio of FITC labelled *E. coli* in buffers from pH 4-7.

2.3.6 Visualisation of pH changes during endosomal traffic in vivo

To monitor changes of pH and concentration of marker during endocytosis (Jenne et al., 1998) vegetative cells were washed with Soerensen buffer and allowed to sit in an observation chamber made of a glass coverslip with a plastic ring. Cells were then exposed to pH-sensitive FITC-dextran (0.4 mg/ml) and pH-independent TRITC-dextran (4 mg/ml) for 1 h. Then single confocal sections were taken showing distribution of FITC-dextran (green at neutral pH) and TRITC dextran (red). Superimposition of the channels yields a yellow colour for neutral vacuoles, while acidic vesicles appear in red.

2.3.7 Secretion of lysosomal enzymes

Cells were harvested by centrifugation and resuspended at a concentration of 1×10^7 cells/ml in Soerensen phosphate with or without addition of sucrose (100 mM). Cells were shaken for up to 6 h and 1 ml samples were harvested by centrifugation at the times indicated. Enzyme assays were performed on the supernatant (extracellular, secreted portion of enzymes) or on the pellets of cells. For this, to 1/5 and 1/10 volume of supernatant for the determination of α -mannosidase activity and of acid phosphatase activity, respectively, Triton X-100 was added to a final concentration of 0.1%. The pellet was resuspended in 200 μ l citrate buffer and lysed by adding Triton X-100 to a final concentration of 0.1%. To assay α -mannosidase and acid phosphatase activity in the pellet fraction, also 1/5 and 1/10 of the pellet sample were used. All four samples were shock-frozen in liquid nitrogen. After thawing, the volume of all samples was equalized to 200 μ l by adding citrate buffer. Then the samples were supplemented with 200 μ l substrate solution. For the measurement of α -mannosidase and acid phosphatase enzyme activity p-nitrophenyl- α -D-mannopyranoside and nitrophenylphosphate was used, respectively. The mixtures were incubated for 30 min at 37°C. The reaction was stopped by adding 600 μ l 0.1 M NaOH and absorbance measured at $\lambda = 405$ nm. Enzyme activity was determined by comparison with a standard curve of 4-nitrophenol. The standard curve was gained by dissolving 4-nitrophenol in 400 μ l citrate buffer and adding 600 μ l 0.1 M NaOH followed by measurement. The range of 4-nitrophenol concentration was 0 -100 μ M (Dimond 1981; Free et al., 1974).

Citrate buffer:

50 mM sodium citrate pH 5.0 (1 part 50 mM citric acid·H₂O and 2 parts 50 mM trisodium citrate·2H₂O)

5 mM benzamidine (stock 0.5 M)

0.5 PMSF (stock 50 mM in isopropanol)

Substrate solutions (in citrate buffer):

For α -mannosidase: 3 mM p-nitrophenyl- α -D-mannopyranoside

For acid phosphatase: 3 mM nitrophenylphosphate

2.4 Immunological methods

2.4.1 Generation of polyclonal antibodies against RacA

For generating polyclonal antisera against RacA the RacA C-terminal peptide B2C generated as described in Materials and Methods 2.2.6 was used to immunise two female white New Zealand rabbits (100 µg/animal; Pineda Antikörper-Service, Berlin, Germany), followed by three boosts of 100 µg each at two-week intervals. After the third boost the antiserum of animal 1 was highly specific for RacA and was affinity purified as follows.

2.4.2 Affinity purification of polyclonal antibodies by the blot method

The recombinant protein that was used to produce the polyclonal antibody, was resolved by SDS-PAGE and the gel was afterwards transferred to a PVDF membrane. The membrane was stained with Ponceau S to confirm the transfer efficiency and the portion of the blot corresponding to the recombinant protein was cut out. The blot was then destained with TBS and blocked by incubating blot for 2 h in buffer I. 1 volume of serum was diluted with 4 volumes of TBS and incubated with the stripes at 4°C for 2 hours. The unbound antibody was washed with TBS 4 x 5 minutes at 4°C. After washing, the antibodies bound to the recombinant protein on the membrane stripes were eluted with 1 ml of buffer II two times for 1.5 min at 4°C. The eluted antibody was neutralised with 100 µl of 1 M Tris (pH 8.0) immediately after elution. The antibody can be stabilised with 0.5% BSA.

TBS: 8 g NaCl, 0.2 g KCl and 3 g Tris/HCl in 1 litre, pH 7.2

Buffer I: 1% BSA, 0.05% Tween 20 in PBS

Buffer II: 0.1 M glycine, 0.5 M NaCl, 0.5% Tween 20, pH 2.6

2.4.3 Indirect immunofluorescence of *Dictyostelium* cells

2.4.3.1 Preparation of *Dictyostelium* cells

Dictyostelium cells were grown in shaking culture to a density of $2-4 \times 10^6$ cells/ml. The desired amount of cells was collected in a centrifuge tube. The cells were then resuspended in fresh axenic medium and grown overnight on glass coverslips in axenic medium. Alternatively, cells from the shaking culture were allowed to attach to the coverslips for 20 min. Thereafter, cells

attached onto the coverslip were fixed immediately by one of the fixation techniques described below.

2.4.3.2 Methanol fixation

After the cells had attached to the coverslip, the supernatant was aspirated and the coverslip was dipped instantaneously into pre-chilled (-20°C) methanol in a Petri dish and incubated at 20°C for 10 min. The coverslip was then taken out from methanol and placed on a parafilm-covered glass plate resting in a humid box with the cell-surface facing upwards. This was followed by 2 washings with 500 µl of PBG for 15 min each and immunolabelling as described in section 2.4.3.4.

PBG, pH 7.4:

0.5 % bovine serum albumin

0.1 % gelatin (cold-water fish skin)

in 1x PBS, pH 7.4

2.4.3.3 Picric acid-paraformaldehyde fixation

After the cells had attached to the glass coverslips the supernatant was gently aspirated from the edge of the coverslip and 200 µl of freshly prepared picric acid-paraformaldehyde solution was directly added. The coverslip was incubated at room temperature for 30 min. After incubation, the picric acid-paraformaldehyde solution was aspirated, the coverslip was picked up with a fine forceps and swirled in 10 mM PIPES buffer, pH 6.0, followed by blotting off the excess solution with a tissue paper. Now the coverslip was swirled in PBS/glycine and placed on a parafilm-covered glass plate resting in a humid chamber. The coverslip was then washed with 500 µl PBS/glycine for 5 min to block free reactive groups followed by postfixation with 500 µl of 70% ethanol for 10 min. This was followed by 2 washings with 500 µl of PBG for 15 min each. After washings, the cells were immunolabelled as described in section 2.4.3.4.

Picric acid-paraformaldehyde solution:

0.4 g paraformaldehyde was dissolved in 5 ml ddH₂O by stirring at 40°C and adding 3-4 drops of 2 M NaOH. After dissolving, the volume was adjusted to 7 ml with ddH₂O. To this paraformaldehyde solution, 10 ml of 20 mM PIPES buffer, pH 6.0, and 3 ml of saturated picric acid was added and the pH was finally adjusted to 6.5.

PBS/glycine:

500 ml PBS
3.75 g glycine in 100 ml distilled H₂O
store at 20°C filter sterilized

20 mM PIPES buffer, pH 6.0:

0.605 g PIPES in 100 ml H₂O
filter sterilized adjust to pH 6.0

2.4.3.4 Immunolabelling of fixed cells

Coverslips with the fixed cells were incubated with 200 µl of the desired dilution (in PBG) of primary antibody for 1-2 h in a humid box at room temperature. After incubation, the excess unattached antibody was removed by washing the coverslip 6 times with PBG for 5 min each. Now the coverslip was incubated for 1 h with 200 µl of a proper dilution (in PBG) of Cy3-conjugated secondary antibody. Following this incubation, two washings with PBG for 5 min each followed by three washings with PBS for 5 min each were performed. After washings, the coverslip was mounted onto a glass slide.

2.4.3.5 Mounting of coverslips

After immunolabelling of the fixed cells, the coverslip was swirled once in deionised water and the extra water was soaked off on a soft tissue paper. Now a drop of gelvatol was placed to the middle of a clean glass slide and the coverslip was mounted (with the cell-surface facing downwards) onto the drop of gelvatol, taking care not to trap any air-bubble between the coverslip and the glass slide. Mounted slides were then stored overnight in the dark at 4°C.

Gelvatol:

2.4 g of polyvinyl alcohol (Mw 30,000-70,000; Sigma) were added to 6 g of glycerol in a 50 ml centrifuge tube and mixed by stirring. To the mixture, 6 ml of distilled water was added and the mixture was incubated at room temperature. After several hours of incubation at room temperature, 12 ml of 0.2 M Tris/HCl, pH 8.5, were added and the mixture was heated to 50°C for 10 min with occasional mixing to completely dissolve the polyvinyl alcohol. The solution was centrifuged at 5,100 rpm for 15 min. After centrifugation, 2.5% of diazabicyclo octane (DABCO), an anti-oxidant agent, was added to reduce the bleaching of the fluorescence. The solution was aliquoted in 1.5 ml microcentrifuge tubes and stored at -20°C.

2.4.3.6 DAPI and phalloidin staining of fixed cells

DAPI staining of *Dictyostelium* nuclei and phalloidin staining of *Dictyostelium* F-actin were performed simultaneously. Staining of F-actin with phalloidin demarcated the cell-boundary, which facilitated determining the number of DAPI stained nuclei within a particular cell. Cells were harvested and the coverslips coated with cells were prepared as explained in Materials and Methods 2.4.3.1. Cells were then fixed by the picric acid-paraformaldehyde fixation method as discussed in section 2.4.3.3. After fixation and usual washings, coverslips were incubated for 30 min with 200 μ l of PBG containing DAPI (1:10,000 dilution of 0.1 mg/ml stock) and TRITC-phalloidin (1:200 dilution of 0.1 mg/ml stock). Thereafter, the coverslip was washed twice with 200 μ l of PBG for 5 min each, followed by three washings with 400 μ l of PBS for 5 min each. After washings, the coverslips were mounted onto the glass slides (see Materials and Methods, 2.4.3.5) for observation under a fluorescence microscope or confocal laser-scanning microscope.

2.5 Tandem affinity purification of RacA

In order to purify RacA under mild conditions thus allowing to additionally co-purify interaction partners we performed the TAP-method. The coding sequence of RacA has been set in frame to an N-terminal epitope into the BamHI site of the TAP-Vector (generously provided by Pauline Schaap, University of Dundee). The epitope comprises two different affinity tags, first the IgG binding units of *Staphylococcus aureus* protein A and second a calmodulin binding peptide (CBP), separated by a cleavage site for Tobacco Etch Virus (TEV) protease. Thus the TAP-method comprises two sequential purifications, interrupted by a protease cleavage step and followed by final elution (Figure 8). After an initial affinity purification step on an IgG matrix, the bound material is released by incubation with TEV protease. The second affinity step involves incubating the first eluate with calmodulin-coated beads in the presence of calcium. In the final step, bound material is released into a solution with EGTA.

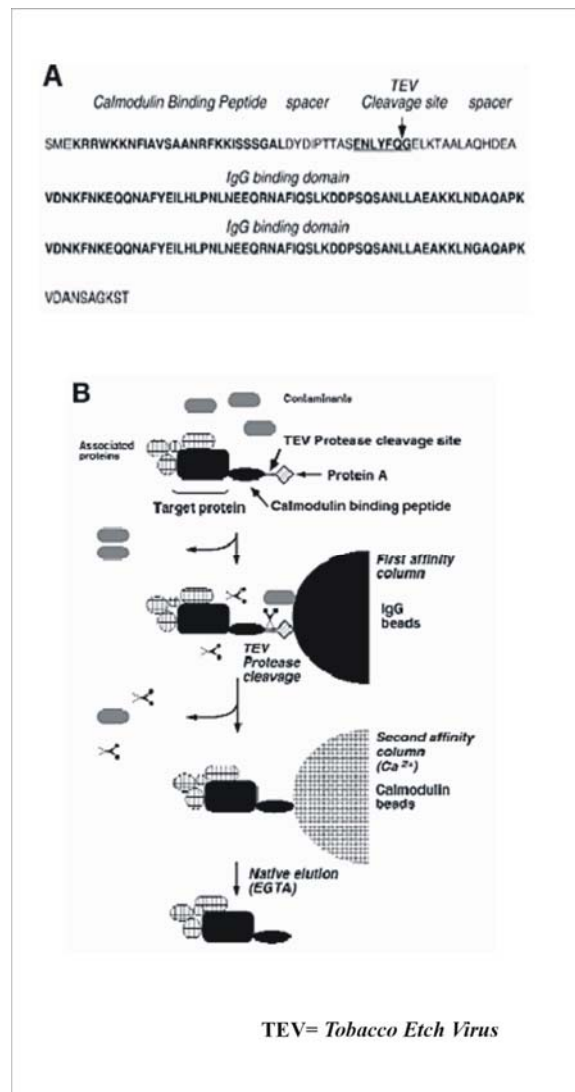


Figure 8: Overview of the TAP procedure. (A) The TAP tag was fused N-terminally to GFP-RacA. The TAP-tag consists of IgG binding units of *Staphylococcus aureus* protein A and a calmodulin binding peptide (CBP) with a cleavage site for Tobacco Etch Virus (TEV) protease between them. (B) The TAP procedure here shown for a C-terminal tag: the first step utilises the binding of the ProtA moiety in the tag to matrix-bound IgG. The complex is released from the beads by cleavage of a seven-amino acid residue recognition sequence located between the two tags by TEV protease. The complex is then immobilized via the calcium-dependent binding of the calmodulin-binding peptide to calmodulin-coated beads and released by the addition of EGTA.

2.5.1 Preparation of the *Dictyostelium* lysate

A *Dictyostelium* culture of cells expressing the NTAP-RacA fusion protein was axenically grown to a density of 3×10^6 cells/ml. 5×10^8 cells were collected by centrifugation (1000 x g for 5 min) and resuspended in MES buffer supplemented with a protease inhibitor mixture (50 μ g/ml leupeptin, 10 μ g/ml pepstatin A, 2 mM benzamidine, 1 mM PMSF). Cells were lysed on ice using a sonicator, and light microscopy was performed to ensure that at least 95% of the cells were

broken. The lysate was centrifuged (10,000 x g for 20 min). The supernatant (10 ml) was utilized for the TAP-purification.

2.5.2 Beads preparation

For the first affinity purification step 200 μ l of IgG sepharose and for the second step 200 μ l of calmodulin beads suspension were used. Both were washed in a small column with 5 ml of IPP150 (IgG beads) or 5 ml of IPP150 calmodulin binding buffer (calmodulin beads) before starting the purification.

2.5.3 Binding to IgG beads

To the extract (10 ml, generated as described in 2.5.1)

- 50 ml 2 M Tris-Cl pH 8.0 (final concentration 10 mM)
- 200 ml 5 M NaCl (final concentration 150 mM)
- 100 ml NP40 10% (final 0.1%)

were added. The mixture was rotated with IgG beads for 2 h at 4°C in the column.

2.5.4 TEV protease cleavage

Then the column was allowed to drain by gravity flow, washed with 30 ml IPP150, followed by a wash step with 10 ml TEV cleavage buffer. In the next step 1 ml TEV cleavage buffer and approximately 100 units of TEV enzyme were added. During the cleavage reaction the column was rotating for 4 h at 4°C. The eluate was then recovered by gravity flow. The solution remaining in the column dead-volume was eluted with an additional 200 μ l of TEV cleavage buffer.

2.5.5 Binding to, and elution from, Calmodulin beads

To the previous 1.2 ml eluate 3 volumes of calmodulin binding buffer and 3 μ l of 1M CaCl₂ per ml of IgG eluate (to titrate the EDTA coming from the TEV cleavage buffer) were added. This mix was transferred into the column containing the washed Calmodulin beads. The column was then rotated for 1 h at 4°C. After binding the column was drained by gravity flow, washed with 30 ml IPP150 calmodulin binding buffer and finally 5 fractions of 200 μ l with IPP150 calmodulin elution buffer. The fractions were mixed with 5 x SDS-buffer, incubated for 3 min at 95°C and

loaded on a 10% SDS-gel or were pooled and TCA precipitated. In the last case the protein precipitate was mixed with 2x SDS-buffer, incubated for 3 min at 95°C and then loaded on the SDS-gel. The gel was either Coomassie- or silver- stained.

TAP-buffers:**IPP150**

10 mM Tris-Cl pH8.0 (0.5 ml of 2 M stock)
150 mM NaCl (3 ml of 5M stock)
0.1% NP40 (1.0 ml of 10% stock)
H₂O to 100 ml final

TEV cleavage buffer

10 mM Tris-Cl pH 8.0 (0.5 ml of 2 M stock)
150 mM NaCl (3 ml of 5 M stock)
0.1% NP40 (1.0 ml of 10% stock)
0.5 mM EDTA (100 ml of 0.5 M stock)
1 mM DTT (100 ml of 1M stock, added just before use)
H₂O to 100 ml final

IPP150 Calmodulin binding buffer

10 mM β-mercaptoethanol (69.7 ml of stock)
10 mM Tris-Cl pH 8.0 (0.5 ml of 2 M stock)
150 mM NaCl (3 ml of 5M stock)
1 mM Mg-acetate (100 ml of 1M stock)
1 mM imidazole (100 ml of 1M stock)
2 mM CaCl₂ (200 ml of 1M stock)
0.1% NP40 (1 ml of 10% stock)
H₂O to 100 ml final

IPP150 Calmodulin elution buffer

10 mM β-mercaptoethanol (69.7 ml of stock)
10 mM Tris-Cl pH8.0 (0.5 ml of 2 M stock)
150 mM NaCl (3 ml of 5 M stock)
1 mM Mg-acetate (100 ml of 1 M stock)
1 mM imidazole (100 ml of 1 M stock)
2 mM EGTA (400 ml of 0.5 M stock)
0.1% NP40 (1ml of 10% stock)
H₂O to 100 ml final

2.6 Microscopy

Visual inspection of *Dictyostelium* cells expressing GFP fusion proteins was performed using an inverted fluorescence microscope (Olympus IX70). Confocal images of immunolabelled specimens were obtained with a confocal laser-scanning microscope TCS-SP (Leica) equipped with a 63x PL Fluotar 1.32 oil immersion objective. A 488-nm argon-ion laser for excitation of GFP fluorescence and a 568-nm helium-neon laser for excitation of Cy3 or TRITC fluorescence were used. For simultaneous acquisition of GFP and Cy3 fluorescence, the green and red contributions to the emission signal were acquired separately using the appropriate wavelength settings for each photomultiplier. The images from green and red channels were independently attributed with colour codes and then superimposed using the accompanying software.

2.6.1 Live cell imaging of *Dictyostelium* cells expressing GFP-RacA and GFP-RacH

To record the distribution of GFP-RacG and GFP-RacH in living cells, cells were grown to a density of $2-3 \times 10^6$ cells/ml, washed in Soerensen phosphate buffer and resuspended at a density of 1×10^7 cells/ml. The cells were then starved for about 1 h with shaking. Starvation facilitated observation as it allowed the cells to digest endocytosed nutrient medium, which is autofluorescent. For observation, cells were initially diluted in Soerensen phosphate buffer at 1×10^6 cells/ml and then 500 μ l of the cell suspension were transferred onto a 18 mm glass coverslip glued to a plastic rim of the same size. Cells were allowed to adhere to the glass coverslip for 10-15 min and confocal images were obtained and processed as described above.

2.6.2 Microscopy of fixed preparations

To visualise the actin and DAPI staining in the fixed preparations, an Olympus IX70 inverse microscope equipped with a 40X LCPlanFI 0.6 and a 10X UplanFI 0.3 objective was used. Images were captured either with a JAI CV-M10 CCD video camera or a SensiCam cooled CCD video camera.

2.6.3 Microscopy of agar plates

To determine development of *Dictyostelium* on phosphate agar plates or on SM-agar plates with *Klebsiella* lawns, an Olympus SZ-4045TR stereomicroscope was used. Images were captured with a JAI CV-M10 CCD video camera.

2.7 Video imaging and chemotaxis assay

Vegetative cells were resuspended at 1×10^7 cells/ml in Soerensen phosphate buffer and starved for 6 to 8 hours. 25-30 μ l of cell suspension were diluted in 3 ml of Sorensen buffer and mixed well by pipetting (25-30 times, with occasional vortexing). This is important to dissociate cells from aggregates. 1.5 ml of the diluted cells were then transferred onto a 5 cm glass coverslip with a plastic ring placed on an Olympus IX70 inverse microscope equipped with a 10x UplanFI 0.3 objective. Cells were stimulated with a glass capillary micropipette (Eppendorf Femtotip) filled with 0.1 mM cAMP (Gerisch and Keller., 1981), which was attached to a microcontroller. Time-lapse image series were captured and stored on a computer hard drive at 30 seconds intervals with a JAI CV-M10 CCD camera (and an Imagenation PX610 frame grabber (Imagenation Corp., Beaverton, OR) controlled through Optimas software (Optimas Corp., Bothell, Washington). The DIAS software (Soltech, Oakdale, IA) was used to trace individual cells along image series and calculate the cell motility parameters (Soll et al., 2001).

2.8 Computer analysis

Analysis of the sequences and homology searches were performed using the GCG software package (Wisconsin package) and the BLAST (NCBI) program. Protein sequences were aligned using the programs ClustalW, BioEdit and TreeView tools (available at the homepages www.bioedit.com and <http://taxonomy.zoology.gla.ac.uk/rod/treeview.html>). For prediction of motif and pattern searches several programs of the ExPaSy server (www.expasy.ch) were used. Annealing temperatures of primers were calculated with the program "Primer Calculator" available in the Internet (www.gensetoligos.com). For processing images, Corel Draw version 9, Corel Photopaint, Adobe Illustrator, Adobe Photoshop and Microsoft Power Point softwares were used. Graphs were prepared using the Microsoft Excel software.

III RESULTS

1 Functional characterisation of RacA

To study RacA function we generated a knock out (KO) strain and analysed its performance in processes depending on the re-organisation of the actin-cytoskeleton. At first, in order to dispose of a powerful tool in the search for RacA-binding partners, to prove the KO on the protein level and to reflect RacA expression levels in the development of WT cells, we generated polyclonal antibodies against RacA. This was followed by studies on a KO-strain and the search for binding partners. Finally, complementary to the KO-analysis, strains were generated overexpressing GFP-RacA fusion proteins and we started to look for localisation of the GFP-RacA fusion proteins and peculiarities of the strains.

1.1 Generation of RacA polyclonal antibody and verification of RacA expression throughout development

1.1.1 Expression of RacA C-terminal peptide for polyclonal antibody production

As the GTPase domain of RacA is quite similar to those of the other Rac proteins in *Dictyostelium* we used the RacA specific C-terminus for polyclonal antibody generation (Figure 9 and Material and Methods 2.2.6). A PCR-amplified cDNA fragment encoding RacA from the second BTB domain (B2C) onwards was cloned into the BamHI site of the bacterial protein expression vector pT7. This vector was transformed into *E. coli* strain MC1061 equipped with an additional plasmid encoding the T7 polymerase, necessary for transcription from the pT7 vector. The transfected cells were used for inoculation of LB-medium and protein expression was induced with Isopropyl β -D-thiogalactoside when the culture reached an OD of 0.6. Culturing was continued for further 3.5 h at 37°C. The cells were lysed and the lysate was split into soluble and pelleted fractions. As B2C resided in the pellet, this was separated by SDS-page, B2C was extracted out of the gel by electroelution and used for the immunisation of two rabbits. Before immunising the rabbits, the identity of the C-terminal peptide was confirmed by excising the protein band out of the SDS-gel and analysing it by MALDI.

The polyclonal antibody obtained after the third immunisation boost recognised the GFP-RacA fusion protein without showing excessive background. Recognition of GFP-RacA was confirmed with a monoclonal antibody against GFP (data not shown).

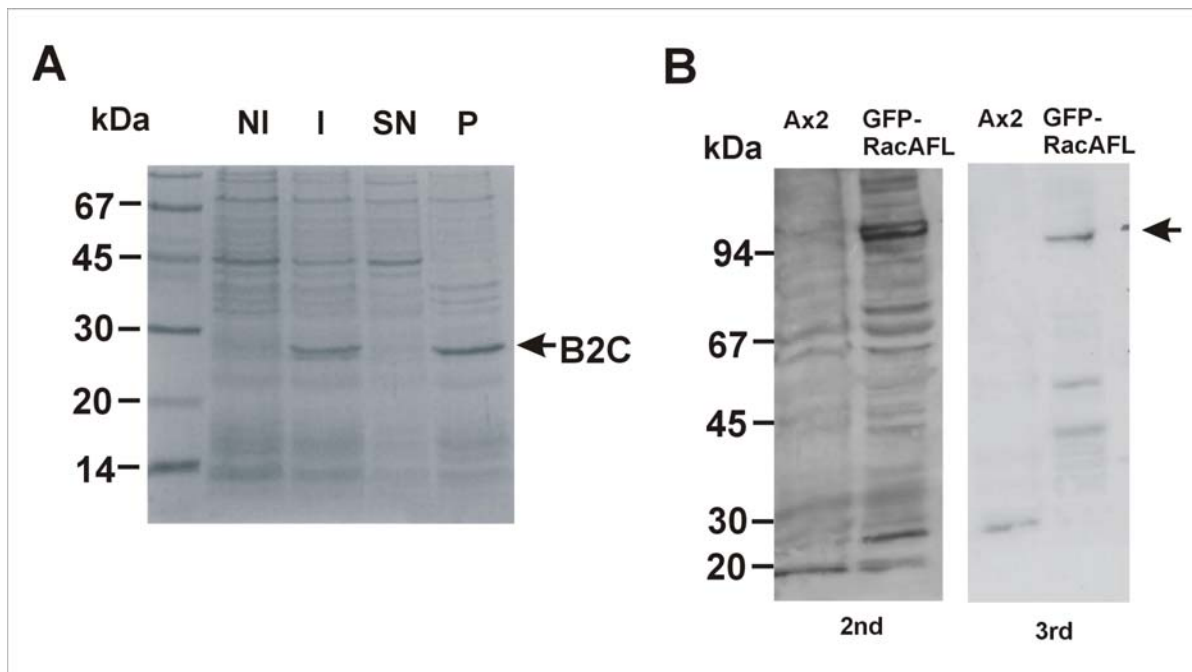


Figure 9: Expression of C-terminal RacA peptide B2C. (A) Coomassie blue stained SDS-polyacrylamide gel (12% acrylamide) showing cell lysates obtained from uninduced (NI) and induced (I) *E. coli* MC1061L cultures expressing the untagged B2C-peptide. Another portion of the induced lysate has been split by ultracentrifugation into soluble (SN) and insoluble (P) fractions. B2C resides in the pelleted membranous fraction, was electroeluted out of the SDS-gel (Materials and Methods 2.2.6) and used for rabbit immunisation. (B) After the 2nd and 3rd immunisation boost the antisera of two rabbits (only the more specific antiserum of animal 1 is shown) have been tested by comparing the lysate of GFP-RacA fusion protein expressing with wild-type cells. The arrowhead indicates the recognized GFP-RacA fusion.

The antiserum was affinity-purified as described (Materials and Methods 2.2.6). In the purified state the antibody was able to detect the endogenous 66 kDA protein on Western blots when used 1:2,500 fold diluted (Figure 14).

1.1.2 Expression of RacA throughout development

Dictyostelium cells grow vegetatively as unicellular amoebae when nutrients are available. Depletion of nutrients triggers a 24 h developmental programme leading to the formation of a multicellular fruiting body. This transition from growth phase to the developmental phase is a consequence of stage specific expression that involves activation of certain genes and repression of others. In Northern blot analysis it was demonstrated that the *racA* gene is transcribed very weakly throughout the developmental cycle of *Dictyostelium* (Rivero et al., 2001). To verify whether the constant level of *racA* transcripts is paralleled by a steady protein expression Western blot analysis of samples taken at various developmental stages (Figure 10)

revealed that RacA is expressed almost constitutively throughout the developmental cycle of *Dictyostelium*.

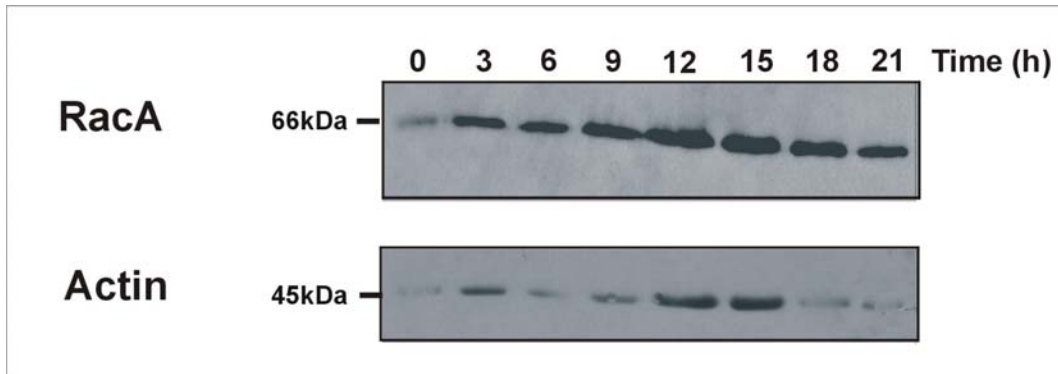


Figure 10: Expression of RacA through the developmental cycle of *Dictyostelium*. Cells were allowed to develop on nitrocellulose filters. Samples were collected at the times indicated and total cell homogenates were resolved in 12% polyacrylamide gels and blotted onto nitrocellulose membranes. Blots were incubated with polyclonal antiserum specific for RacA (1:2,500 dilution) and with mAb Act1-7 specific for actin as a control for loading.

1.2 Generation and functional analysis of a RacA deficient strain

1.2.1 Generation of a RacA deficient strain

To define the function of RacA, we attempted to generate mutants that lack the protein. Two genomic sequences were used for the construction of the targeting vector (Figure 11). The sequences were fused together such that 200 bp of the first BTB domain were removed. The blasticidin-resistance-cassette (bsr) was inserted in the *Cl*I site resident in the first BTB domain (B1). Since this construct still allowed the transcription of an mRNA encompassing the GTPase domain, a frameshift has been introduced by deleting the *Pst*I restriction site at the base pair position 172 of the coding region. *Dictyostelium* cells were transformed with the linearised targeting vector, spread on several Petri dishes and blasticidin selection was applied until single colonies became apparent. The blasticidin resistant transformants were subcloned in 96 well plates in Ax2 medium containing blasticidin or grown in replica on a bacterial lawn.

1.2.2 Screening for a RacA deficient strain

In order to analyse a large number of clones in a fast procedure, so that we could reduce the number of candidates to be further tested, a negative PCR-screen was carried out. In this screen

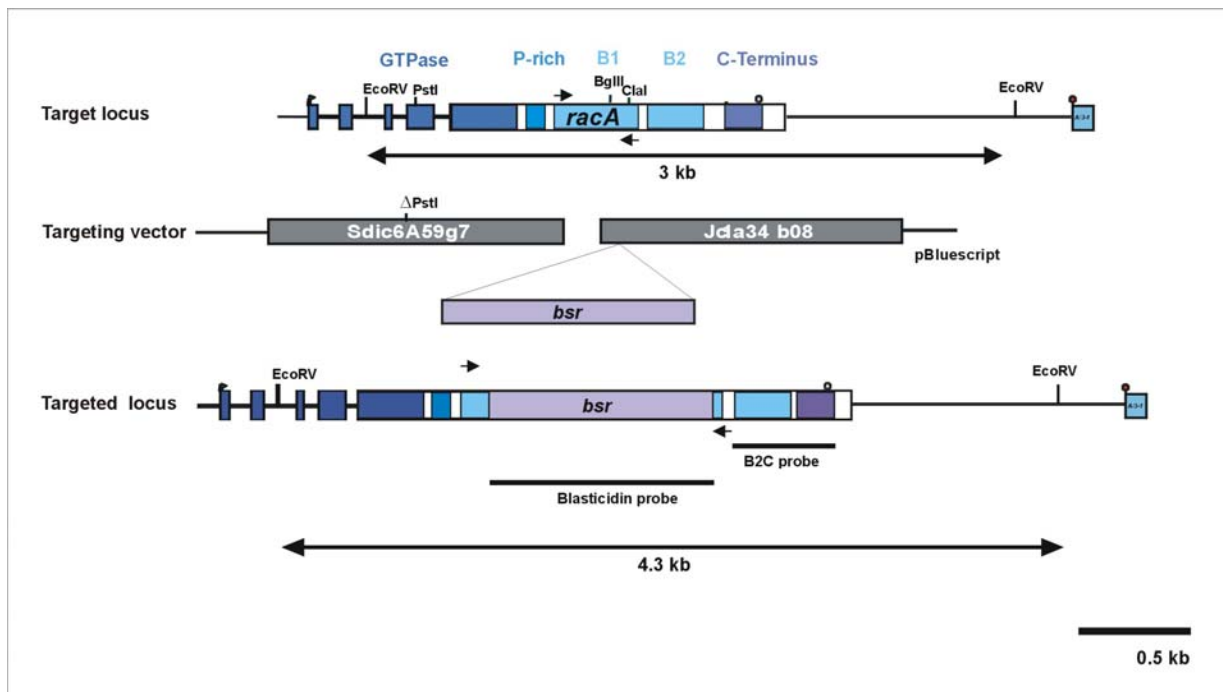


Figure 11: Disruption of the *racA* gene. The RacA knock out has been generated using a targeting vector consisting out of two genomic sequences fused together sparing out 200 bp of B1 domain encoding sequence. The blasticidin selection cassette (*bsr*) has been inserted in the endogenous *ClaI* site. Additionally, a frameshift has been created by removing the endogeneous *PstI* site. Primers used for the first two rounds of screen by PCR (see Figure 12) flanking the B1 domain are shown. The probes utilised for Southern blotting are indicated. The deletion of part of the coding region and the insertion of the *bsr* cassette brought about a shift of the encoding 3 kb band to a 4.3 kb band after digestion with *EcoRV* (see Figure 12C).

KO candidates should be detected by lack of a PCR-product. More than 900 clones were examined in this negative PCR screen using B1-flanking primers (Figure 12 A). For this, genomic DNA of the clones was gained by a fast method (Materials and Methods 2.2.4). The DNA quality just allowed a negative screen solely allowing amplification of short PCR products. Thus the negative screen aimed to exclude WT-clones that gave rise to the 500 bp B1-product from further steps of analysis. Forty potential knock out clones were further analysed by positive PCR. To this end high quality genomic DNA was purified (Materials and Methods 2.2.3). Due to *bsr* insertion PCR with the B1-flanking primers yield a 1.8 kb long product (Figure 12 B). Twenty clones passed the second screening and were further analysed by Southern blotting (Figure 12 C). Genomic DNA of wild type and transformants was digested with *EcoRV*. The digested DNA was resolved on an agarose gel, transferred onto a nylon membrane and the blot was probed with two different ^{32}P labelled probes, one complementary to the second BTB domain and the following C-terminus, the other hybridized to the *bsr*-sequence. We selected three independent clones (#20, #40 and #69) where a gene replacement event has occurred at the *racA* locus.

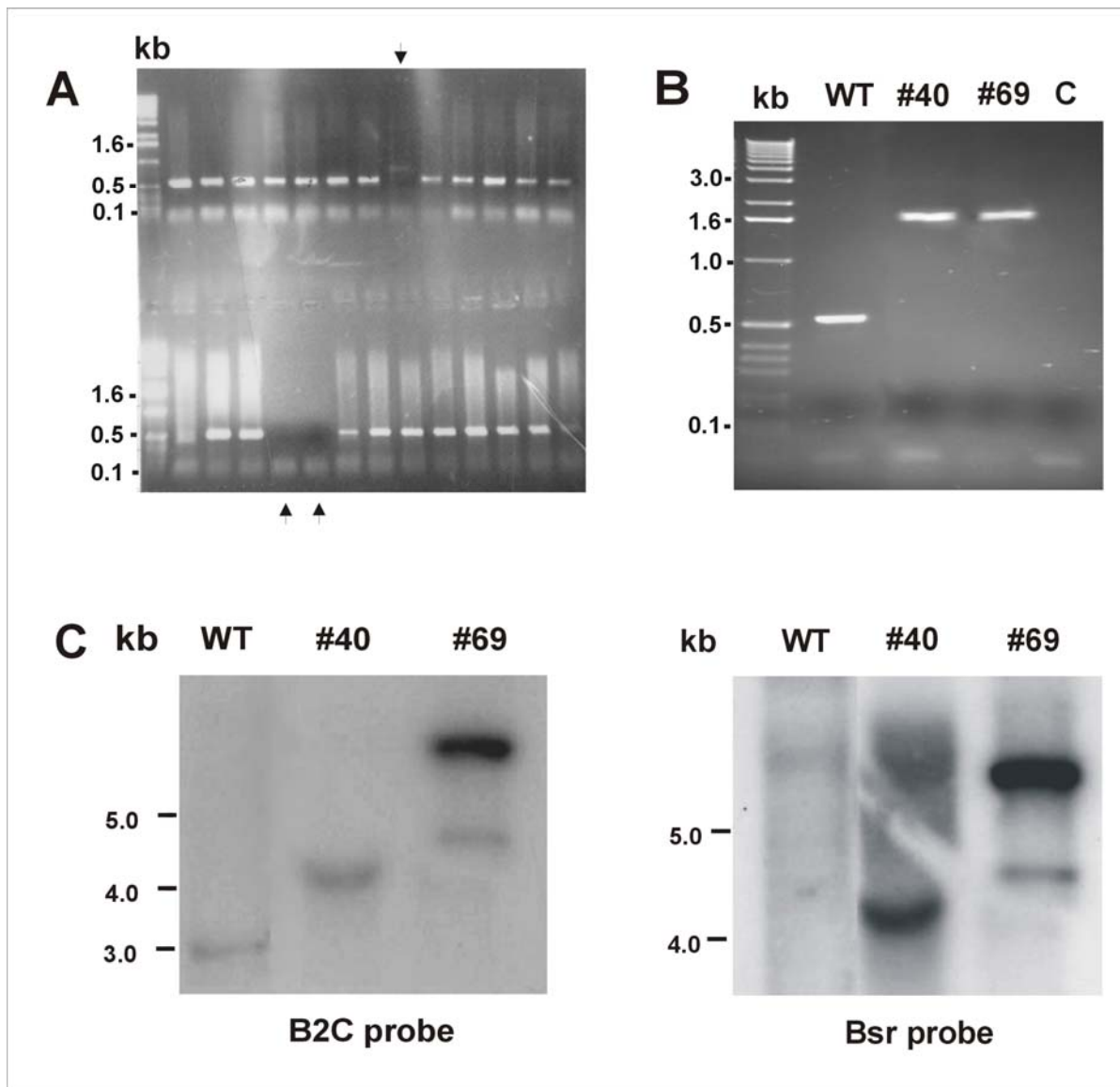


Figure 12: RacA-KO screening. The number of potential knock out clones was reduced by performing a large-scale negative PCR screen (A). For this, primers flanking the B1 sequence were used (see Figure 11). Clones that did not give rise to the 500 bp endogenous band (indicated by arrowheads) have been further analysed. (B) PCR-screening with highly purified genomic DNA and (C) Southern Blot analysis followed. For the Southern blotting genomic DNA was digested with EcoRV and the probes presented in Figure 11 were used. RacA-KO-clones #40 and #69 yield a 1.8 kb PCR-product indicating the insertion of the *bsr* into B1. RacA-KO clone #40 was confirmed by Southern blotting as it displays a 4.3 kb band whereas WT clones show a 3.0 kb. The *racA* gene of clone #69 seems to be disrupted as well. A band of higher molecular weight indicates multiple integration of the targeting vector.

Proper homologous recombination took place in clone #20 and #40. Both clones (only #40 is shown in Figure 12 C) showed the 4.3 kb band enlarged by insertion of the *bsr*-cassette in contrast to the 3.0 kb band of the WT. In clone #69 multiple integration of the targeting vector took place as indicated by a large and intense band.

1.2.3 *racA* transcript is still synthesised

The insertion of the *bsr*-cassette with its termination sequence into the *racA* locus might have caused transcriptional termination and degradation of the *racA* mRNA. Therefore we tested the KO clones, #20 and #40 used for the knock out studies, for the presence or absence of the *racA* transcript – thus in the absence of the transcript another means to confirm the KO or in its presence raising the demand for final Western blot-confirmation at the protein level.

RT-PCR (Figure 13) revealed that the clones still synthesised the *racA* mRNA transcript. In the KO clones every domain with the exception of the B1-domain gave rise to a product of the expected length. The WT control yielded a 500 bp with the B1 flanking primers thus confirming that the lack of product in the RacA deficient clones is due to insertion of the *bsr*-cassette.

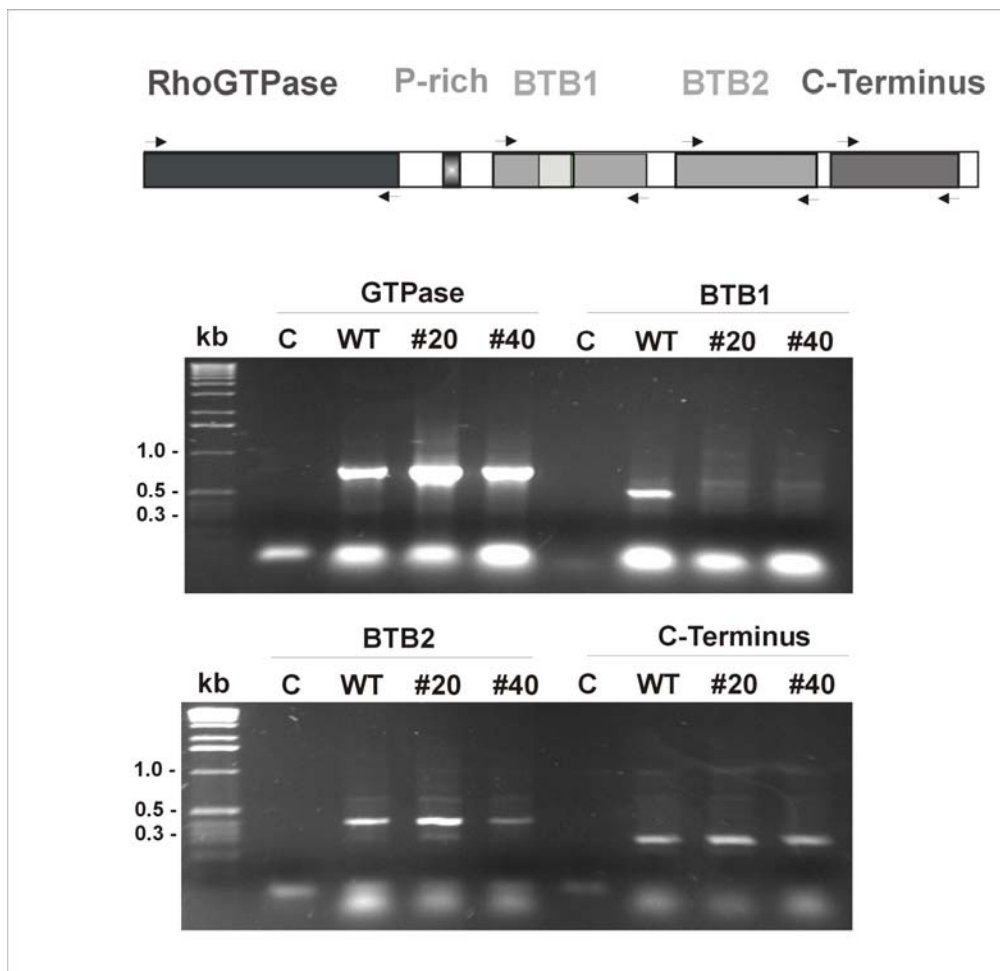


Figure13: RT-PCR analysis of the RacA-KO strains. Total RNA of the RacA-KO strains was isolated as described in Materials and Methods 2.2.5. The primers used for RT-PCR analysis are indicated in the upper pannel. RT-PCR of the two KO-clones #20 and #40 demonstrates that the *racA* transcript is still synthesised. Only the B1-RT-reaction does not give rise to a product. This was assumed as in KO-clones the B1 domain should harbour the selection cassette and the RT-PCR conditions just allowed amplification to products below 1 kb.

1.2.4 Confirmation of RacA knock out by Western blot

The absence of the RacA protein was finally verified by immunoblot analysis using the RacA affinity-purified polyclonal antiserum (Figure 14). Total cell homogenates of WT, GFP-RacA-overexpressors, RacA deficient cells and RacA deficient cells expressing the GFP-RacA fusion protein (Rescue) were analysed.

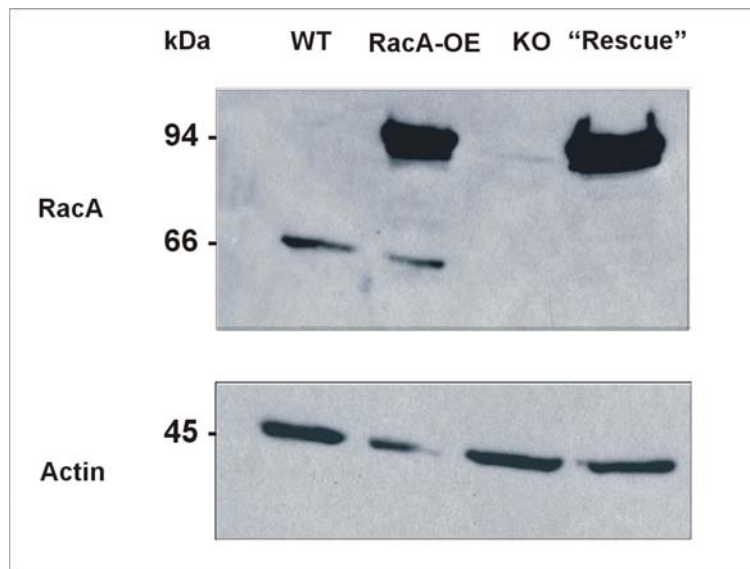


Figure14: Confirmation of the RacA-knock out on the protein level. Total cell homogenates of 4×10^5 cells were resolved in polyacrylamide gels and blotted onto nitrocellulose membranes. AX2, RacA-KO, GFP-tagged RacA overexpressor and a KO-strain expressing GFP-RacA ("Rescue") were analysed. The blot was incubated with the polyclonal antiserum specific for RacA (1:2,500 dilution) and mAb Act 1-7 for labelling of actin as loading control.

The antibody recognised the 66 kDa endogenous RacA protein in WT and GFP-RacA-overexpressors. This band was absent in RacA-KO and Rescue cells. As expected, a band of 97 kDa corresponding to the GFP-RacA fusion protein appeared in the overexpressor and Rescue.

1.2.5 Characterisation of the RacA deficient strain

1.2.5.1 Growth in axenic medium

Since cell growth is a result of the interplay between many cellular processes involving rearrangements of the actin cytoskeleton, the growth rate of RacA-KO was compared with that of the WT. Growth curves were determined under standard conditions (shaking at 160 rpm and 21°C) with starting cell densities of 2×10^5 cells/ml. WT cells attained maximum cell densities of 13×10^6 cells/ml. RacA-KO cells had a severe growth defect. They were just able to grow to a

density slightly over 1×10^6 cells/ml (Figure 15 A). We looked whether this growth defect can be compensated by re-expression of RacA. This was partly the case as rescue cells showed intermediate growth rates reaching a cell density of 8×10^6 cells/ml with a doubling rate of 26.4 h vs. 14.5 h of Ax2.

The growth defect of RacA-KO cells was abrogated when grown attached to a surface showing that the defect is conditional. In order to obtain the amount of cells needed for the KO assays we cultured the RacA deficient as well as the WT control and the Rescue cells on Petri dishes and resuspended them prior to the experiments.

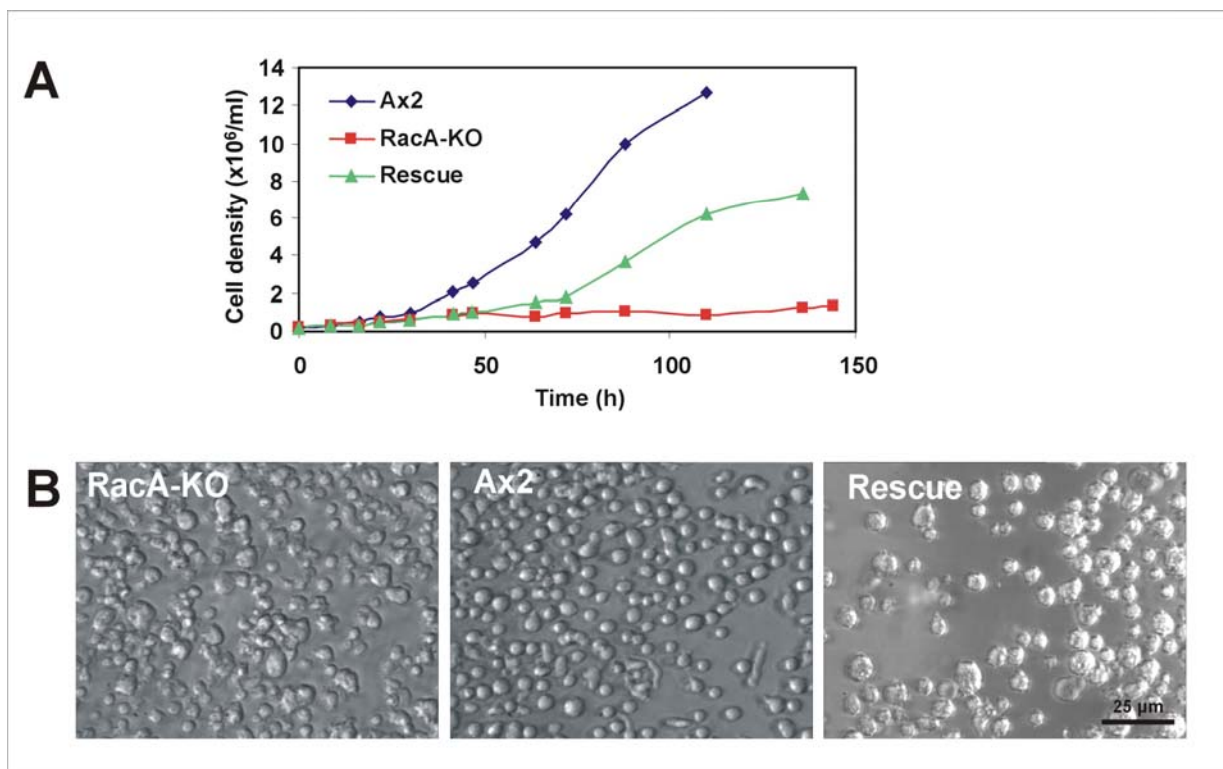


Figure 15: Growth of RacA-KO and “Rescue” cells in axenic medium. Cultures were inoculated at 2×10^5 cells/ml and grown at 21°C with shaking at 160 rpm. Cells were counted at the indicated time points. Growth is impaired in the RacA-KO cells. The “Rescue” is partially impaired in growth. The data are the average of three independent experiments. (B) Cell morphology of the respective cells grown in suspension. Cells were resuspended in Soerensen phosphate buffer containing 20 mM EDTA. The cell size of RacA-KO cells is very inhomogeneous and cells do not round up as extensively as WT and Rescue cells do.

Then we had a closer look at the cell morphology of RacA-KO and Rescue cells grown in suspension (Figure 15 B). In order to be able to compare the cell size of the respective strains, we made the cells round up by exposing them to EDTA. For this the cells were resuspended in Soerensen phosphate buffer containing 20 mM EDTA. The RacA-KO cells were very inhomogeneous in size. Their surface appeared very “rough” in comparison to WT cells and they

did not round up as the Ax2 cells did. Morphology of rescue cells resembled more the WT than the KO cells. They were more similar in size and their surface seemed to be smoother although not as plain as WT cells.

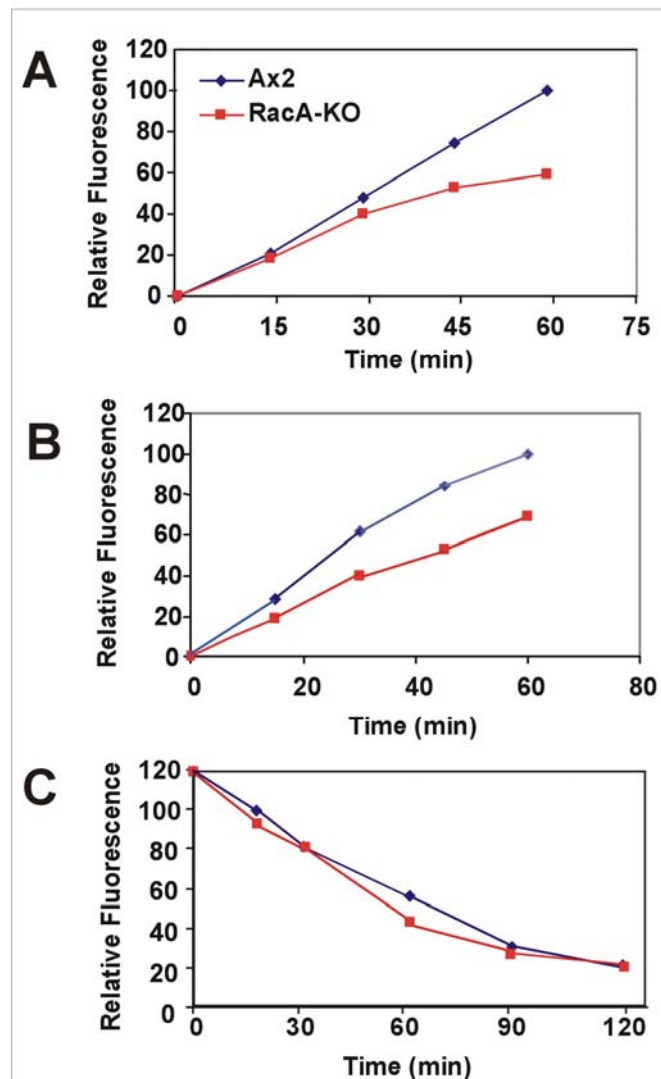


Figure 16: Phagocytosis, fluid-phase uptake and exocytosis of the RacA-KO strain. (A) Phagocytosis of TRITC-labelled yeast cells. *Dictyostelium* cells were resuspended at 2×10^6 cells/ml in fresh axenic medium and challenged with fivefold excess fluorescent yeast cells. Fluorescence from internalised yeasts was measured at the designated time points. (B) Fluid-phase endocytosis of FITC-dextran. Cells were resuspended in fresh axenic medium at 5×10^6 cells/ml in the presence of 2 mg/ml FITC-dextran. Fluorescence from the internalised marker was measured at selected time points. (C) Fluid-phase exocytosis of FITC-dextran. Cells were pulsed with FITC-dextran (2 mg/ml) for 2 hours, washed, and resuspended in fresh axenic medium. Fluorescence from the marker remaining in the cells was measured. Data are presented as relative fluorescence, Ax2 being considered 100%. All values are the average of at least three independent experiments. For the sake of clarity, error bars are not shown.

1.2.5.2 Endo- and exocytosis

Rho GTPases participate in the regulation of endocytic and exocytic pathways (Qualmann and Mellor, 2003) through remodelling of the actin cytoskeleton. Therefore we examined the ability of RacA-KO cells to internalise fluorescently labelled yeast particles (Figure 16 A) and the fluid phase endocytosis marker FITC-dextran (Figure 16 B). Furthermore the exocytosis capacity of RacA-KO cells was examined using FITC-dextran (Figure 16 C). In comparison to the WT, RacA-KO cells performed in phago- as well as in pinocytosis slightly worse, reaching approximately 60% and 70%, respectively, of the WT-level. RacA-KO cells exocytosed FITC-dextran at the same rate as WT cells.

1.2.5.3 Cytokinesis and F-actin organisation of RacA-KO cells

As Rho GTPases are reportedly involved in the regulation of cytokinesis (Laroche 1996; Dumontier et al., 2000) we investigated whether RacA has an impact on cell division. We analysed cells grown attached to a surface and under shaking conditions after staining. We fixed and stained the cells as described (Materials and Methods 2.4.3.2-6) and counted the number of nuclei per cell. When grown attached to a surface, RacA-KO cells showed a cytokinesis

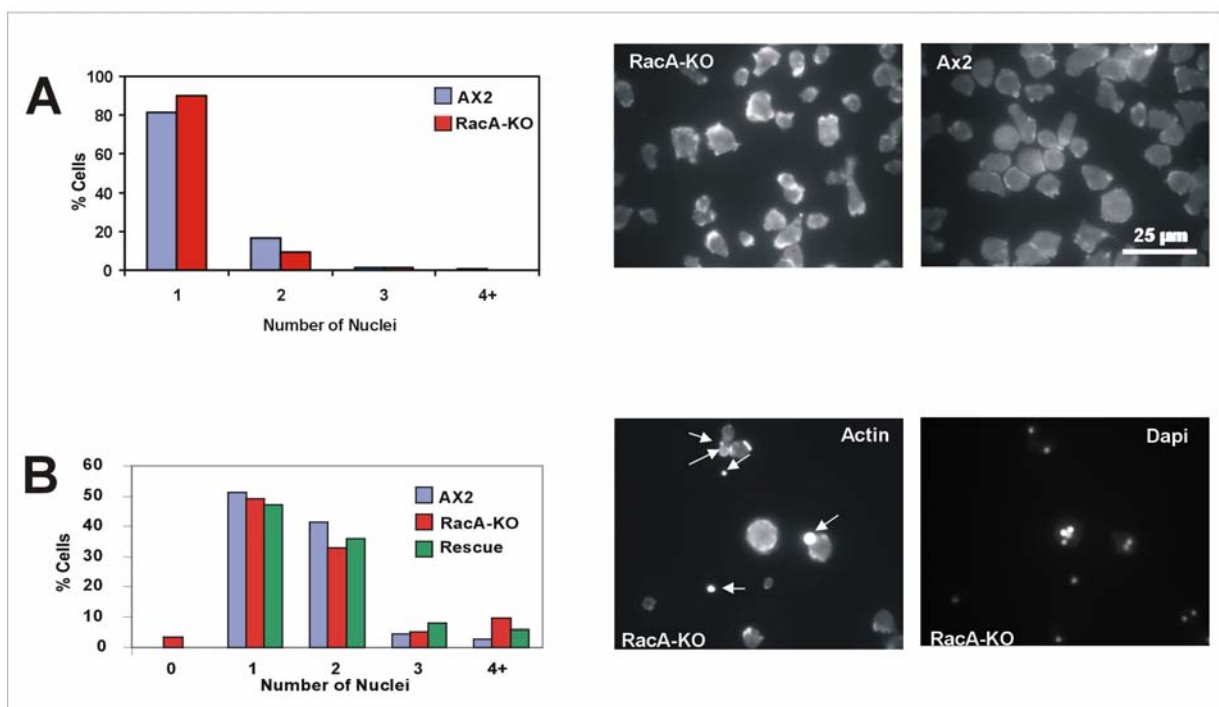


Figure 17 (previous page): Quantification of nuclei of RacA-KO and RacA-overexpressing RacA-KO/“Rescue” cells. Fluorescence images after DAPI staining of the nuclei of the AX2 and RacA-mutant cells grown on coverslip (A) and in suspension (B). Cells were allowed to sit for 20 min on coverslips or were grown on coverslips for two days. Cells were fixed with picric acid/paraformaldehyde and stained with actin-specific mAb Act 1-7 followed by Cy3-labelled anti-mouse IgG. For all strains, nuclei of 250-300 cells were counted. When grown on coverslips WT and RacA-KO cells are quite alike. When grown in suspension wild-type AX2 cells are mainly mononucleated or binucleated, whereas RacA-KO shows a higher percentage of cells possessing 4 or more nuclei. In particular RacA-KO cells exhibit many cellular fragments that do not contain a nucleus when grown in suspension (arrowheads).

behaviour as WT cells. Under these circumstances the general cell morphology and F-actin organisation resembled the WT although F-actin seemed to be particularly accumulated at some foci in the cells (Figure 17 A). By contrast, when cultured in suspension the cytokinesis behaviour of RacA-KO slightly diverged from the mainly mono- or binucleated Ax2 cells. More than 10% of RacA-KO cells possessed 4 or more nuclei in comparison to 2% of WT cells. In particular RacA-KO cells exhibit many cellular fragments (on average 1 particle in a field of 20 cells) devoid of a nucleus. Additionally we observed that F-actin does not form a circle surrounding RacA-KO cells as present in almost every WT cell. We verified whether the defect in cytokinesis (Figure 17 B) and the unusual F-actin pattern (Figure 18) is due to RacA ablation by studying performance in cytokinesis and morphology of the Rescue cells. The percentage of Rescue cells possessing 4 or more nuclei lies between that of KO and WT. As WT cells, Rescue cells do not exhibit nuclei-free cellular fragments and resembled Ax2 cells exhibiting F-actin circles at the cell periphery.

1.2.5.4 Chemotaxis and F-actin polymerisation responses upon cAMP stimulation

Stimulation with cAMP elicits fast and highly transient changes in the F-actin content that allow the aggregation competent cells move towards the cAMP gradient (Hall et al., 1988). As Rho-regulated signalling pathways have been shown to be involved in this process (Weeks 2004; Rivero et al., 2002) we tested whether RacA is involved in the F-actin polymerisation response and chemotactical movement. In the test RacA-KO behaved as WT cells (Figure 19). When stimulated with cAMP both cell types showed a rapid and transient 1.5-fold increase in the amount of F-actin followed immediately by a second much lower peak that lasted until approximately 60 seconds.

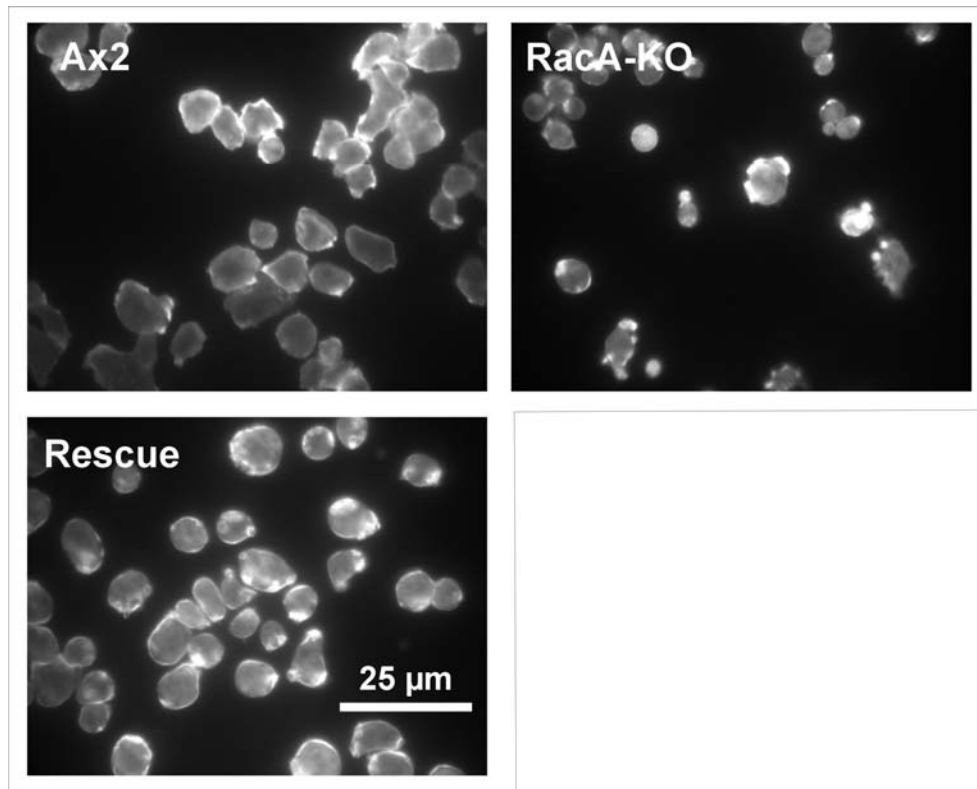


Figure 18: F-actin organisation of RacA-KO cells. Suspension culture cells were allowed to sit for 20 min on coverslips. Cells were fixed with picric acid/paraformaldehyde and stained with actin-specific mAb Act 1-7 followed by Cy3-labelled anti-mouse IgG. RacA-KO cells did not possess an F-actin circle around the cell periphery but rather contained concentrated F-actin aggregates. Rescue cells resembled Ax2 cells showing in most cells an F-actin cortex at the cell periphery.

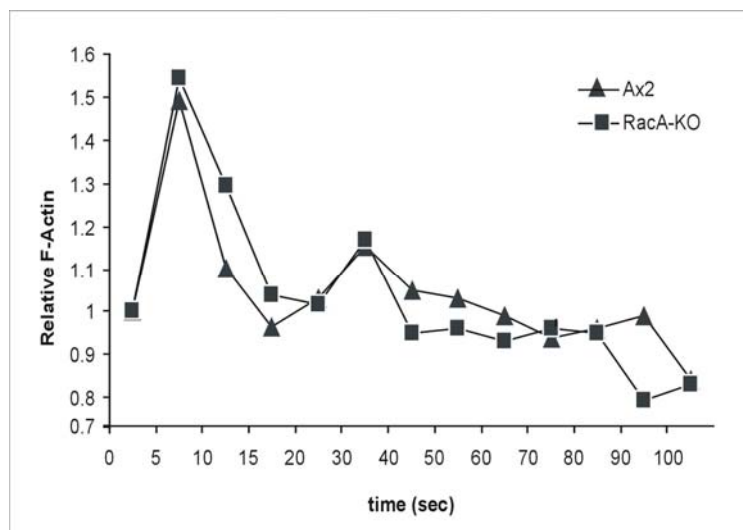


Figure 19: F-actin polymerisation responses upon cAMP stimulation of aggregation competent cells. The relative F-actin content was determined by TRITC-phalloidin staining of cells fixed at the indicated time points after stimulation with 1 μ M cAMP. The amount of F-actin was normalised relative to the F-actin level of unstimulated wild-type cells.

Next, we looked at the parameters of movement, at its speed, persistence and directionality. We performed a chemotaxis assay combined with time-lapse video microscopy (Materials and Methods 2.7). Aggregation competent cells were allowed to migrate towards a micropipette filled with 0.1 mM cAMP and time-lapse image series were taken and used to generate migration paths and calculate cell motility parameters (Figure 20 and Table 1). In the absence of cAMP the chemotactical parameters of AX2 and RacA-KO strain were almost alike. In the presence of cAMP RacA-KO cells moved moderately but significantly slower than WT cells (7.53 vs. 10.51 $\mu\text{m}/\text{min}$). Otherwise, as the path illustration shows (Figure 20), RacA-KO cells became polarised, formed streams and migrated toward the tip of the micropipette almost as WT cells. Though the angle of their directional changes was strikingly higher than the one of the WT (42.01 vs. 33.05). As the value of persistence was also lower (2.34 and 3.05 $\mu\text{m}/\text{min-deg}$) this lead in total to a significantly lower directionality (0.52 vs. 0.61).

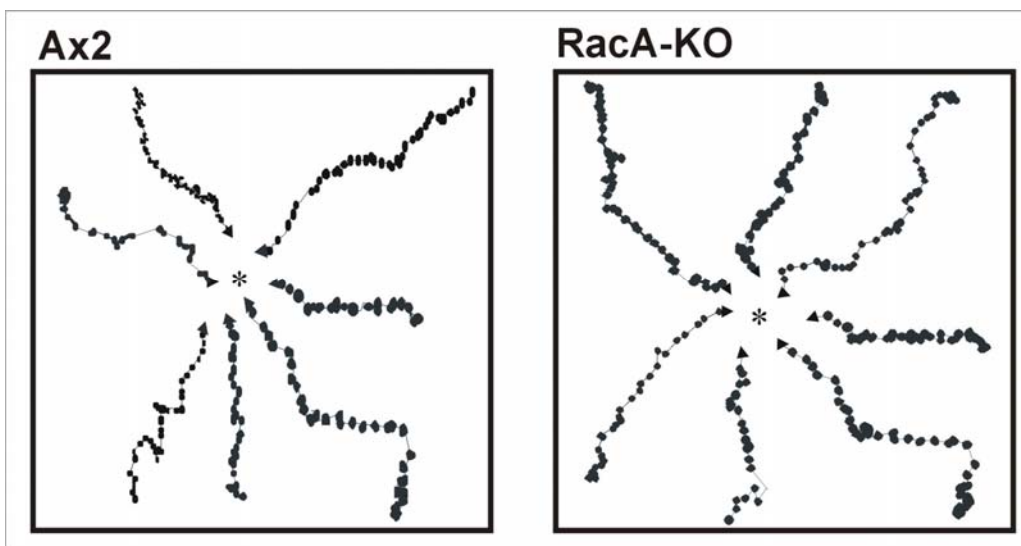


Figure 20: Chemotactic movement of RacA-KO cells. Cells were starved for 6 hours, allowed to sit on a glass coverslip and stimulated with a micropipette filled with 0.1 mM cAMP. Images of chemotaxing cells were captured every 30 seconds. Cell movement was analysed with the DIAS software. RacA-KO strain behaved almost like Ax2.

Table 1: Analysis of cell motility of the RacA-KO strain

	Ax2	RacA-KO
Buffer		
Speed (um/min)	5.23 ± 3.26	5.46 ± 2.79
Directionality - Total	0.28 ± 0.13	0.33 ± 0.12
Direction Change (deg)	57.60 ± 7.60	57.45 ± 11.56
Persistence (um/min-deg)	0.91 ± 0.77	1.44 ± 0.72
cAMP		
Speed (um/min)	10.51 ± 1.92	7.53 ± 4.62*
Directionality - Total	0.61 ± 0.03	0.52 ± 0.12*
Direction Change (deg)	33.05 ± 6.69	42.01 ± 12.08
Persistence (um/min-deg)	3.06 ± 1.46	2.34 ± 1.08*

Time-lapse image series were captured and stored on a computer hard drive at 30 seconds intervals. The DIAS software was used to trace individual cells along image series and calculate motility parameters. Objects whose speed was $<2 \mu\text{m}/\text{min}$ were excluded from the analysis. Persistence is an estimation of movement in the direction of the path. Directionality is calculated as the net path length divided by the total path length, and gives 1.0 for a straight path. Directional change represents the average change of angle between frames in the direction of movement. Values are mean \pm standard deviation of 60 to 140 cells from at least three independent experiments. * $P < 0.05$ relative to AX2 in the same condition (Student's t test)

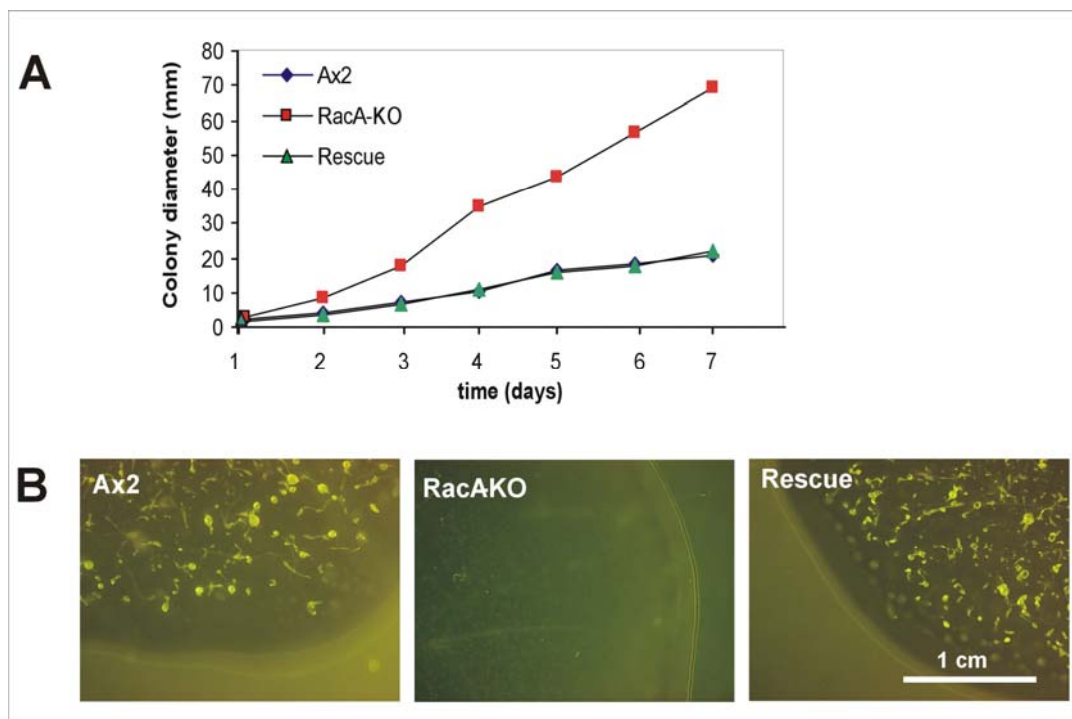


Figure 21: Development on bacterial lawn. Cells were plated on nutrient agar in the presence of *K. aerogenes* and allowed to develop at 21°C. (A) The diameter of the colonies has been measured at the indicated time points. (B) Colonies of the WT, RacA-KO and the “Rescue” strain are depicted. WT and “Rescue” colonies look alike. The size of the central colony region of RacA-KO strain comprising fully developed aggregates corresponds to those of the WT and “Rescue”. This core region was surrounded by a large rim of single amoebae. Due to this rim the colony diameter of RacA-KO in (A) was that large.

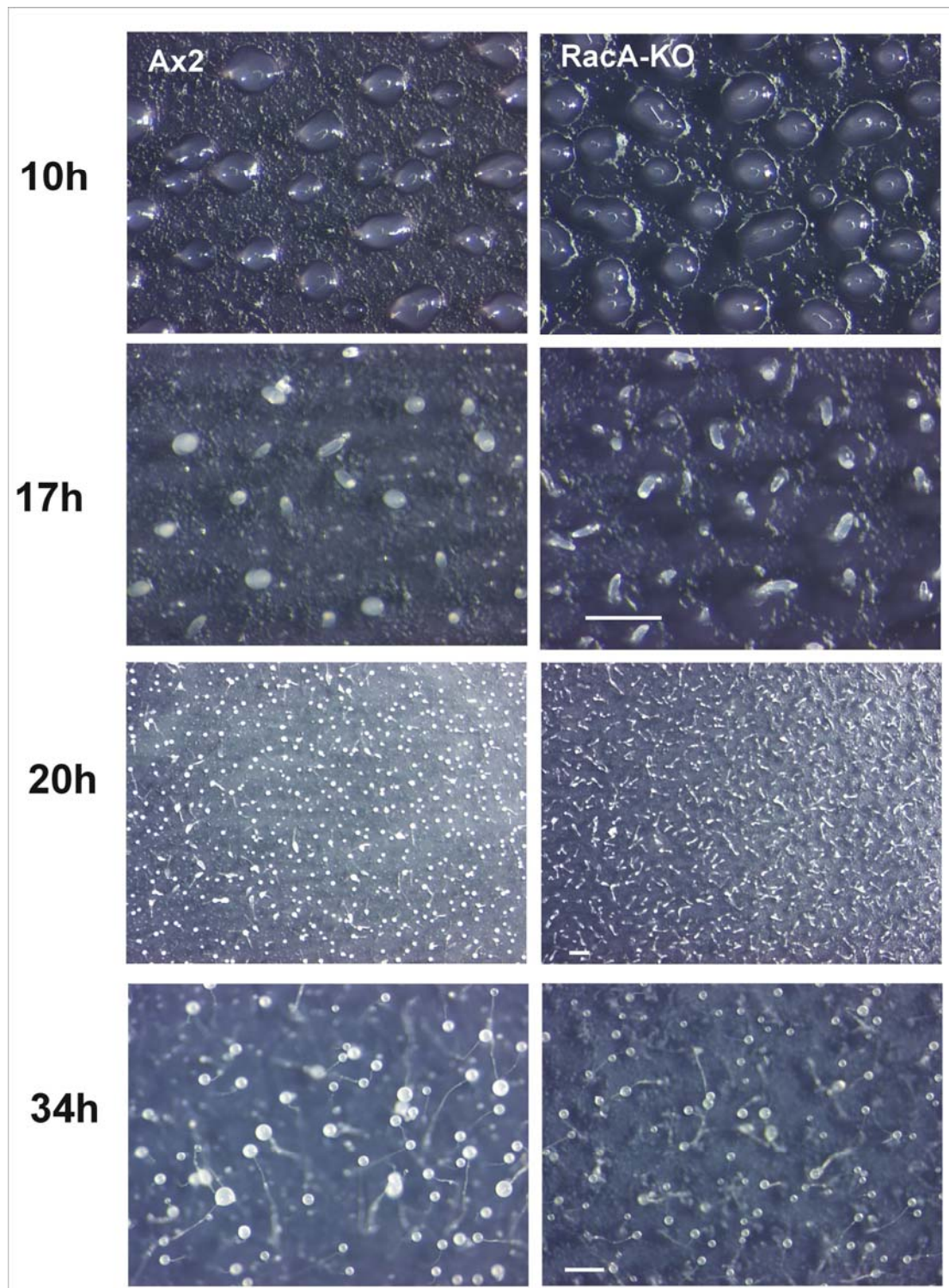


Figure 22: Development of cells lacking RacA. Cells were starved at a cell density of 5×10^7 cells/plate on phosphate agar plates and images were taken at the indicated time points using a stereomicroscope. RacA-KO cells show the same developmental behaviour as AX2 cells at post-aggregation stages. Bar, 1mm.

1.2.5.5 RacA deficient cells spread faster on bacterial lawn

We also tested growth of AX2 and RacA-KO cells on SM agar plates in the presence of *Klebsiella aerogenes* as their food source. The cells were inoculated in the centre of SM agar plates previously overlaid with *Klebsiella aerogenes*. The increase in the colony diameter was taken as a relative measure of growth (Figure 21 A). The RacA-KO cells spread very fast on the bacterial lawn showing growth rates twice of the WT. The plaque diameter of rescue cells corresponds to the WT. The size of the central colony region of all three strains is similar and comprises fully developed aggregates. What makes the difference in the colony diameter is a large rim of single amoebae surrounding the core region.

1.2.5.6 Development of RacA deficient cells

Deprived of nutrients, *Dictyostelium discoideum* undergoes a developmental program that lasts about 24 h and starts with the formation of aggregates that undergo morphological changes before culminating into a fruiting body. The developmental timing and performance of RacA-KO cells resembled the WT (Figure 22). Both strains formed tight aggregates after 10 h of starvation followed by formation of finger like structures after 17 h, which then become fruiting bodies by a culmination process after 20-24 h of starvation.

The only difference in the development was that the aggregate territories (the region encompassing cells that stream to its middle) of RacA-KO were smaller than those of the WT and Rescue (Figure 23) although the size of the fruiting bodies was not notably smaller.

1.2.6 Identification of potential binding partners of RacA

In order to detect RacA binding partners, we first used the tandem affinity purification approach but failed in this effort. So we continued with conventional immunoprecipitation. Additionally, suspecting the binding of RacA by cullins, this was assayed by means of the yeast-two-hybrid system.

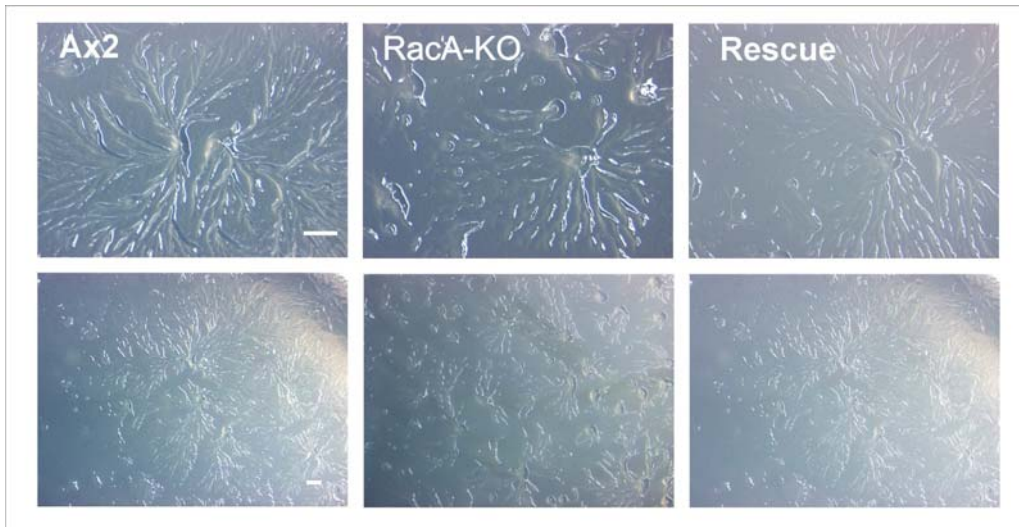


Figure 23: Aggregation of RacA mutants on phosphate agar plates. Cells were starved at a cell density of 5×10^7 cells/plate on phosphate agar plates and images were taken at the indicated time points using a stereomicroscope. After 4 hours of starvation cells start to aggregate. The aggregation territories of RacA-KO cells are notably larger than the ones of WT cells. The aggregation area of the “Rescue” resembles the ones of the WT. Bar, 1mm.

1.2.6.1 Tandem affinity purification

In order to purify RacA under mild conditions, thus allowing to additionally obtain its interaction partners, we used the TAP-method. GFP-RacA was N-terminally fused to an epitope consisting of two tags separated by a protease cleavage site (Materials and Methods 2.5.1 and Figure 8). Although we repeated the TAP purification several times and modified many parameters, such as salt concentration, the amount of NP40, the duration and temperature of the TEV cleavage step, different approaches to concentrate the eluate and finally to stain the gel, we never obtained a protein band additional to the one of GFP- RacA. The method has been successfully utilised in *Dictyostelium discoideum* to purify the Arp2/3 complex but turned out not to be promising in any other application (P. Schaap, personal communication).

1.2.6.2 Immunoprecipitation of RacA

Alternatively to the TAP approach we performed immunoprecipitations (IPs) (Materials and Methods 2.2.7) using the affinity purified polyclonal anti-RacA antibody. The immunoprecipitated protein samples were resolved by SDS-PAGE, the gel subsequently Coomassie-stained (Figure 24) and the protein bands dissected from the gels in order to be analysed by MALDI-mass spectroscopy. The proteins of two independent IPs identified by MALDI-MS and exhibiting a

significant score above 50 are listed in Table 2. As expected, in both IPs we found RacA itself. In both IPs besides RacA we only could detect one protein: an uncharacterised, 172 kDa protein with a Dead-like-helicase domain. Two significant candidates for RacA-binding partners are a 86,9 kDa uncharacterised protein containing a BTB domain and additional KELCH domains and a protein involved in ubiquitin-dependent protein catabolism that contains a ubiquitin carboxyl-terminal hydrolase (UCH) domain.

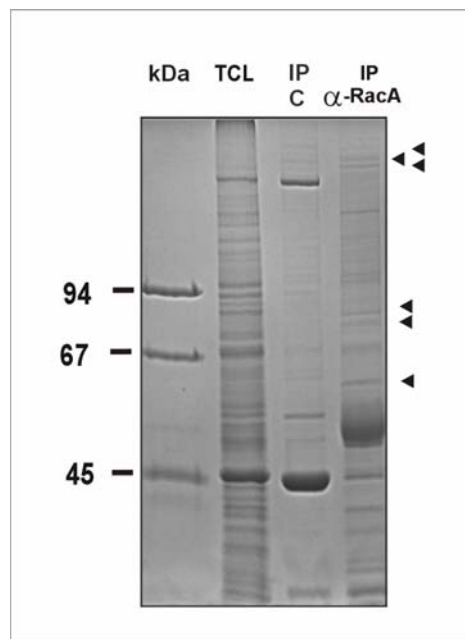


Figure 24: Immunoprecipitation with the polyclonal α -RacA antibody. Immunoprecipitation was performed as described in Materials and Methods 2.2.7. In the control-IP (C) addition of α -RacA antibody has been omitted. Bands (marked by arrowheads) of the α -RacA-IP that were not present in the control and appeared stronger in comparison to the total cell lysate were analysed by MALDI-MS.

1.2.6.3 Identification of *Dictyostelium discoideum* cullins

As binding of BTB proteins to cullins (Geyer et al., 2003; Pintard et al., 2003) and in particular of mammalian RhoBTB 2 to cullin 3 (Wilkins et al., 2004) was reported, we tested whether the *Dictyostelium discoideum* RhoBTB-homologue RacA also interacts with cullins.

We identified 5 cullins when searching the *Dictyostelium* genome database using the known amino acid sequences of the *Homo sapiens* cullin set (Table 3). Two of the *Dictyostelium* matches were already characterised as cullins and designated Cul A and Cul B. The three additional cullins we simply called Cul III, Cul IV and Cul V reflecting the order of their identification.

Table2: Potential RacA interaction partners revealed by immunoprecipitation followed by MALDI-analysis

Gene Name, Dicty Base ID	DDB0217656	gtr2, DDB0169506	DDB0217480	DDB0205392	DDB0205031	gluS, DDB0231321	hspE, DDB0185047
Protein	uncharacterized	starch synthase-like protein	uncharacterized**	uncharacterized	uncharacterized	Glutamate-tRNA ligase	Hsp70 protein
Genome Position (Chromosome, locus)	2, 5413156 to 5422669	2, 6269013 to 6276434	2, 3863067 to 3867838	3, 725541 to 728648	3, 637282 to 639630	5, 296841 to 299227	2, 2827228 to 2829126
# Amino Acids, MW (kDa)	2991; 343	2473; 275	1487;172	996, 114	782; 86,9	764; 85.6	632; 69.8
Score, Peptide Matches	100, 32	136, 26	106 and 117, 22 and 24	121, 25	89, 17	86, 15	73, 12
Characteristic Domains	Ubiquitin carboxyl-terminal hydrolase (UCH)	α amylase catalytic domain	DEAD-like helicase, 5e-04	none	K+ channel tetramerisation /BTB domain, KELCH	tRNA synthetases class I	Hsp70 protein
Molecular Function	ubiquitin thiolesterase activity	α mannosidase activity	unknown	unknown	voltage-gated potassium channel activity	glutamate- tRNA ligase activity	cysteine-type endopeptidase
Biological Process	ubiquitin-dependent protein catabolism	carbohydrate metabolism	unknown	unknown	potassium ion transport	glutamyl-tRNA aminoacylation	proteolysis
Blast, e value*	ubiquitin specific protease 34 (Hs), 1e-83	no characterized homologues	unknown	actin binding protein(Dd), 2e-10	PRED: similar to actinfilin (Dr), 9e-23		
Gene Name, Dicty Base ID	DDB0192211	DDB0185867	rpI3, DDB0191094	rpI4, DDB0218032	elf2alpha, DDB0229412	smlA, DDB0191525	DDB0187793
Protein	uncharacterized	uncharacterized	60S ribosomal protein L3	60S ribosomal protein L4	elf2A	Phenotype KO: small aggregates	uncharacterized
Genome Position (Chromosome, locus)	6, 3523472 to 3525259	4, 1620371 to 1621940	6, 944011 to 94226	2, 8414158 to 8415373	2, 931678 to 933132	5, 459691 to 460542	5, 1124804 to 1126249
# Amino Acids, MW (kDa)	595; 70,7	409; 46.8	398; 45,3	369; 40,3	341; 39,6	283; 33,3	265; 29
Score, Peptide Matches	91, 13	51, 8	133, 17	162, 15	50, 5	196, 15	148, 16
Characteristic Domains	DUF1 ⁰ 43, 2e-13	none	Ribosomal protein L3	Ribosomal protein L4/L1	Euk translation initiation factor 2 α	none	Hyaluronan / mRNA binding family
Molecular Function	unknown	unknown	RNA binding, ribosomal component	oxidoreductase activity	translation initiation factor activity	unknown	unknown
Biological Process	unknown	unknown	protein biosynthesis	protein biosynthesis	regulation of translational initiation	positive regulation of aggregate size	unknown
Blast, e value*	no significant matches	no significant matches	no significant matches	no significant matches	no characterized homologues	no characterized homologues	no characterized homologues

*indicated when closest match in Dd is an uncharacterized protein; ** protein detected in both MALDI analyses; (a) domain of unknown function

Table 3: *Dictyostelium discoideum* cullins

Dd cullins	Dicty Base ID	Genome position	# aa	Blast e-value to cullins (Hs)
Cul A	DDB0185191	6, 967540 to 970465	770	to Cul-1: 0.0
Cul B	DDB0191260	1, 544536 to 547751	771	to Cul-2: 2e-133
Cul III	DDB0186248	4, 2554904 to 2552143	769	to Cul-3: 0.0
Cul IV	DDB0184551	6, 1988814 to 1991381	801	to Cul-4B: 0.0
Cul V	DDB0188264	5, 2232384 to 2238643	750	to Cul-1: 2e-111

Cullins show the lowest similarity in their N-termini and the highest in their C-termini. This is also the case for the *Dictyostelium discoideum* cullins (Figure 25). The divergence in their N-termini allows the cullins to cluster with closely related cullins of the same and homologous cullins of other organisms into classes. Four classes, namely 1, 2 & 5, 3, 4 have been described (Pintard et al., 2003). We compared the N-termini of the *Dictyostelium discoideum* cullins: Dd has a representative of every class (Table 3 and Figure 25). The names for Cul III and Cul IV were luckily significant as they belonged to the classes 3 and 4, respectively. This was not the case for Cul V, that does not belong to any class. The representative of the class 1 is Cul A and Cul B is a member of the class 2 & 5.

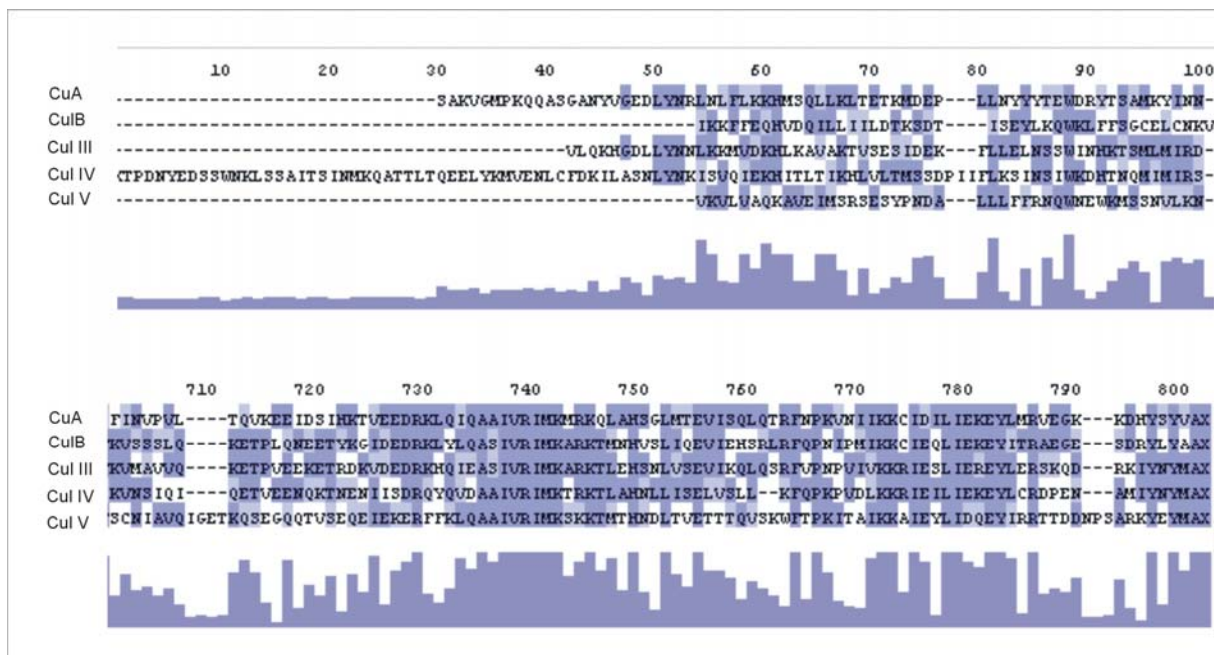


Figure 25: Alignment of the *Dictyostelium discoideum* cullins. All 5 *Dictyostelium discoideum* cullins comprise around 770 amino acids except Cul IV that is preceded by a stretch of about 90 amino acids (only the last 30 aa of this stretch are shown) that starts with a poly-asparagine sequence. The N-termini of cullins (alignment on top) show the lowest similarity between the cullins making them cluster with homologues of other organisms into cullin classes. The cullin C-termini show the highest degree of similarity (alignment below).

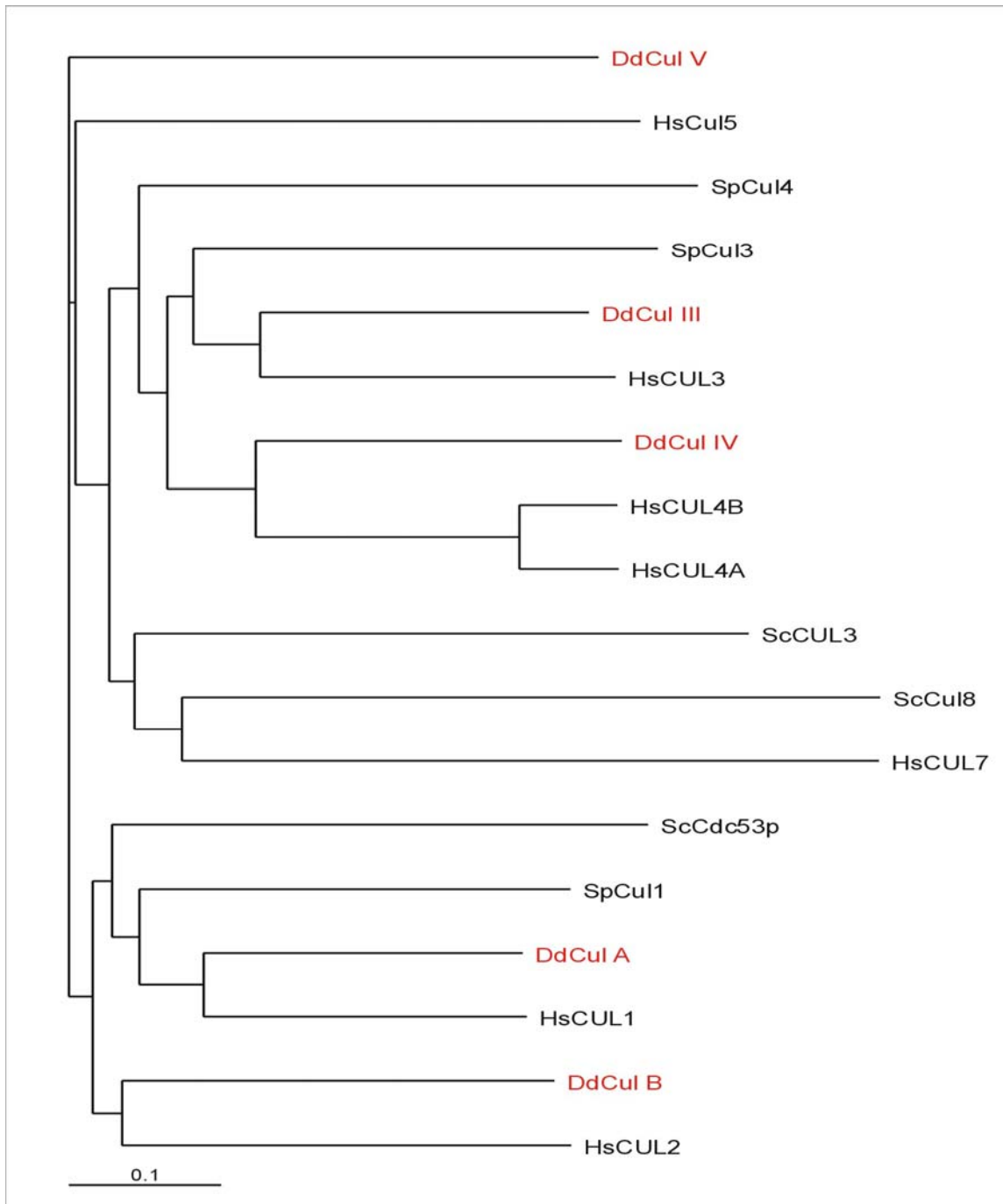


Figure 26: Phylogenetic tree of Cullins. Sequences of *Dictyostelium discoideum* (Dd), *Saccharomyces cerevisiae* (Sc), *Schizosaccharomyces pombe* (Sp) and *Homo sapiens* (Hs) were aligned using ClustalX and the tree was constructed using Treeview. The *Dictyostelium* Cullins are highlighted in red. Bar represents 10% divergence.

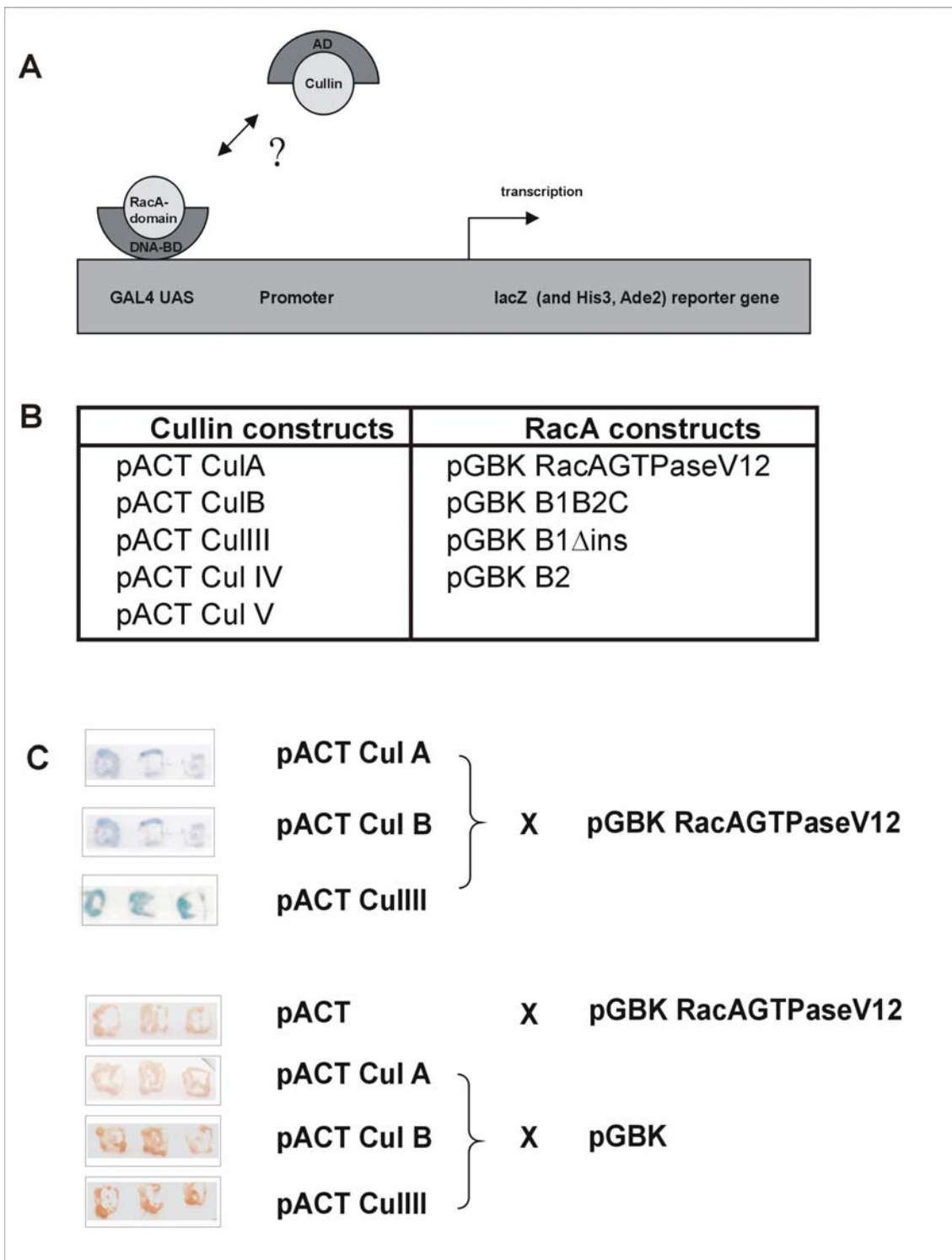


Figure 27: Potential interaction of *Dictyostelium discoideum* cullins with RacA has been analysed with the yeast-two-hybrid method (A). Constructs used for the analyses are listed in B. The constitutively active RacA GTPase domain and different subsets of the BTB-domain containing RacA C-terminus have been cloned as bait proteins and were tested for interaction with the *Dictyostelium discoideum* cullin proteins (B1 = BTB domain 1; B2 = BTB domain 2; C: residual C-terminus; B1 Δ ins = BTB1 domain devoid of a short high variable region). (C) The constitutively active RacA GTPase domain interacts with cullin A, B and III (upper part). Below the appropriate controls are shown.

To show the clustering of homologues belonging to a common cullin class, we constructed a phylogenetic tree with the cullin sets of *Dictyostelium discoideum*, *Saccharomyces cerevisiae*, *Schizosaccharomyces pombe* and *Homo sapiens* (Figure 26). The protein sequences were aligned using ClustalX and the tree was constructed using Treeview.

1.2.6.4 Interaction of RacA with cullins analysed by yeast-two-hybrid

To test the *Dictyostelium discoideum* cullins for interaction with RacA we cloned them into the yeast-two-hybrid vector pACT (Figure 27 A, B) (Cul B in the pACT vector was kindly provided by R.A. Firtel, University of California, San Diego, La Jolla). We requested cDNA-clones from the National Institute of Genetics, Japan that were used as PCR-templates (clones are listed in the Appendix). In the case of Cul IV and V the EST clones did not encompass the entire sequence although the largest C-terminal part of the proteins was covered. The missing N-termini were obtained by RT-PCR. The overlapping N-terminal and C-terminal fragments were then joined by an additional PCR step.

Although we could show by means of the yeast-two-hybrid analysis that Cul A, B, and III interact with the constitutively active RacA GTPase domain (Figure 27 C), an interaction of the RacA C-terminus, in particular the BTB domains, with any of the cullins could not be proven.

1.3 Overexpression of RacA, its mutant variants and single domains

To study the function of RacA in vivo, we have generated stably transformed cell lines that overexpress the wild-type (WT) and the constitutively active (Gly12→Val) and dominant negative (Thr-17→Asn) forms of RacA. Additionally, we overexpressed single domains of RacA: the GTPase domain and its mutant variants, the whole C-terminus (RacA without the GTPase domain) and single domains of the C-terminus (for a list of constructs, see: Materials and Methods 1.9). In the case of the first BTB domain, an additional construct has been created in which a short sequence that diverges highly from other BTB domains and may be a specific effector site of RacA has been omitted (B1Δ ins). By expressing single RacA domains we aimed to see possible dominant negative effects. In order to study the localisation of RacA, its mutant variants and single domains in the cell we have expressed all the proteins as GFP fusions (Figure 28). Partly the overexpression was performed in a tetracycline-controlled inducible system recently adapted for *Dictyostelium* (Blaauw et al., 2000). Furthermore as expression of the GTPase domain might have an effect only if equipped with a prenylation motif and thus

become localised to endomembranes or the plasma membrane, GFP-GTPase fusions of the WT and mutant variants extended by a CAAX-motif have been generated.

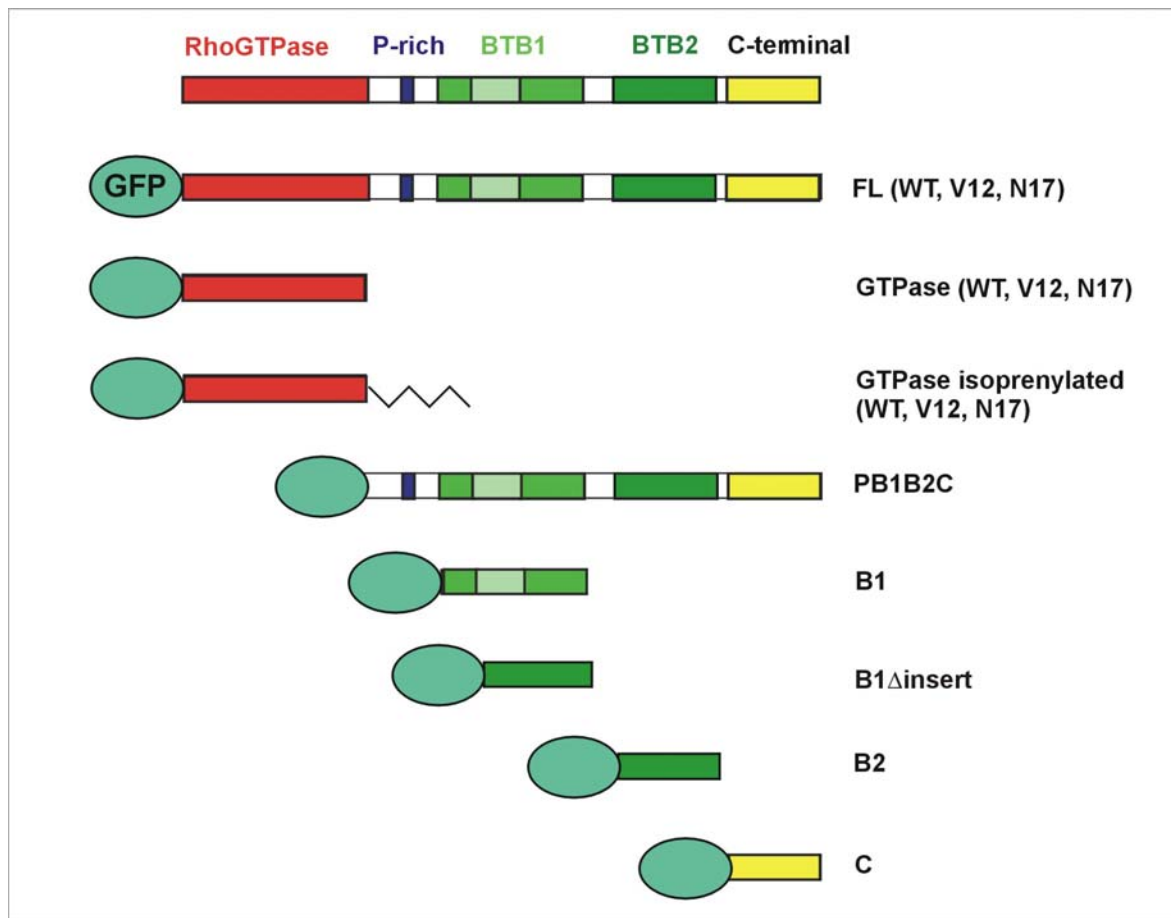


Figure 28: Overexpression of GFP-RacA fusion proteins. On top the domain architecture of RacA is shown (for details: see Introduction 5). Below the GFP fusion proteins of full-length (FL) WT or constitutively active (V12) and dominant negative (N17) variants of RacA or GFP fusions of parts of RacA expressed in stably transformed cell lines are depicted. The GTPase domain has been constructed either with or without prenylation motif.

Expression of the respective fusion proteins has been confirmed by Western blot analysis using GFP-antibody. All the fusion proteins showed an indistinct localisation pattern, mainly cytosolic. The behaviour of stably transfected cell lines overexpressing single domains of RacA-C-terminus in cytokinesis, growth and phagocytosis has been surveyed. The only noteworthy results were that these strains, namely B1, B2 and C, showed, as if eliciting a dominant negative effect, impaired growth (Figure 29 A). These strains, as well as the strain overexpressing the constitutively active GTPase domain, revealed a cytokinesis defect when grown in suspension (Figure 29 B). In particular among the cells, overexpressing the first BTB domain, there were many cells containing around ten nuclei. As for RacA-KO cells, these

cytokinesis defects were conditional and did not appear when cells were grown attached to a surface.

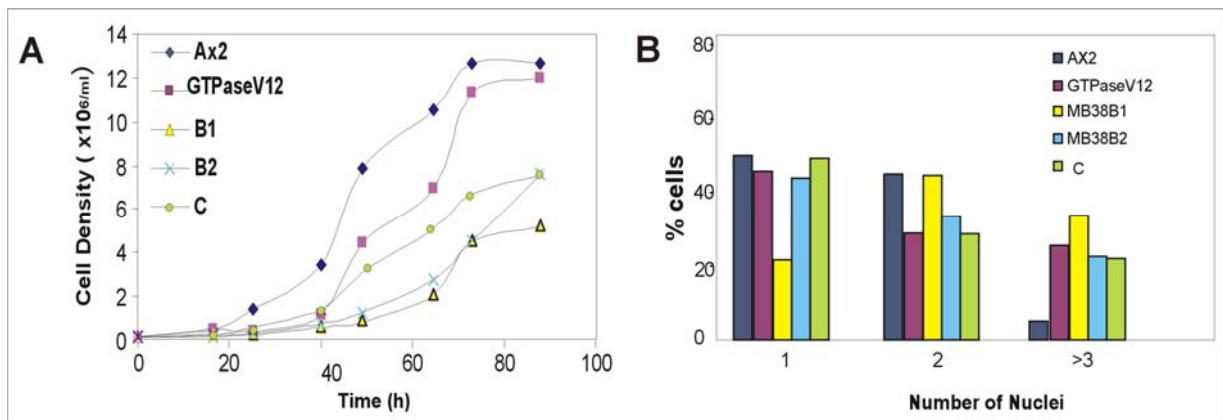


Figure 29: Growth and cytokinesis of strains overexpressing single domains of RacA. (A) Growth of stably transfected cell lines overexpressing the constitutively active RacAGTPase domain, the first BTB domain (B1), the second BTB domain (B2) and the residual C-terminus (C). (B) Quantification of nuclei of cells taken from suspension culture. In growth, cells overexpressing the constitutively active GTPase domain behaved as Ax2. B1-, B2- and C-overexpressing strains showed deficient growth. All overexpressor strains, B1 in particular, were impaired in cytokinesis when prior cultivated in suspension. Growth assay and cell fixation/quantification of nuclei were performed as described in the legends of figures 17 and 18.

2 Functional analysis of RacH

To investigate the function of RacH we used a *racH*-KO strain provided by Dr. Miho Iijima (Johns Hopkins University School of Medicine, Baltimore, USA). For some experiments stably transformed cell lines were generated that overexpress RacH-WT (Somesh, 2002) and a mutant RacH-variant lacking the Rho insert.

2.1 Confirmation of RacH knock out and overexpressor strains

The *racH* gene was deleted by homologous recombination (Figure 30 A) and the recombination event verified by Southern (Figure 30 B) and Western analysis (Figure 31). A polyclonal antiserum generated against RacH (Somesh, 2002) recognised a protein of approximately 25 kDa in total cell homogenates of Ax2 that was absent in the knockout strain. In cells overexpressing a GFP fusion of RacH-WT the antiserum recognised an additional protein of approximately 50 kDa that corresponds to the predicted size of GFP-RacH.

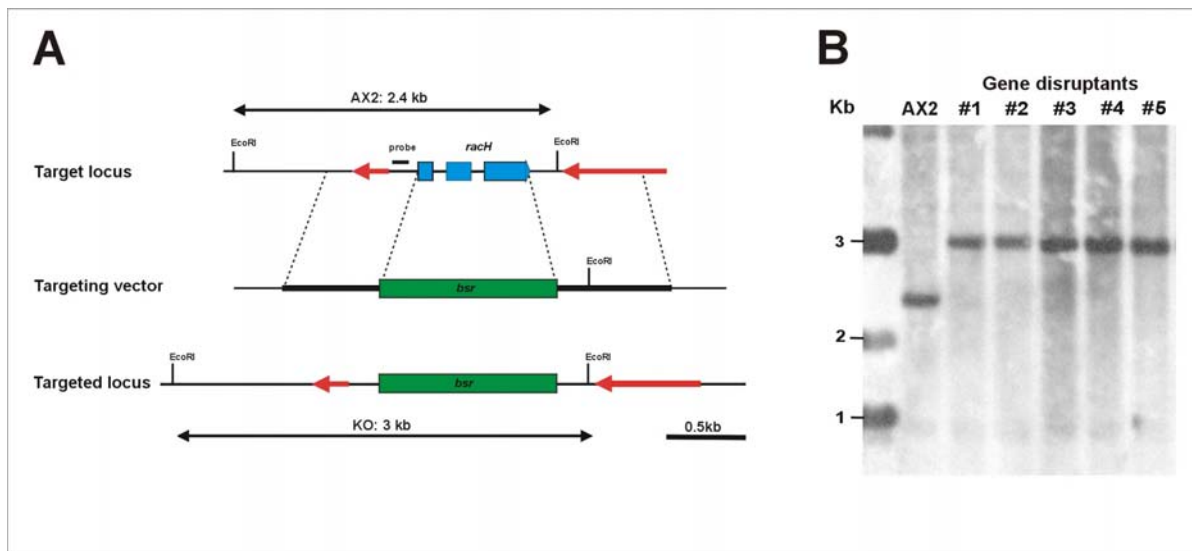


Figure 30: Disruption of the *rach* gene. (A) Diagram of the *Dictyostelium rach* gene and its disruption by the blasticidin resistance cassette (*bsr*). A targeting vector was used with the blasticidin cassette flanked on the left by a 850 bp long arm homologous to the 5'-region and on the right by a 960 bp long arm homologous to the 3'-region of *rach*. (B) Screening for homologous recombinants was performed by Southern blotting. Genomic DNA was digested with *EcoRI* and the blot probed with a ^{32}P -labelled probe in the 5' region of the *rach* gene. A shift of the 2.4 kb wildtype band to a 3 kb band in the knockout is apparent (Southern blot provided by Dr. Miho Iijima).

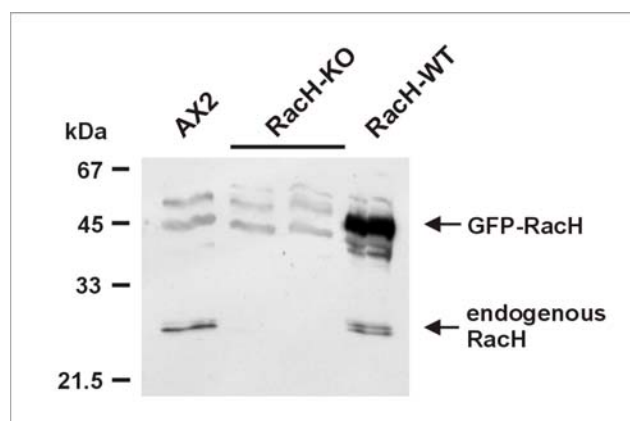


Figure 31: Confirmation of *Rach*-KO on the protein level. Western blot analysis of Ax2, *Rach*-KO (two independent clones) and GFP-tagged *Rach*-WT overexpressor. Total cell homogenates of 4×10^5 cells were resolved in polyacrylamide gels and blotted onto nitrocellulose membranes. The blot was incubated with a polyclonal antiserum specific for *Rach* (1:2,000 dilution).

2.2 Growth and endo/exocytosis of *Rach* mutants

The pattern of subcellular localisation of *Rach* at endomembranes (Somesh, 2002 and Results 3) and the fact that Rho GTPases participate in the regulation of endocytic and exocytic pathways (Qualmann and Mellor, 2003) prompted us to examine vesicle trafficking processes in *Rach* mutants in more detail. We examined the ability of *Rach* mutant cells to internalise

fluorescently labelled yeast particles (Figure 33A) or the fluid-phase marker TRITC-dextran (Figure 33 B). RacH-KO showed normal rates of particle uptake.

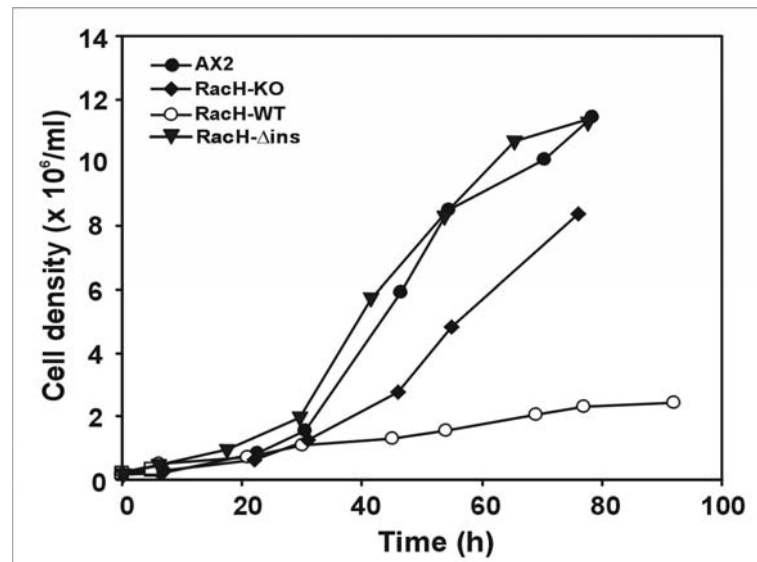


Figure 32: Growth of RacH-KO, RacH-WT-overexpressor and RacHΔins-overexpressor in suspension. Cultures were inoculated at 2×10^5 cells/ml and grown at 21°C with shaking at 160 rpm. Cells were counted at the indicated time points. The RacH-WT overexpressor but not the RacH-KO shows impaired growth. Data are the average of three independent experiments.

RacH-KO cells were able to internalise the fluid phase marker TRITC-dextran to a lesser extent (approximately 50%) than the control Ax2 cells. The rates of pinocytosis roughly correlated with the growth rates of these mutants in suspension (Figure 32). RacH-WT cells had a severe growth defect: they were able to grow only to a density slightly over 2×10^6 cells/ml with a very prolonged doubling time (36.5 h). RacH-KO cells were slightly impaired: they grew slowly (10 to 12 h vs. 8.5 h for Ax2) and reached densities below that of Ax2 (around 8×10^6 cells/ml vs. 10×10^6 cells/ml). Finally, we quantitated exocytosis rates of the fluid phase marker TRITC-dextran and found that RacH-KO cells showed a slower rate of exocytosis. In contrast to RacH-KO cells RacH-WT overexpressor cells were severely impaired in growth. The growth defect of RacH-WT overexpressor correlated with a strong deficiency in both, phago- and pinocytosis. Exocytosis in RacH-WT overexpressor was just slightly impaired (Fig. 34 C). RacH-WT overexpressor cells showed almost no uptake of fluid phase and reached a phagocytosis rate of 30% in comparison to Ax2. The behaviour in growth, pino-, phago- and exocytosis of the RacHΔins strain did almost not differ from the performance of Ax2 cells, indicating that the

RacH-specific effector site plays an important role in the dominant negative effect on these processes provoked by RacH-WT overexpression.

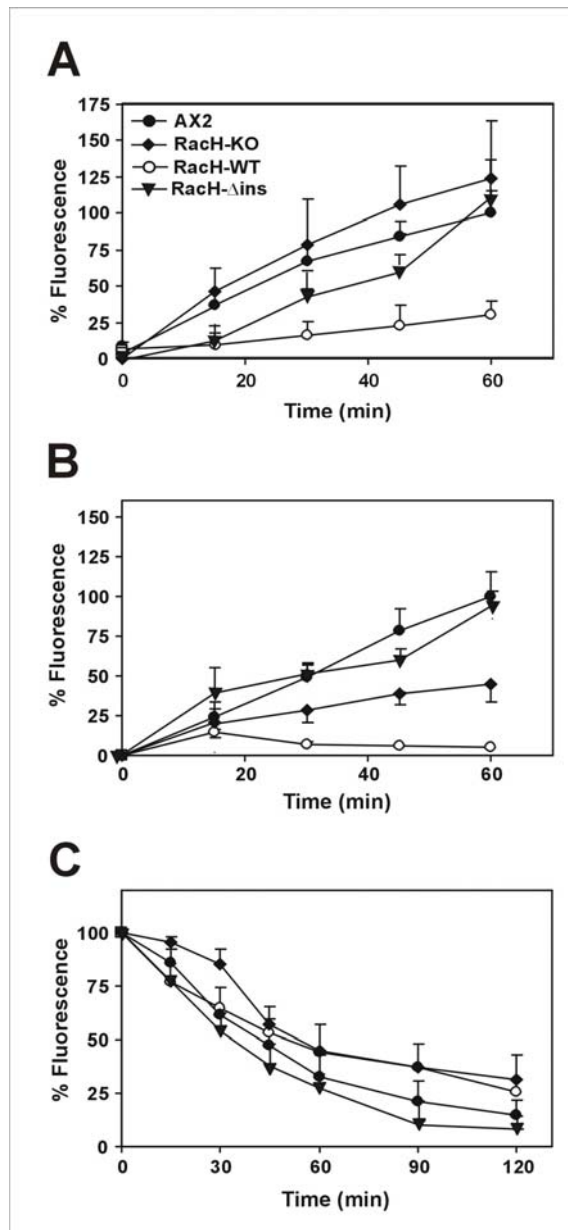


Figure 33: Phagocytosis, fluid-phase uptake and exocytosis of RacH-mutants. (A) Phagocytosis of TRITC-labelled yeasts. Cells were resuspended at 2×10^6 cells/ml in fresh axenic medium and challenged with fivefold excess fluorescent yeast cells. Fluorescence from internalised yeasts was measured at the designated time points. (B) Fluid-phase endocytosis of TRITC-dextran. Cells were resuspended in fresh axenic medium at 5×10^6 cells/ml in the presence of 2 mg/ml TRITC-dextran. Fluorescence from the internalised marker was measured at selected time points. (C) Fluid-phase exocytosis of TRITC-dextran. Cells were pulsed with TRITC-dextran for 3 hours, washed, and resuspended in fresh axenic medium. Fluorescence from the marker remaining in the cell was measured. Data are presented as relative fluorescence, Ax2 being considered 100%. All values are the average of at least three independent experiments.

2.2.1 Detailed analysis of endocytosis in RacH deficient cells

2.2.1.1 RacH-KO cells show deficient acidification of early endosomes

As RacH seems to play a role in the regulation of endocytosis, we further analysed the endosomal and vacuolar system of RacH-KO cells. First we monitored the change of endosomal pH during early phases of pino- and phagocytosis following a 10 min pulse of FITC-dextran (Figure 34 A) or FITC-labelled bacteria (Figure 34 B). In Ax2 cells endosomal acidification was rapid and reverted during the next 30 min. By contrast, in RacH-KO cells endosomes became on average less acidic. As endosomes are acidified by $V(H^+)$ -ATPase we compared the levels of VatA, a component of the peripheral catalytic domain of the $V(H^+)$ -ATPase, in RacH-KO and Ax2 cells. The levels of VatA did not differ between RacH-KO and Ax2 cells (Figure 34 C).

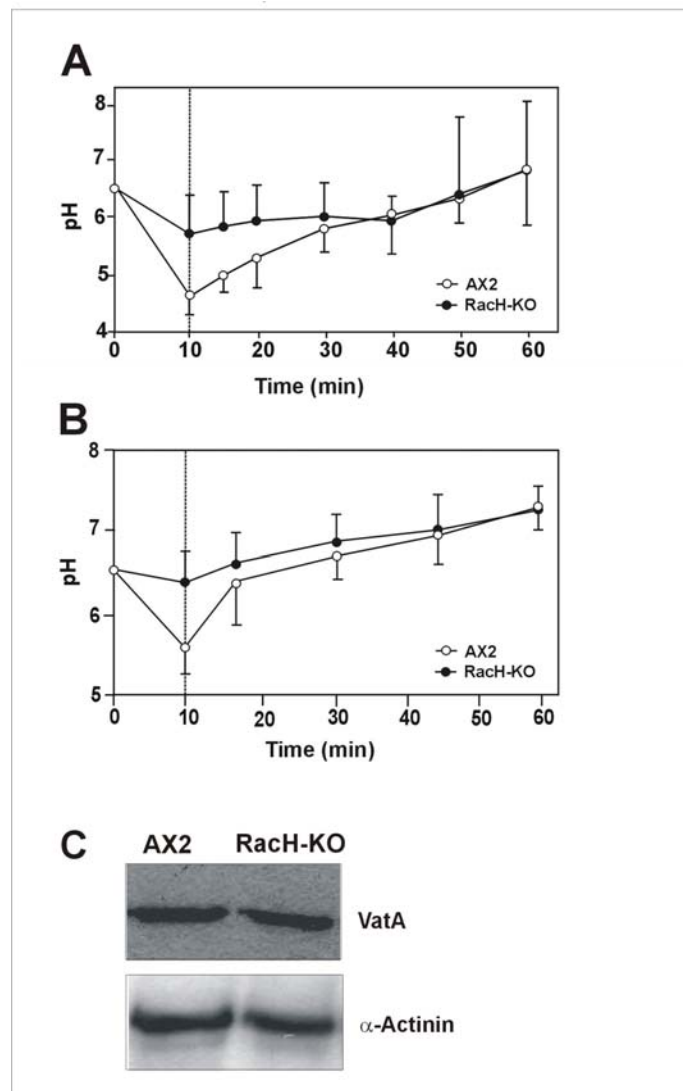


Figure 34 (previous page): Change of endosomal pH during transit of a fluid or a solid phase marker. Cells were pulsed with with FITC-dextran (2 mg/ml) (A) or FITC-labelled *E. coli* B/r (5×10^9 *E. coli*1 $\times 10^6$ *Dictyostelium* cells) (B) for 10 minutes, then washed and resuspended in fresh nutrient medium. Samples were collected at the indicated time points, and dual excitation ratio was used to calculate the endosomal pH. In the *RacH* deficient cells endosomes turn significantly less acidic than in the wild type. (C) *VatA* levels are comparable in *Ax2* and *RacH*-KO cells. Total cell homogenates of 4×10^5 cells were resolved in 12% polyacrylamide gels and blotted onto nitrocellulose membranes. The blot was probed with mAb 221-35-2 for detection of *VatA* and mAb 47-62-17 for labelling of α -actinin as loading control.

2.2.1.2 Visualisation of pH changes during endosomal traffic in vivo

Additionally we visualised pH changes during endosomal traffic in vivo. We exposed *RacH*-KO cells to medium containing pH-sensitive FITC-dextran and pH-independent TRITC-dextran. After 1 hour, when cells have reached an equilibrium of endo- and exocytosis, images of both markers were collected (Figure 35 A) and the distribution of acidic and neutral vesicles was calculated. We did not notice significant alterations: *RacH*-KO cells displayed 82.7% acidic and 17.3% neutral endosomes and *Ax2* cells 84.8% acidic and 15.2% neutral endosomes. Furthermore we investigated the ability of endosomes to concentrate their contents by measuring the intensity of TRITC-dextran in vesicles compared to its concentration in the medium. The marker concentration in acidic and neutral endosomes of *Ax2* and *RacH*-KO cells did not differ significantly (Figure 35 B).

2.2.1.3 Secretion of lysosomal enzymes

Like other lower eukaryotes, *Dictyostelium* cells partly secrete lysosomal enzymes, likely due to incomplete retrieval from the postlysosomal compartment (Dimond et al., 1981). Measuring the activity of lysosomal enzymes provides a means to quantify the relative amounts of exocytosis versus recycling of lysosomal enzymes. Some lysosomal enzymes, like acid phosphatase, enter endosomes early in the pathway to profit from the acidic luminal pH value and may be efficiently recycled and re-used. Other enzymes, like α -mannosidase, are delivered to endosomes later, when their pH has returned to neutral, and tend to be secreted at higher rates and thus accumulate in the medium. Secretion of lysosomal enzymes can be stimulated by non-metabolisable sugars, like sucrose, that induce endosomal swelling, thus counteracting membrane retrieval processes (Crean and Rossomando, 1979). We compared the secretion of acid phosphatase (Figure 36 A) and α -mannosidase (Figure 36 B) in *RacH*-KO and *AX2* cells. In the absence of sucrose, lysosomal secretion of both enzymes was comparable in *RacH*-KO and *AX2*. Sucrose generally provokes an increase of lysosomal enzyme secretion rates, especially

acid phosphatase. In the case of α -mannosidase no major differences were found between RacH-KO and AX2; by contrast, RacH-KO cells showed almost no increase of secreted phosphatase activity.

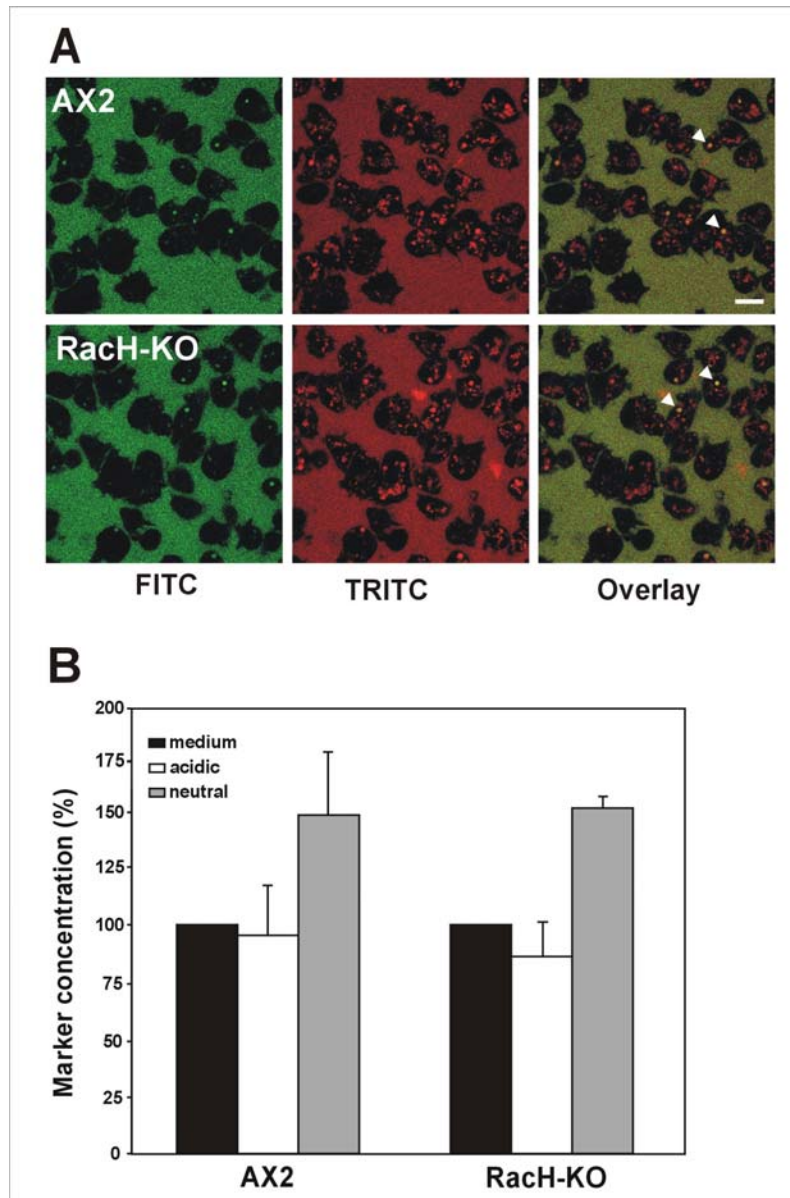


Figure 35: Visualisation of pH changes during endosomal traffic in vivo. Wild type and RacH-KO cells were allowed to sit on a glass surface and were incubated with nutrient medium containing the pH-sensitive FITC-dextran and the pH-independent TRITC-dextran. (A) Single confocal sections showing distribution of FITC-dextran (green) and TRITC-dextran (red). Superimposition of the channels yields a yellow colour for neutral vacuoles (examples are marked with arrowheads), while acidic vesicles appear in red. Note that vesicular staining can be of higher intensity than extracellular medium, indicating concentration of marker during passage through the endocytic pathway. Scale bar, 10 μ m. (B) Marker concentration determined from acidic and neutral vesicles of AX2 and RacH-KO cells. Fluorescence intensity of TRITC-dextran in the vesicles was quantitated relative to the intensity in the medium from digital images similar to the ones shown in (A) for more than 200 vesicles each. Values are average \pm standard deviation.

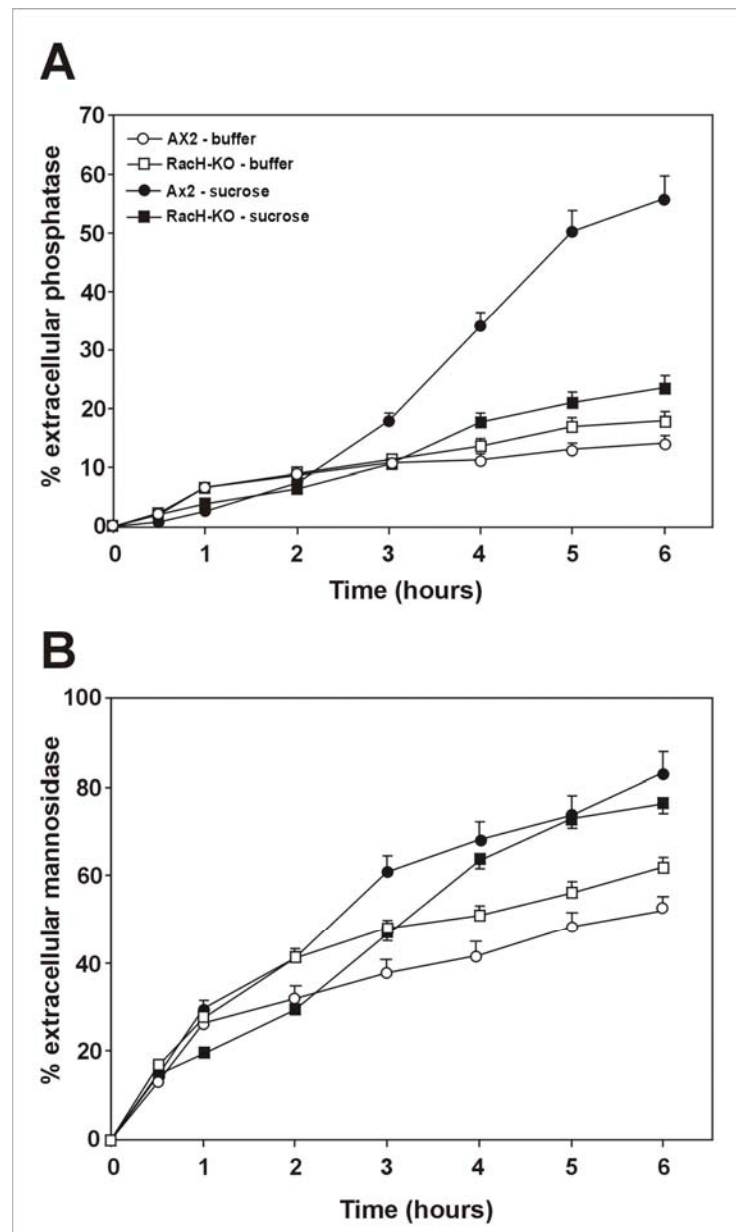


Figure 36: Secretion of lysosomal enzymes. Cells were harvested by centrifugation and resuspended at a concentration of 1×10^7 cells/ml in Soerensen phosphate buffer with or without addition of sucrose (100 mM). The acid phosphatase (A) and α -mannosidase (B) activities were measured both in the supernatant and in cell lysates at the indicated time points and results expressed as percentage of extracellular enzyme activity. Values are the average \pm standard deviation of two independent experiments. In comparison to AX2 the RaH-KO mutant does not respond with higher acid phosphatase secretion in the presence of sucrose.

2.2.1.4 Subcellular distribution of vacuolin is affected in RaH deficient cells

The pattern of subcellular localisation of RaH at the endomembranes of the ER and mainly Golgi apparatus and the trafficking defects observed in RaH-KO cells led us to investigate

whether ablation of RacH would lead to alterations of compartments that constitute the stages of endocytic transit. In fixed cells we studied the distribution of comitin, PDI, VatA, a lysosomal antigen and vacuolin. Comitin marks the Golgi apparatus, PDI the ER, VatA early endosomes and the contractile vacuolar system and vacuolin the post-lysosomal compartment that acquires endocytic markers shortly before exocytosis. Except for vacuolin, the distribution of none of these markers was noticeably altered in RacH-KO cells (Figure 37) and for this reason not shown at higher magnification.

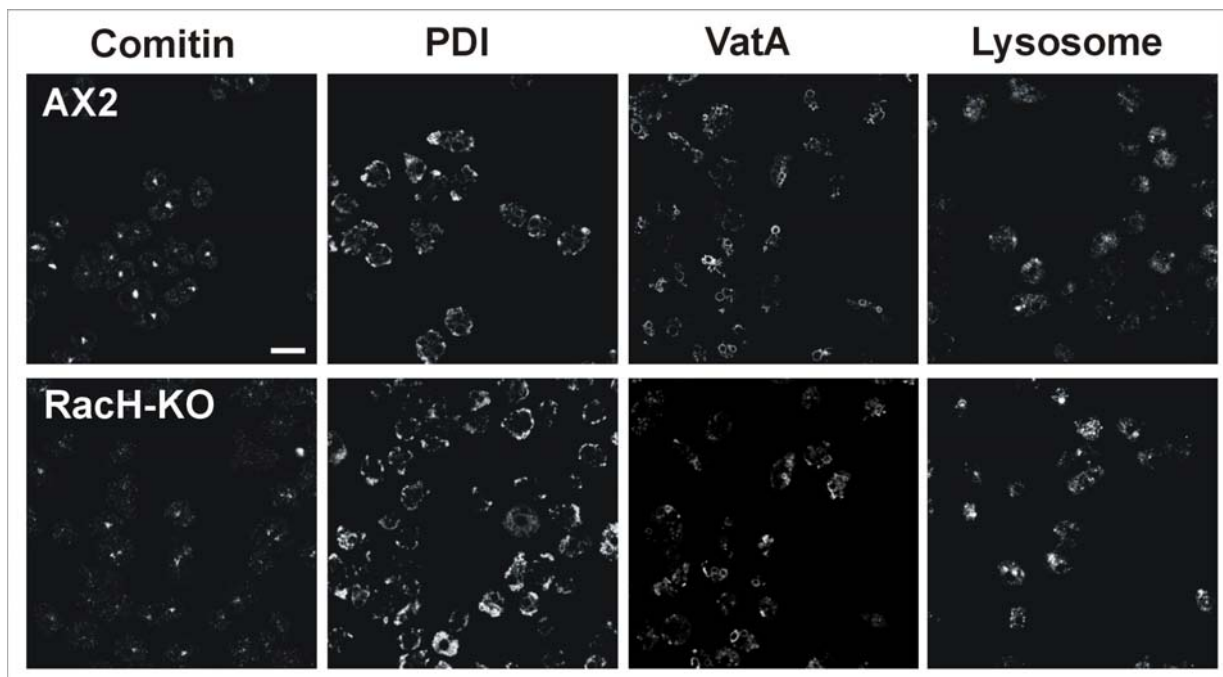


Figure 37: Distribution of membrane compartments in cells lacking RacH. Ax2 and RacH-KO cells were fixed in cold methanol and incubated with monoclonal antibodies against the following membrane compartment markers: the Golgi marker comitin (mAb 110-340-2), the ER marker protein disulfide isomerase (PDI, mAb 221-135-1), a marker for the contractile vacuolar system (VatA, mAb 221-35-2) and a marker for the lysosomal compartment (a carbohydrate antigen, mAb 221-342-5). Images are confocal sections. Bar, 10 μ m.

By contrast, the vacuolin distribution of RacH-KO cells was remarkably distinct from the one of Ax2 cells (Figure 38). While over 50% of Ax2 cells exhibited 1 to 3 large vacuoles, only 22% of RacH-KO cells showed this morphology. In 66% of RacH-KO, but only in 23% of AX2 cells, vacuolin staining is dominated by a pattern of small vacuoles dispersed all over the cell (Figure 39 B). Thus RacH seems to influence the morphology of the postlysosomal system.

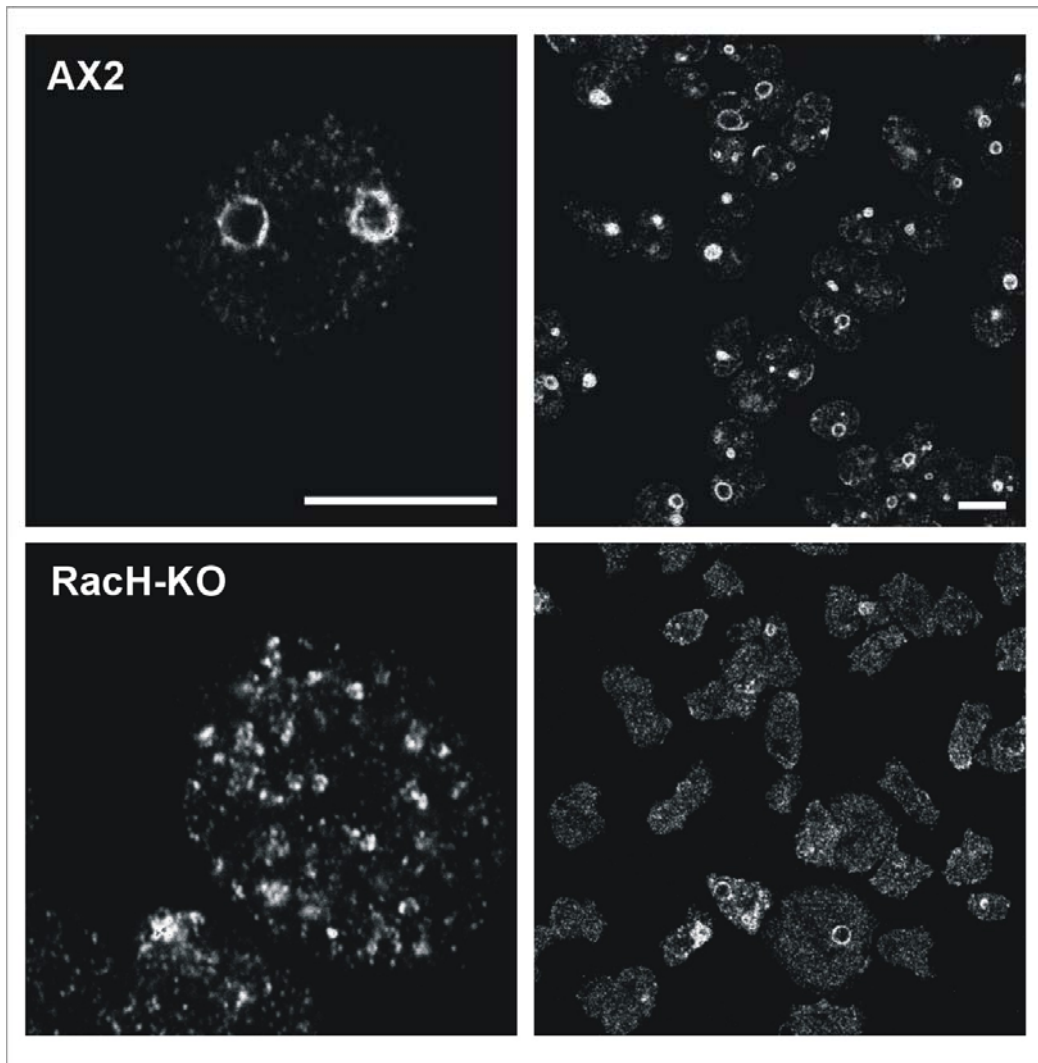


Figure 38: Distribution of vacuolin is disturbed in RacH deficient cells. (A) WT and RacH-KO cells were fixed and labelled with mAb 221-1-1 for vacuolin followed by Cy3-labelled secondary antibody. Images are confocal sections. In RacH-KO cells the vacuolin labelled vesicles appear smaller and dispersed over the whole cell. Scale bars, 10 μ m.

Examination of the vacuolin distribution in overexpressor mutants supported this observation: in cells overexpressing RacH-WT and RacH-N18 the proportion of cells containing large vacuoles was severely reduced, and most cells had numerous middle-size vacuoles. In RacH-V13 cells the proportion of cells with small intense vacuoles was unusually large, and in many cases vacuolin accumulated intensely at the plasma membrane (Figure 39 A and 39 B).

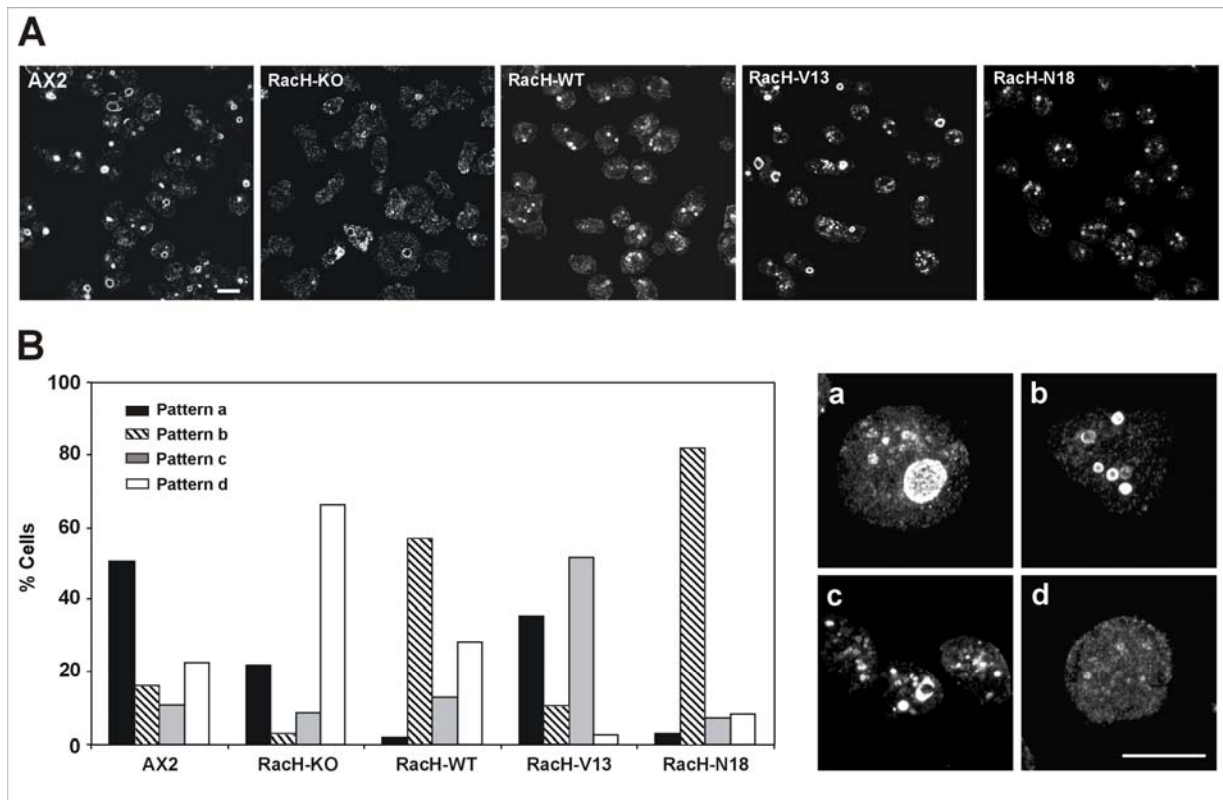


Figure 39: Distribution of vacuolin is disturbed in RacH mutants. (A) Cells were allowed to sit on glass coverslips, fixed and labelled with mAb 221-1-1 followed by Cy3-labelled secondary antibody. Images are confocal sections. In RacH-KO cells the vacuolin labelled vesicles appear smaller and dispersed over the whole cell. Scale bars, 10 μ m. (B) Patterns of vacuolin staining in RacH mutants. Cells have been categorised into four classes according to the morphology of their vacuolar system. One example of each class is shown on the right panels: a, one (occasionally 2 or 3) large prominent vacuole; b, numerous middle size vacuoles; c, numerous small vesicles; d, diffuse punctuate pattern. 300 cells of each strain have been scored.

2.2.1.5 Co-localisation of RacH with early and late endosomes and lysosomes was noticeable but not pronounced

To substantiate whether the effect of RacH on the morphology of the postlysosomal system is rather direct or indirect, we looked for co-localisation of RacH and postlysosomal vesicles. For this, we stained GFP-RacH-WT overexpressing cells for vacuolin. Moreover, as we observed impaired acidification and divergent secretion of lysosomal enzymes, we verified eventual co-localisation of RacH and endocytic compartments containing the proton pump and lysosomes, respectively. The proton pumps were stained as described above by means of the VatA marker directed against a subunit of the $V(H^+)$ -ATPase. Like this, staining of the contractile vacuole, where 90% of the $V(H^+)$ -ATPase is located, and the endo/lysosomal system, where the rest of the $V(H^+)$ -ATPase resides, was achieved (Figure 40 B). Thus only a part of the VatA pattern

represented the endosomal system suggesting probable co-localisation with RacH. The lysosomes were visualised using a marker against a lysosomal antigen (Figure 40A). Co-localisation with Vata, vacuolin and lysosomes was apparent in some instances, but was not pronounced.

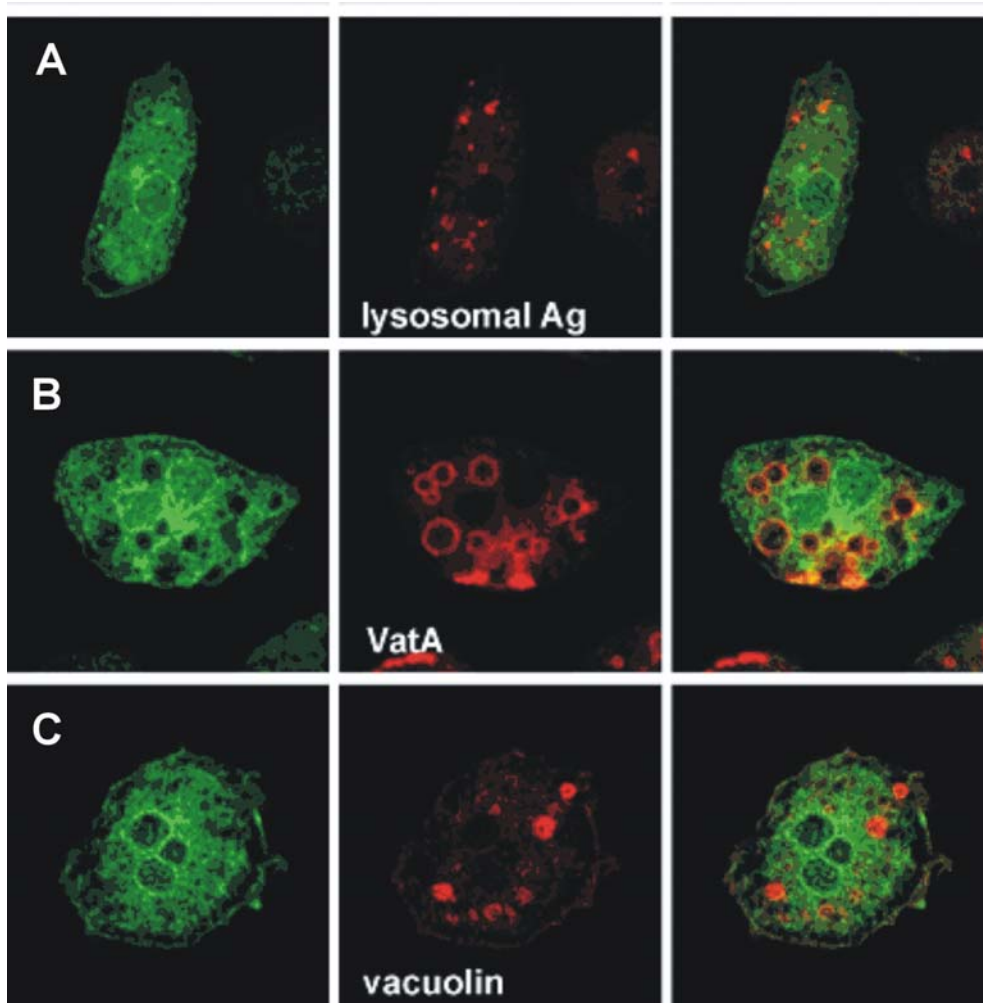


Figure 40: Localisation of GFP-RacH-WT and endocytic compartments. Cells expressing GFP-RacH-WT were fixed in cold methanol and were incubated with monoclonal antibodies that recognize specific membrane compartments followed by incubation with Cy3-labelled anti-mouse IgG. The markers used were: a lysosomal marker (mAb 221-342-5), a marker for the vacuolar H^+ -ATPase (vatA, mAb 221-35-2) present at the contractile vacuole system and to a lesser extent at endosomes, and a marker for a postlysosomal compartment (vacuolin, mAb 221-1-1). Images are confocal sections. Bar, 10 μ m.

2.3 Cytokinesis and development of RacH mutants

Rho-mediated signalling pathways have been shown to participate in the regulation of cytokinesis in diverse eukaryotic organisms (Prokopenko et al., 2000). We were therefore interested in investigating whether overexpression of RacH provoked any alteration in this

process. We analysed cells grown under shaking conditions or on a solid substrate after staining with the DNA-binding dye DAPI (Figure 41). Ax2 cells are usually mono or binucleate under any of these conditions. RacH-KO cells were indistinguishable from Ax2, suggesting that RacH does not play a major role in regulating cytokinesis. By contrast, RacH-WT overexpressor strain, when grown under shaking conditions, showed impaired cytokinesis with 30% of the cells having 3 or more nuclei. Interestingly, the distribution of nuclei in RacH-overexpressing strain grown on coverslips for two days did not differ from that of Ax2 (not shown), indicating that the cytokinesis defect of these strains is conditional. As already observed in growth and endo/exocytosis, the defects observed in the RacH-overexpressing strain were not provoked by overexpression of RacH Δ ins.

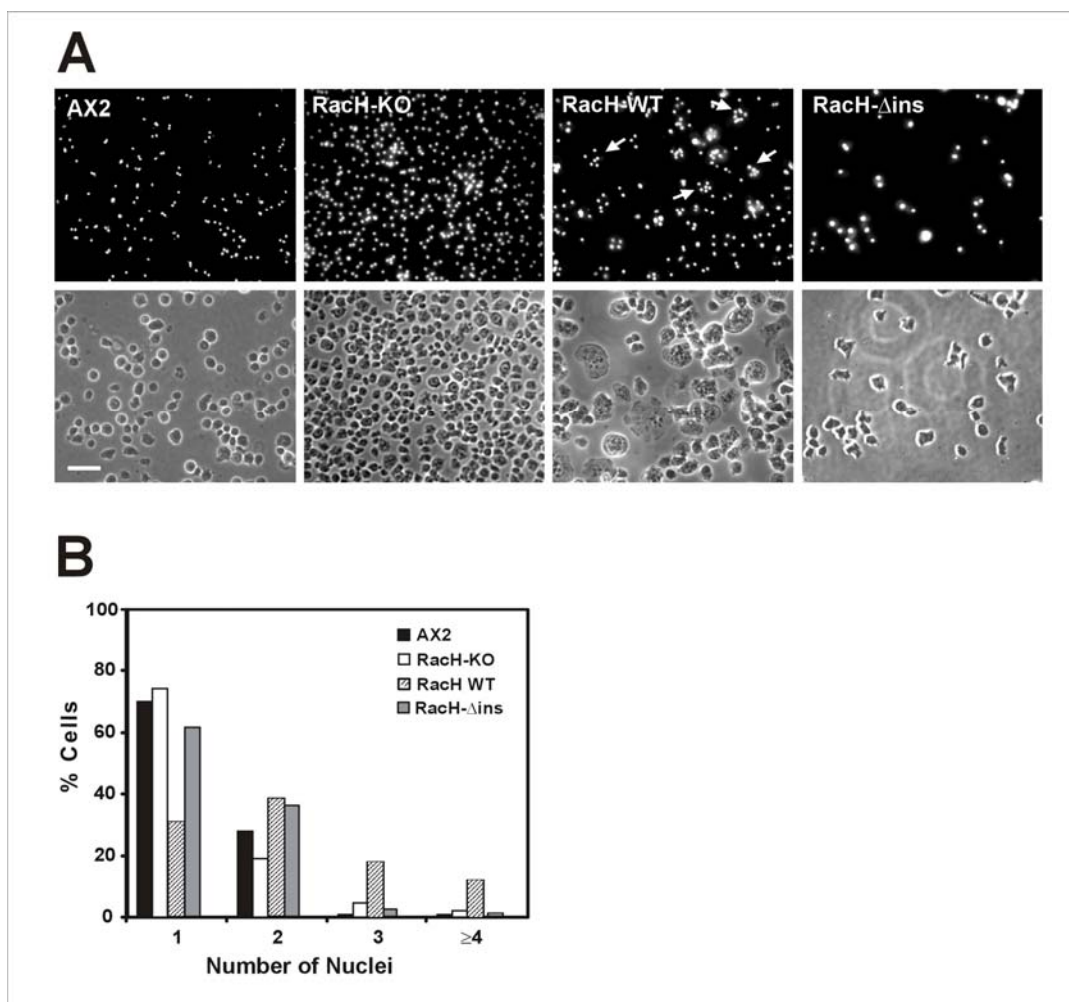


Figure 41: Cytokinesis of RacH mutants. (A) Fluorescence and phase contrast images of cells grown in shaking culture. Cells were allowed to sit for 20 min on coverslips, were fixed with picric acid/paraformaldehyde and nuclei were stained with the DNA-binding dye DAPI. Arrows indicate multinucleate cells. Scale bar 25 μ m. (B) Quantification of nuclei of cells grown in shaking suspension. Samples were processed as in A. For every strain nuclei of 250-300 cells were counted.

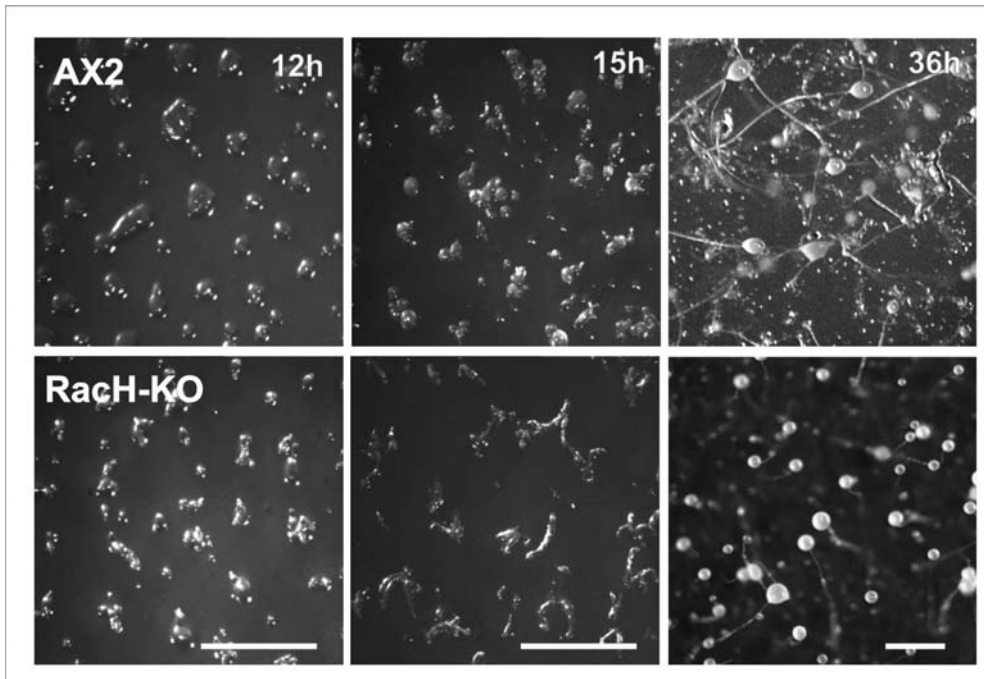


Figure 42: Development of cells lacking RacH. Cells were starved at a cell density of 5×10^7 cells/plate on phosphate agar plates and images were taken at the indicated time points using a stereomicroscope. RacH-KO cells show the same developmental behaviour as AX2 cells. Bars, 1mm.

As RacH is expressed at a constant level throughout development (Somesh 2002) there was no reason for assuming that the GTPase played a major role in this process. However we verified whether ablation of RacH affected development, a process depending besides different transcriptional regulation mainly on rearrangements of the cytoskeleton. As expected, when starved on phosphate buffered agar, RacH-KO cells did not differ significantly from Ax2 in the timing and morphology of the developmental process (Figure 42).

2.4 Chemotaxis, cell motility and F-actin polymerisation

Aggregation competent cells move actively toward a cAMP gradient. Stimulation with cAMP elicits fast and highly transient changes in the F-actin content that correlate with changes in cell behaviour (Hall, 1998). Rho-regulated signalling pathways have been shown to be involved in this process (Park et al., 2004; Rivero and Somesh, 2002). It was therefore of interest to investigate to which extent ablation or overexpression of RacH alters actin polymerisation and the motile behaviour of aggregation competent cells. In Ax2 cells stimulation with cAMP resulted

in a rapid and transient 1.9-fold increase in the amount of F-actin followed immediately by a second much lower peak that lasted until approximately 60 seconds. A similar response was observed in RacH-KO and RacH-WT cells (Figure 43 A) although the second peak was abolished.

In a micropipette-based chemotaxis assay Ax2 and all mutant strains exhibited a similar rate of locomotion (4 - 6 $\mu\text{m}/\text{min}$) in the absence of cAMP (Table 4). Parameters like persistence, directionality and directional change were indicative of random movement with frequent turns. In the presence of cAMP RacH-KO cells displayed a moderately lower speed in comparison to Ax2, otherwise the RacH-KO strain behaved as Ax2: cells became polarised, formed streams and migrated toward the tip of the micropipette (Figure 43 B).

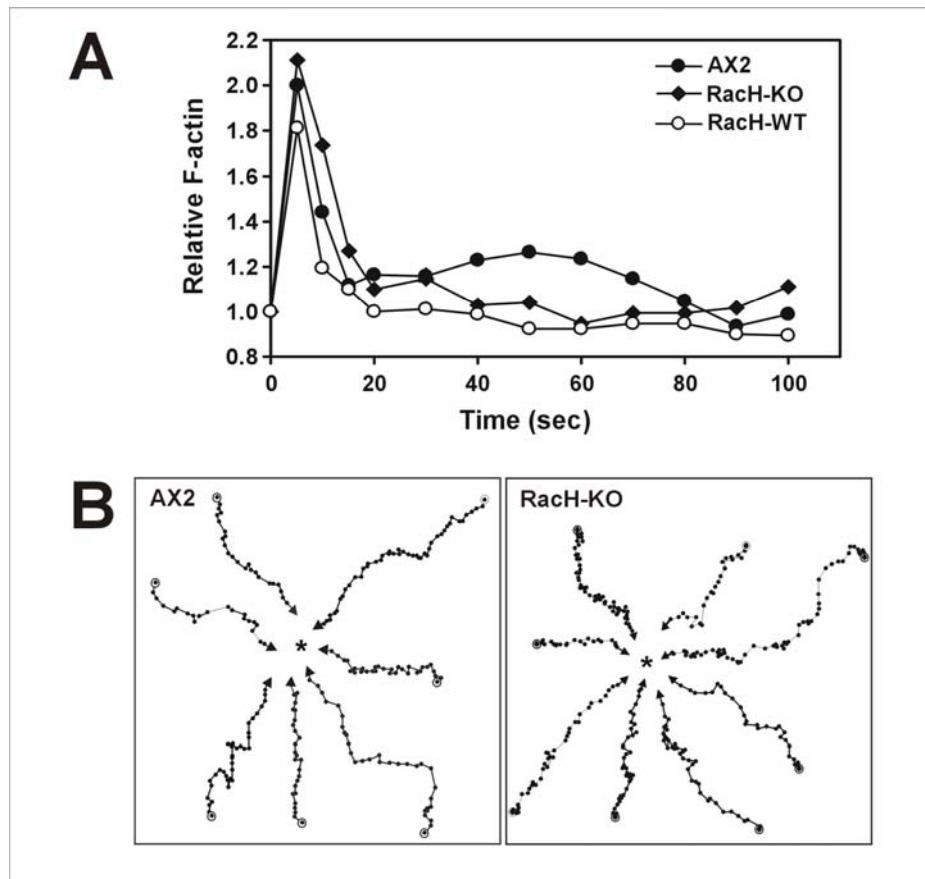


Figure 43: Chemotaxis of RacH-mutants. (A) Actin polymerisation response upon cAMP stimulation. The relative F-actin content was determined by TRITC-phalloidin staining of cells fixed at the indicated time points after stimulation with 1 μM cAMP. The amount of F-actin was normalised relative to the F-actin level of unstimulated cells. (B) Chemotactic movement to a micropipette containing cAMP. Cells were starved for 6 hours, allowed to sit on a glass coverslip and stimulated with a micropipette filled with 0.1 mM cAMP. Images of chemotaxing cells were captured every 30 seconds. Cell movement was analysed with the DIAS software.

Table 4: Analysis of cell motility of the RacH-KO strain.

	Ax2	RacH-KO
Buffer		
Speed ($\mu\text{m}/\text{min}$)	5.61 ± 3.37	5.98 ± 2.57
Directionality - Total	0.40 ± 0.25	0.33 ± 0.21
Direction Change (deg)	47.07 ± 18.71	57.92 ± 17.06
Persistence ($\mu\text{m}/\text{min-deg}$)	1.71 ± 1.59	1.55 ± 1.07
cAMP		
Speed ($\mu\text{m}/\text{min}$)	11.83 ± 3.30	$8.94 \pm 2.83^*$
Directionality - Total	0.72 ± 0.19	$0.52 \pm 0.23^*$
Direction Change (deg)	24.61 ± 10.77	$43.21 \pm 18.08^*$
Persistence ($\mu\text{m}/\text{min-deg}$)	3.96 ± 2.04	$2.65 \pm 1.39^*$

The analysis was performed as explained in Table 1. Chemotaxis of RacH-KO cells exposed to a cAMP gradient differed from Ax2 significantly in all parameters. * $P < 0.05$ relative to AX2 in the same condition (Student's t test).

3 Determinants of RacH subcellular localisation

It has been previously shown that RacH GFP fusion protein associated to internal membrane compartments: GFP-RacH clearly colocalised with interaptin (nuclear envelope) and comitin (Golgi apparatus), and to a great extent also with PDI (ER) and occasionally colocalisation with VatA, vacuolin and lysosomes was apparent, but was not pronounced (RacH localisation at the ER and Golgi was established by Somesh, 2002).

In this study, we sought to investigate the molecular determinants of the subcellular localisation pattern exhibited by RacH. RacH was apparently localised in the inner membranes and not at the plasma membrane even though RacH has a prenylation motif. But as RacH exhibits numerous negatively charged residues in the polybasic stretch the net positive charge of this region is reduced. In order to verify whether solely this lack of positive charge prevented RacH-targeting to the plasma membrane, we chose two approaches. First (this was described in Somesh, 2002), as RacG possesses both signals, a CAAX motif and a highly positive-charged hypervariable region, we exchanged the C-termini of RacH and RacG and looked at the targeting properties of the chimerae. And secondly, we neutralised the aspartic residues of the RacH polybasic stretch by alanine exchange.

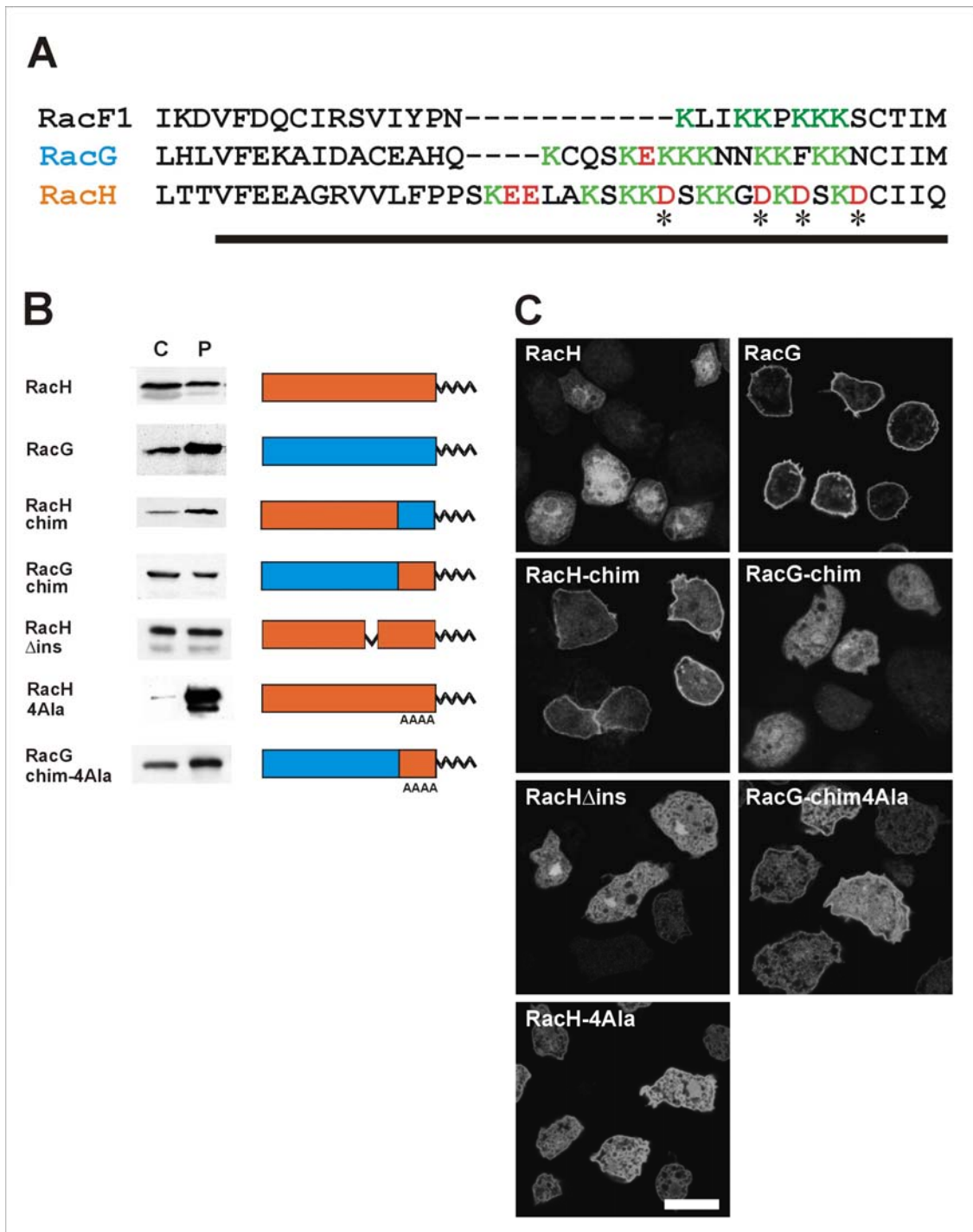


Figure 44: Determinants of RacH subcellular localisation. (A) The C-terminal membrane association region of RacH in comparison with RacF1 and RacG. All three Rho proteins end with a CAAX prenylation motif. Note the presence of numerous negatively charged residues (red) in the polybasic stretch (green) of RacH that have been neutralised by alanine exchange (asterisks). The bar below the sequences denotes the part exchanged in the chimeric constructs. (B) Fractionation of *Dictyostelium* cells overexpressing GFP fusions of RacH, RacG, and further constructs as indicated on the right. Cells were lysed by sonication and cytosolic (C) and particulate (P) fractions were separated by ultracentrifugation. Samples were resolved in 12% polyacrylamide gels and blotted onto nitrocellulose membranes. Blots were incubated with anti-GFP mAb K3-184-2. (C) Confocal sections of *Dictyostelium* cells expressing the GFP fusions indicated in B. Cells were fixed with cold methanol. Bar, 10 μ m (Data on RacGchim and RacHchim are taken from Somesh 2002).

In the tail swap experiments between RacH and RacG it was noticed that the RacH chimeric construct was enriched at the plasma membrane, resembling RacG. RacG-chim distributed homogeneously throughout the cell including the nucleus, but was not enriched at any particular membranous structure. This indicates that the net positive charge at the C-terminus is an important determinant but other requirements are responsible for enrichment of RacH at particular membrane compartments that RacG-chimera does not exhibit. In addition to the chimera studies we rised the positive charge of RacH hypervariable region by alanine exchange of aspartic acid residues. Interestingly, both RacH-4Ala and RacG-chim-4Ala constructs displayed increased, but not predominant, accumulation at the plasma membrane. A similar behaviour was observed in a RacH-2Ala mutant (not shown). This confirms that net charge of the hypervariable region is important but is not the only determinant for proper targeting of RacH, suggesting the presence of an additional targeting mechanism in RacH.

We next investigated the role of the insert region. This region is characteristic of Rho proteins and is required for activation of some effectors but not others. It is usually about 13 residues long, but in RacH it only comprises 6 residues. Remarkably, insert-deleted RacH (RacH Δ ins) displayed a homogeneous pattern of localisation, with enrichment in the cell nucleus, indicating that the insert region is essential for correct subcellular localisation of RacH. The subcellular localisation of these mutants was further studied by differential centrifugation of lysates followed by Western blot analysis of the resultant cytosolic and particulate fractions (Figure 44 B). In the case of RacH approximately 60% of the protein was cytosolic and 40% was membrane associated. RacG was predominantly membrane-associated, 70% being present in the particulate fraction. These proportions became reversed in the chimeric mutants. The alanine exchange mutants displayed an increased proportion of membrane-associated protein, particularly the RacH-4Ala mutant, whereas the RacH Δ ins mutant appeared equally distributed between the cytosolic and the membrane fractions.

IV DISCUSSION

1 RacA potential binding partners and RacA-KO conditional defect indicate a signal transduction pathway downstream of RacA

In order to elucidate the function of RacA we studied RacA deficient cells. In combination with previously described RacA effectors, they give a hint to the signal transduction pathway downstream of RacA. Furthermore we tried to identify additional RacA interaction partners.

1.1 Putative RacA-binding partners

1.1.1 Previously described RacA binding partners

Effectors of the RacA GTPase domain (Figure 45) have been identified previously by means of yeast-two-hybrid analysis using the constitutively active GTPase domain as prey: three PAK (p21 activated kinase) proteins, PAK a, b, c and d, WASP (Wiskott-Aldrich syndrome protein) and WRP1 (WASP-related protein 1) (Park et al., 2004; De la Roche et al., 2005 and unpublished results).

In PAK kinases the catalytic domain is placed at the C-terminus and is preceded by a regulatory domain that harbours a p21-binding domain (PBD) that mediates binding to Rac. In the currently accepted model inactive PAK exists in a folded conformation in which an autoinhibitory domain that overlaps with the PBD inhibits the kinase domain. This interaction is disrupted upon binding of activated Rac or Cdc42, bringing about an open conformation that exposes multiple phosphorylation sites. Subsequent autophosphorylation of these sites leads to maximal kinase activity through prevention of interaction of the catalytic and the regulatory domains.

WASP/Scar proteins share a central proline-rich region and a C-terminal region composed of one or two WASP-homology 2 (WH2) domains that bind actin monomers and one acidic region that interacts with Arp2/3. The proline-rich region binds the G-actin-binding protein profilin as well as SH3 domains from a variety of proteins. In contrast to Scar, WASP additionally possesses a p21-binding domain (PBD) that allows WASP to interact with RacGTPases and Cdc42. WASP exists in an autoinhibited state where the PBD blocks the C-terminal region. Upon binding of activated Rac or Cdc42 and PIP₂ the C-terminal region of WASP is exposed and binding of the Arp2/3 complex and activation of actin nucleation are enabled (Higgs 2001).

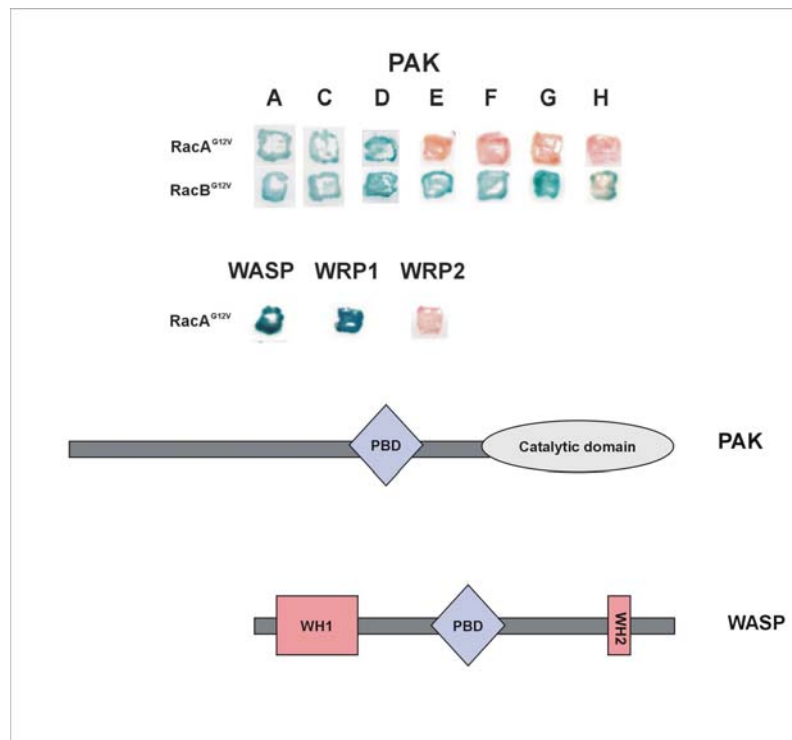


Figure 45: Identification of RacA effectors PAK a, c, d, WASP and WRP1 (WASP-related protein) by yeast two hybrid analysis. PAK proteins consist of a catalytical C-terminal kinase and a p21-binding domain (PBD) that mediates RacGTPase binding. WASP proteins are composed of two WASP homology domains that bind monomeric actin and a PBD domain.

These results of the yeast-two-hybrid analysis should be confirmed by co-immunoprecipitation in GFP-PAKb- as well as GFP-WASP expressing strains using GFP and RacA antibodies.

1.1.2 Analysis of cullin-RacA interaction by means of the yeast-two-hybrid system

In the last two years it became evident that many BTB domain-containing proteins are components of the E3 ubiquitin ligase complex of the ubiquitinylation pathway. The E3 ubiquitin ligases provide two distinct functions: catalysing isopeptide bond formation and targeting of the substrate. Cullins, endowed with scaffolding properties, constitute another subunit of the complex. Different cullin classes appear in E3 ligase complexes of different composition (see Introduction 1.8). In cullin 3 complexes the role of the substrate specificity adaptor is mostly maintained by a BTB domain-containing protein. All three BTB domain proteins of *S. pombe* bind to cullin 3 (Xu et al., 2003) and all *C. elegans* cullin 3 interacting partners contain BTB domains (Pintard et al., 2003). In mammalian cells BTB proteins also turned out to be substrate adaptors for cullin 3 ubiquitin ligases (Geyer et al., 2003). It has been reported that cullin 3 binds the

respective BTB domain via its N-terminus (Furukawa et al., 2003; Geyer et al., 2003; Pintard et al., 2003; Xu et al., 2003). For RhoBTB proteins cullin 3 binding has been reported recently by Wilkins et al. (Wilkins et al., 2004). They suggest a model in which RhoBTB2 acts as a tumor suppressor by recruiting proteins to the Cul 3 ubiquitin ligase complex for degradation (Wilkins et al., 2004).

By means of the yeast-two-hybrid system we could not reveal binding of RacA via its BTB domains to any of the five *Dictyostelium* cullins. Only the constitutively active RacAGTPase domain bound to Cul A, B, and III. This can be either an artefact (although all appropriate controls were negative) or have no significance in *Dictyostelium* cells for the full-length RacA protein. It could also represent a mechanism by which subcellular localisation of the cullin complex is achieved. Seenadheera et al. showed that cellular localisation of cullin complexes is achieved via the binding of cullin C-termini to Rho GTPases (Senadheera et al., 2001).

Anyway, as besides RacA there exist just two further BTB domain containing proteins in *Dictyostelium* - one, migA (DDB01911409) seems to be essential for efficiently assessing chemical gradients (Escalante et al., 1997) and another 806 aa comprising still uncharacterised protein (DDB0220694)- binding of the Rho BTB protein to cullins, in particular cullin3, is quite probable and will be further analysed. For expression in *Dictyostelium* we already prepared vectors encoding the N-termini of *Dictyostelium* cullins as GFP fusion proteins. *Dictyostelium* strains expressing these fusion proteins will be generated and will be used for co-immunoprecipitations with either GFP- or RacA antibodies.

1.1.3 Potential RacA binding partners detected by immunoprecipitation

Apart from the cullin binding analysis immunoprecipitation experiments with polyclonal RacA antibodies resulted in a series of molecules, which will need to be further analysed in detail. Interesting candidates for RacA binding is a BTB domain and C-terminal KELCH repeats containing protein. It might possess F-actin binding capacity as it is related to mammalian actinfilin (Blast e-value 9×10^{-23}), a brain-specific Kelch protein, which interacts with F-actin and contains an amino-terminal POZ/BTB domain. Moreover MALDI-analysis revealed the protein *smlA*. *SmlA* and *racA* null cells share a common, although in RacA deficient cells less severely expressed, phenotype: when starved, *smlA* null cells form large numbers of small aggregates, thus revealing small aggregation areas. Another probably significant candidate is a protein involved in the ubiquitin-dependent protein catabolism. The large protein of 343 kDa, DDB0217656, contains a ubiquitin carboxyl-terminal hydrolase (UCH) domain and hence

possesses ubiquitin thiolesterase activity. UCH proteins are deubiquitinating enzymes playing a role in maintaining the homeostasis of protein degradation via the ubiquitinylation pathway.

1.2 Conditional defects in growth, cytokinesis and F-actin organisation of RacA deficient cells correspond to phenotypes of myosin II and PAKa null cells

RacA-KO cells have a severe growth defect when cultured in suspension, attached to a surface they are able to multiply almost as fast as WT cells. They also show a conditional cytokinesis defect: when grown in suspension RacA-KO cells are more often multinucleated and, strikingly, exhibit many cellular fragments without a nucleus. Also the F-actin distribution is altered when RacA deficient cells are axenically cultured. Instead of being surrounded by an actin cortex like most of the WT cells, they reveal separate F-actin aggregates. They also show a slight chemotaxis defect with respect to speed and directionality and, additionally, are slightly impaired in pino- and phagocytosis. The lower directionality might provoke the fast spreading on bacterial lawn. All these features seem to be RacA specific as they can be “rescued” by RacA expression in RacA null cells.

The correspondence in phenotypes of RacA and myosin II deficient cells is striking. Conventional myosin (myosin II) deficient cells show all peculiarities of RacA deficient cells in an even stronger expression: a conditional growth and cytokinesis phenotype, as the cells cannot undergo cytokinesis in suspension and form large, multinucleate cells (Knecht and Loomis, 1988; Lozanne and Spudich, 1987). During cytokinesis myosin II is typically accumulated on both sides of the cleavage furrow, suggesting that it plays a role in stabilising the furrow and restricting its position to the midzone of the cell (Neujahr et al., 1997b). However, when grown on a substratum, the cells cleave by traction-mediated cytokinesis (Fukui et al., 1990). Myosin II is also involved in the regulation of chemotaxis by its polarised localisation in the posterior of the cell making the posterior detach from the substratum (Clow and McNally, 1999; Moores et al., 1996). Wild-type cells predominantly form a single pseudopod at the leading edge; *myoII* null cells produce lateral pseudopodia, possibly due to reduced cortical tension (Pasternak et al., 1989) and have difficulty lifting the cell’s posterior (Jay et al., 1995). This leads to a slower and less efficient chemotaxis.

Also the phenotype of PAKa null cells corresponds to the observations in myosin II lacking cells. This is of particular interest, as PAKa constitutes a potential binding partner of RacA. PAKa null cells are defective in completing cytokinesis in suspension. PAKa is also required for maintaining the direction of cell movement, suppressing lateral pseudopod

extension, and proper retraction of the posterior of chemotaxing cells. Chung et al. showed that PAKa is a major regulator of myosin II assembly (Chung and Firtel, 1999): PAKa null cells are defective in myosin II assembly, as the myosin II cap in the posterior of chemotaxing cells and myosin II assembly into cytoskeleton upon cAMP stimulation are absent in these cells, while constitutively active PAKa leads to an upregulation of myosin II assembly. The proposed mechanism involves negative regulation of the *Dictyostelium* myosin II heavy chain kinase (Chung and Firtel, 1999). PAKa colocalises with myosin II to the cleavage furrow of dividing cells and the posterior of polarised, chemotaxing cells (Chung and Firtel, 1999). Moreover Chung et al. proved that during chemotaxis, Akt/PKB activates PAKa by phosphorylation and mediates its proper subcellular localisation (Chung et al., 2001). Akt/PKB is a PH domain-containing protein that translocates to the leading front in response to cAMP. Thus, activation by Akt/PKB links PAKa and myosin II assembly to PI3 kinase-regulated pathways responsible for establishment of cell polarity in response to chemoattractants (Chung et al., 2000).

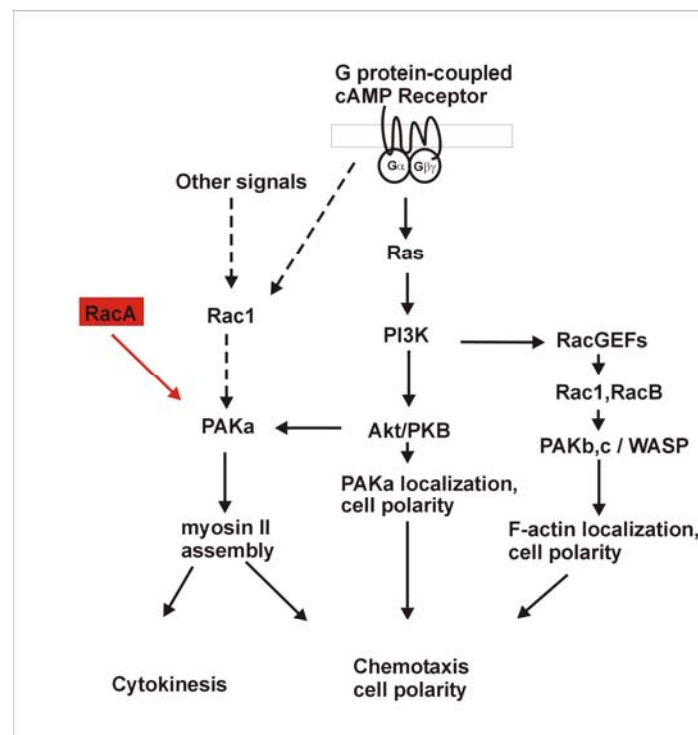


Figure 46: Model for the key role of PAKa in the control of the actin-cytoskeleton-depending processes, cytokinesis and chemotaxis, as proposed by Chung et al. 2001. RacA is placed working in concert with the Rac1 GTPases and in parallel with the Ras-PI3K-KB-pathway. PI3K probably plays a broader role in regulating subcellular structure and cell polarity. *pi3k1/2* null cells show a significantly greater loss of axial polarity than do myosin II or *paka* null cells, suggesting that there are multiple branch points in the pathways, thus PI3K having further effectors besides PKB, and PAKa.

Hence the conditional defects in growth, cell shape, F-actin distribution and the slight chemotaxis defect of RacA lacking cells could be explained by reduced activation of PAKa leading to reduced myosin II polymerisation. As speed and directionality reduction upon cAMP of RacA null cells is not as prominent as in PAKa and myosin II null cells, RacA might regulate PAKa in parallel to the PI3-kinase/PKB-pathway (Figure 46).

Furthermore neither PI3K1/2 nor PKB null cells exhibit cytokinesis defects, indicating that PI3K and PKB are not required for PAKa function in this process. Also Rac1 GTPases are assumed to regulate PAKa activity. Rac1 GTPases play a role in growth, motility, endocytosis, cytokinesis and development of *Dictyostelium*, all processes that depend on the re-organisation of the cortical actin cytoskeleton (Dumontier et al., 2000). Overexpression mutants of Rac1A, Rac1B and Rac1C all had identical phenotypes (Dumontier et al., 2000). Expression of constitutively activated forms of the Rac1 proteins resulted in an increase in the assembly of F-actin, while dominant negative forms had the opposite effect (Chung et al., 2000; Palmieri et al., 2000). The overexpression of the mutated Rac1 proteins resulted in a slight defect in cytokinesis when cells were grown in suspension, and activated Rac1 inhibited both phagocytosis and pinocytosis (Dumontier et al., 2000; Palmieri et al., 2000).

Thus the PAKa, myosin II, RacA and Rac1 mutant strains all reveal the conditional defect most probably caused by defective myosin II assembly leading to the destabilisation of the actin cytoskeleton. Gerald et al. showed that *Dictyostelium* cells have less overall F-actin in suspension compared to adherent conditions (Gerald et al., 1998). This is also the case for mammalian cells (Cunningham, 1995). Thus, an attachment-mediated signalling pathway exists that promotes the polymerisation of actin in both systems. Therefore, any mutation that causes a destabilisation of the cortex may be expressed differently in attached or suspended conditions. When the cells are adhered to a substrate, the increased level of F-actin may be sufficient to stabilise the cortex and suppress any phenotype. In suspended conditions, the reduced level of F-actin may enhance the defect in cortical organisation and result in an observable phenotype.

The observed cellular particles without nucleus in axenically grown RacA-KO cell culture might arise from reduced cortical tension also seen in myosin II cells. Bleb formation during cytokinesis due to reduced cortical tension has already been observed in cells lacking RacE cultured in suspension (Gerald et al., 1998). RacE null cells do not reveal a decreased F-actin content. Also RacA null cells normally perform F-actin-polymerisation upon camp stimulation. But as RacA null cells, cells lacking RacE contain abnormal F-actin aggregates. RacE function in organisation of the cortical cytoskeleton can, as noticed in RacA, PAKa and myosinII null cells, be bypassed by other signalling pathways induced by adhesion to a substrate.

The major impact of RacA might really be concentrated on its effector PAKa, as depicted in the model (Figure 46), or alternatively the phenotype of RacA-KO cells might in part or mainly arise by reduced stimulation of the other putative RacA effectors. In the first case, other Rac proteins, for instance RacB, might exert higher influence on the additional putative RacA effectors, presented in the next section.

Cells overexpressing activated PAKb are, like RacA-KO cells, unable to complete cytokinesis when grown in suspension. Additionally they exhibit increased rates of phagocytosis and pinocytosis (Lee et al., 2004). As PAKb null cells only revealed mild chemotaxis defects (DelaRoche et al., 2005), it is not probable that the influence of RacA ablation on PAKb activity is apparent, especially when considering that PAKb interacts with a bunch of Rac proteins: besides RacA, with Rac1a/b/c, RacB, RacC, and RacF1. In contrast to PAKa, PAKb is concentrated within the leading edge of migrating *Dictyostelium* cells, where it regulates the actin cytoskeleton via controlling the activity of myosin I isozymes (Jung et al., 1996; Monita et al., 1996; Novak et al., 1995; Novak and Titus, 1998). The opposing distributions of PAKa and PAKb strongly suggest that these two proteins do not have overlapping functions, at least in migrating cells. Moreover the strong phenotype of PakA null cells support the view that PAKa has unique cellular functions that cannot be compensated by PakB (Chung and Firtel, 1999; Chung et al., 2001).

The lack of phenotype of PAKb null cells can be explained with redundant function of other *Dictyostelium* protein kinases. For this, PAKc might be a probable candidate. Cells disrupted in the gene encoding PAKc exhibit a loss in polarity and produce multiple lateral pseudopodia when placed in a chemoattractant gradient. *pakB/pakC* doubly disrupted strains exhibit a severe loss of cell movement, suggesting that PAKb and PAKc have cooperative effects (Lee et al., 2003). Both kinases might be mainly regulated by RacB, as RacB-KO cells exhibit defects in chemotaxis and the associated F-actin polymerisation (Park et al., 2004). Ablation of RacB was accompanied by reductions in the activation of PAKc (Park et al., 2004). Consistent with this result, binding studies have indicated that PAKc preferentially interacts with RacB (Lee et al., 2003). Lee et al. proposed that RacB is normally involved in the control of cortical actin polymerisation, as cells overexpressing dominant negative RacB appeared morphologically normal, while cells overexpressing RacB-WT became flattened. Furthermore, most of the cells expressing constitutively active RacB became detached from the substrate. In the same study it was shown that RacB was activated upon chemoattractant stimulation and that this activation was partially controlled by PI3 kinase.

PI3Ks are principal regulators of cell motility and polarity (Funamoto et al., 2001; Funamoto et al., 2002) acting through their products (such as PIP₃) that bind to the PH

(Pleckstrin Homology) domain of PKB and thus recruit PKB to the plasma membrane. Most RacGEFs also contain PIP₃-binding PH domains, allowing PI3Ks to couple to Rac activation. Upon PIP₃ production WASP as well is recruited to the plasma membrane. WASP is activated by signalling pathways through the binding of GTP-bound Rac/Cdc42 to the PBD, resulting in a conformational change, which leads to activation of the Arp2/3 complex followed by F-actin-polymerisation. These steps enable the cells to move, as Myers et al. reported. They suggest that the spatial and temporal control of WASP localisation and activation is essential for the regulation of directional motility (Myers et al., 2005).

So PAKb, PAKc and WASP might parallel the two-branched PAKa signal transduction cascade, either sharing one branch with PAKa when responding to rather conditional stimuli with cell polarisation and movement or more probably acting in this function in a different subcellular localisation and regulating different effectors.

In summary a model, in which RacA can be added to Rac1 GTPases as a regulator of PAKa activity working in parallel to the PI3-kinase/PKB pathway that elicits PAKa, PAKb, PAKc and WASP activity upon chemoattractant stimulation, can be assumed. By lowering the myosin II assembly via PAKa, absence of RacA disturbs the actin cytoskeleton leading to defective cytokinesis, chemotaxis and cell shape. Whether PAKa regulation by RacA is mediated by controlling its protein level or the normal mechanism of GTPases, acting as molecular switch, remains to be elucidated. Therefore the search for interaction partners complemented by localisation studies with the GFP-RacA fusion protein overexpressors and analysis of their F-actin organisation have to be continued.

2 RacH is a regulator of endocytosis and depends in this function on its subcellular localisation

2.1 Role of RacH in endocytosis

2.1.1 Observations leading to a detailed analysis of endocytosis

The localisation of RacH at membranes of the ER and Golgi apparatus along with the defects in endo- and exocytosis observed in a RacH deficient strain and the ability of RacH to induce actin polymerisation (Somesh, 2002) suggests a role for RacH in vesicle trafficking mediated by

regulating the actin cytoskeleton. The severe defects in growth, phago- and pinocytosis observed in RacH-WT cells might be RacH-specific as RacH Δ ins overexpressing strains, yielding RacH without its specific effector site, do not show the defects of RacH-WT overexpressors. However expression levels of RacH-WT were very high and thus might give rise to artefacts. Results from overexpressors have to be interpreted very cautiously. So in this study the striking RacH-WT behaviour was rather taken as a hint for probable RacH function. The role of RacH in those processes was further elucidated by RacH-KO studies on a RacH deficient strain. This strain showed a 50% decrease in fluid phase uptake and a moderate exocytosis defect. In order to further define the function of RacH in endocytosis we analysed this process more closely in the RacH deficient strain.

2.1.2 Impact of RacH on early endocytosis

In summary endocytosis in RacH deficient cells differed from the wild type strain in several aspects. RacH-KO cells showed deficient acidification of early endosomes, a process driven by accumulation of vacuolar V(H⁺)-ATPase. Lack of RacH causes the distortion of the post-lysosomal compartment of *Dictyostelium*, marked by vacuolin. Additionally RacH-KO cells secreted lower amounts of acid phosphatase in the presence of sucrose. Finally exocytosis was slightly impaired in RacH deficient cells. As RacH-KO cells showed decreased fluid phase uptake and exocytosis rates, divergent endosomal pH and a different pattern of the neutral compartment, RacH-KO reveals defects in all four steps of the endocytic pathway (see Introduction 1.4). However the localisation of the major part of RacH at the Golgi and the ER and the inability of the RacH-KO strain to acidify early endosomes, imply a role in early vesicle processing triggering the defects apparent in later stages. For instance the slight delay in exocytosis could be provoked by incomplete digestion due to unsuitable pH. Since targeting of RacH to the plasma membrane (RacH-chim mutant), while stimulating the formation of filopods, does not elicit any alteration in fluid phase uptake or release, we assume that in RacH-KO cells the by 50% reduced fluid uptake and the moderate exocytosis defect cannot be attributed to the fraction of RacH that appears to localise at the plasma membrane. We suggest that the defect arises due to alterations in trafficking away from the plasma membrane rather than to deficient signalling at this location and we assume that the main function of RacH in early endocytosis might be the retrograde transport (recycling) of lysosomal enzymes and proton pumps from the later endosomes to the newly formed ones. This is in contrast to Rho GTPases that regulate the initial phase of endocytosis by acting at the plasma membrane, like the well established Rac1

and RhoA in mammalian cells (Qualmann and Mellor, 2003; Symons and Rusk, 2003) and presumably RacF1, Rac1, RacC and RacG in *Dictyostelium* (Dumontier et al., 2000; Palmieri et al., 2000; Rivero et al., 1998; Seastone et al., 1998).

The roles of Rac1, Cdc42 and RhoA in the initial phase of endocytosis at the plasma membrane in mammalian cells is well established, particularly during phagocytosis and clathrin-independent internalisation, although there is also evidence for a regulatory role in clathrin-mediated endocytosis. However, the actions of Rho GTPases are not restricted to the plasma membrane. Diverse studies point to a function of specific Rho GTPases in endocytic trafficking pathways in intracellular compartments. For example, RhoD regulates the motility of early endosomes (Randazzo, 2003), whereas RhoB is involved in transport to lysosomes (Gasman et al., 2003). Cdc42 also functions at the Golgi apparatus, where it is recruited through interaction with the COPI vesicle coat protein coatamer and triggers Arp2/3-dependent actin assembly (Luna et al., 2002).

Clarke et al. (Clarke et al., 2002) have shown that in *Dictyostelium* most of the proton pumps delivered to a new endosome are retrieved from late endosomes. This might be one of the roles of RacH. The overall protein level of Vata, a component of the V(H⁺)-ATPase, in RacH-KO cells was not affected. This was not surprising as 90% of the proton pump is localised on vesicles of the contractile vacuole system, a compartment that does not exchange membranes with the endolysosomal compartment.

The lower amounts of secreted acid phosphatase observed in RacH-KO cells in the presence of sucrose might be related to a deficient acidification of endosomes: previous reports in *Acanthamoeba* indicated that hydrolase transport and secretion is pH-dependent (Hohman and Bowers., 1986). In addition the divergent phosphatase secretion pronounces the role of RacH in the delivery of early endosomes. Souza et al. revealed that two classes of lysosomal enzymes are delivered to endosomes with different time courses. The first class (those modified with N-acetylglucosamine-1-phosphate residues; e.g. phosphatases and proteinases) was found in endosomes after about 3 minutes, whereas the second (those modified with mannose-6-phosphate residues; e.g., α -mannosidase and β -glucosidase) was found in endosomes after about 15 minutes.

2.1.3 Disturbance of the post-lysosomal system in RacH deficient cells

The post-lysosomal system is characterised by its marker vacuolin. Vacuolin, which exists as two isoforms, is a member of the PHB (prohibitin homology) domain family that also includes flotillins and related proteins of higher eukaryotes frequently associated to lipid rafts (Morrow and

Parton, 2005). While vacuolin A is dispensable, disruption of vacuolin B results in markedly impaired exocytosis, enlargement of the neutral post-lysosomal compartment and accumulation of fluid phase marker (Hacker et al., 1997; Jenne et al., 1998; Rauchenberger et al., 1997). Due to this observation it was speculated that by neutralisation of the vesicle, vacuolin can associate with the vesicle membrane to prevent further cycling and homotypic fusion. Except of a moderate exocytosis defect, none of the defects, revealed by vacuolin deficient cells, could be observed in *RacH*-KO cells, suggesting that in spite of its altered distribution, function of vacuolin is not affected and suggesting that the perturbed vacuolin pattern is caused by defects at earlier stages of endocytosis. As vacuolin association at the endosomal membranes occurs upon neutralisation and endosomes in *RacH*-KO cells gain a neutral pH earlier in comparison to *Ax2*, one can speculate that this leads to vacuolin association prior to major endosomal fusion, causing the dispersed pattern of small vacuolin-marked post-lysosomes. More exactly, first coronin re-associates with vacuole membranes at the beginning of this neutral phase and thus the signal that directs coronin to these vacuoles could be linked to a pH change in the lumen of the vesicle. One endosomal coat protein for which pH-dependent membrane binding has been described is β -COP (Aniento and Gruenberg, 1995). Both proteins, coronin as well as β -COP, contain WD-repeats, leading Rauchenberger et al. to speculate that the motif might act as a target of a pH-sensor protein. Coronin re-association is accompanied by Scar and Arp2/3, which act together to provide the endosome with a coat of filamentous actin. Major changes in the composition of membrane lipids in the course of the neutral phase have been described (Nolta et al., 1994). Such changes could favour the binding of vacuolin to the late vacuoles, either directly or mediated by another protein, resulting in gradual replacement of coronin.

Prior to vacuolin association homotypic fusion reduces the number of endosomes in the endocytic pathway to about 10–20 per cell. The process is under control of PI 3-kinases and protein kinase B (Rupper et al., 2001), and requires the protein *rtoA* that may act as a vesicle tethering protein (Brazill et al., 2000). In the respective mutants, particles or other endocytosed markers remain in individual, small endosomes throughout endocytic transit thus revealing a vacuolin pattern that resembles the one observed in the *RacH*-KO cells. Hence *RacH* might act through PI 3-kinase and protein kinase B mediated signal transduction coordinating the actin cytoskeleton. Conflicting with this assumption is that in *ddpik1/2* cells, lacking two of the three PI 3-kinases of *Dictyostelium*, endosomal pH is increased (Buczynski et al., 1997; Rupper et al., 2001). Thus *RacH* might act in a complementary signal transduction cascade to the cytoskeleton, both of them necessary for tuning endocytosis appropriately. Otherwise *RacH* might just partly mediate the effects elicited by PI 3-kinase. Anyhow the correspondence in phenotype of Δ *ddpik1/ddpik2* and *RacH*-KO cells, impaired growth in axenic culture

accompanied with smaller and more irregular size, impaired pino- but normal phagocytosis and lack of large postlysosomal vacuoles is conspicuous (Buczynski et al., 1997). Li et al. (1995) proposed that a PI 3-kinase regulates the fusion of early vesicles by activation of Rab5 in mammalian cells (Li and D'Souza-Schorey, 1995). In *Dictyostelium* no Rab5 encoding gene has been isolated (Bush et al., 1994). It has been shown that a Rab4-like GTPase (named RabD) regulates lysosome to postlysosome transport (Bush et al., 1994). Thus one model is assumable that Rab5 function in mammalian cells is carried out by RacH in *Dictyostelium*.

2.1.4 RacH might affect endocytosis by regulating the actin cytoskeleton

Besides the fact that RacH induces actin polymerisation, the hypothesis that RacH has an impact on endocytosis through the actin cytoskeleton is supported by the following studies: the progression of endocytic marker from a late endosomal to a lysosomal stage in mammalian cells or from acidic to neutral phase in *Dictyostelium* can be disrupted with cytochalasin (Durrbach et al., 1996; vanDeurs et al., 1995) and thus depends on the F-actin cytoskeleton. Furthermore treatment with different actin-depolymerising agents has shown that minor depolymerisation of the actin cytoskeleton can stimulate vesicle budding. Greater depolymerisation of actin was found to prevent budding of clathrin-coated vesicles, suggesting that local remodelling of the actin cytoskeleton (i.e. a combination of polymerisation and depolymerisation) is required for proper endosome processing (Lamaze, 1997). Additionally it has been reported that the Golgi membranes nucleate and polymerise actin as do phagosomes (Valderrama et al., 2000), endosomes and lysosomes (Taunton et al., 2000). This could represent the site of action of RacH. Evidence towards an actin-cytoskeleton regulating function of RacH is provided by the similarities of the phenotypes with RacH deficient cells observed in cells lacking the following regulators of the actin cytoskeleton: myosin Ib, coronin and CAP (cyclase-associated protein, regulator of the G-actin/F-actin ratio). Coronin-null mutants show strongly reduced rates of fluid-phase uptake by macropinocytosis as do *myoA⁻B⁻* double mutants. Furthermore, *myoA⁻B⁻* mutants possess numerous small vesicles and a reduced growth rate in axenic culture (Novak et al., 1995). Sultana et al. (2005) showed that CAP is essential for maintaining the structural organisation, integrity and functioning of the endolysosomal system, as distribution and morphology of V(H⁺)-ATPase-decorated membranes and the post-lysosomal vesicles were disturbed in cells lacking functional CAP accompanied by an increased endosomal pH (Sultana et al., 2005). Here also, the post-lysosomal system consisted of many small-sized vesicles. Furthermore it was reported that CAP is associated with Rab GTPases (Sultana et al., 2005).

However, CAP seems to have an overall function in the structural organisation of the endolysosomal system and probably also in the contractile vacuolar system. CAP might act more directly *and*, although this sounds contradictory, more generally, as it shows, in comparison to RacH, a much higher degree of co-localisation to the early and late endolysosomal system, represented by the markers VataA and vacuolin, respectively, and interacts directly with the V(H⁺)-ATPase (Sultana et al., 2005). The common feature of the CAP and RacH null mutants, the disturbed postlysosomal system, might be only elicited by increased endosomal pH.

2.1.5 RacH localisation points to its function in endocytosis and its effectors

The diversity of localisation matches the diversity of function reported for the Rho family of proteins. In some cases localisation suggests function. For example, the ER and Golgi localisation of Cdc42 is consistent with its ability to bind γ COP and regulate ER to Golgi transport (Wu et al., 2000). The mechanism of RacH action is not clear at the moment. Localised as Cdc42 at the Golgi and ER, RacH could be involved in vesicle transport within and from the Golgi apparatus by promoting actin-driven vesicle movement as it is well established that progression of vesicles along the endocytic pathway depends on actin (Drengk et al., 2003; Jenne et al., 1998; Luna et al., 2002). However, RacH does not interact with WASP or any other effector carrying a CRIB domain ((DelaRoche et al., 2005; Park et al., 2004) and our unpublished observations). RacH also does not interact with IQGAP-related proteins (our unpublished observations), which have been reported to associate with Cdc42 at Golgi membranes (McCallum et al., 1998). In mammalian cells RhoD regulates motility of early endosomes through interaction with a Diaphanous-related formin (Gasman et al., 2003). Therefore formins may constitute a candidate family of RacH effectors to be addressed in future studies. In particular the finding that formins can nucleate actin polymerisation, providing a second parallel pathway to activation of the Arp2/3 complex, is thereby of interest (Chang and Peter, 2002).

The specific involvement of several Rho proteins at particular stages of vesicular trafficking in correlation with their different localisation at membrane compartments is strongly verified for mammalian cells (Qualmann and Mellor, 2003; Symons and Rusk, 2003). In analogy, it is also most probable that RacH, which localises to inner membranes, regulates a specific process of endocytic pathway enabling regular endosomal progression.

2.1.6 RacH function is restricted to endocytosis

The impact of RacH function seems to be limited to endocytic processes and thus the vesicular pattern. Development and cytokinesis were not affected in the RacH-mutants. The slight reduction in cell motility of RacH-KO cells could be a result of the impaired membrane flow from the endosomes back to the plasma membrane. Membrane flow models for cell locomotion, in which the advance of the leading edge is provided by membrane from internal pools, have been proposed (Bretscher, 1996). Aguado-Velasco et al. proved that the endocytic cycle of Ax2 cells appears capable of delivering sufficient membrane surface area to advance the cells' fronts during migration.

2.2 Determinants of RacH targeting

Besides elucidating the role of RacH in endocytosis we analysed the importance of the CAAX motif and the second signal in the hypervariable region close to the CAAX motif for targeting and functionality of *Dictyostelium* RacH. As previously emphasised, RacH is predominantly cytosolic, but 40% of the protein is targeted to the perinuclear region, Golgi apparatus and ER, closely resembling the behaviour of human Cdc42 and Rac2 (Michaelson et al., 2001). We initially attributed this localisation of RacH to lack of a functional second signal: negatively charged residues in this region lower the net positive charge to +2 (Figure 40). It has been shown that a net positive charge of four or more is required to target K-ras4B to the plasma membrane (Hancock et al., 1990; Hancock et al., 1991) and indeed human Cdc42 and Rac2, which have a weak polybasic region, are targeted predominantly to internal membranes (Michaelson et al., 2001). By contrast, in those *Dictyostelium* Rho GTPases that are targeted to the plasma membrane, like Rac1a/1b/1c (Dumontier et al., 2000), RacC (Larochelle et al., 1997), RacE (Larochelle et al., 1996), RacF1 (Rivero et al., 1998) and RacG, the hypervariable region has charges that range from +4 to +8, similar to human Rac1 (Michaelson et al., 2001). Chimeric constructs of RacG and RacH in which the C-terminal region was exchanged appeared to confirm the role of the net positive charge of the hypervariable region: the RacH chimeric construct was targeted to the plasma membrane, whereas the RacG chimeric construct was retained at endomembranes. This is in line with the results obtained with human Cdc42 and TC10 (a Cdc42-related GTPase). TC10 possesses both a palmitoylation signal and a polybasic stretch and localises on the plasma membrane and on endosomes. A chimeric construct in which the C-terminal 20 amino acids were replaced by the homologous region of Cdc42 displayed a localisation identical to Cdc42 (Michaelson et al., 2001). These and other results

reported by Michaelson et al. led to propose that subcellular localisation of Rho GTPases is determined primarily by the hypervariable region and by the capacity to bind RhoGDI. A role for RhoGDI in the localisation of RacG or RacH, however, can be excluded, because neither of both proteins interacts with RhoGDI (Rivero et al., 2002). A more detailed analysis using alanine exchange mutants revealed that further sequences upstream of the polybasic region within the 38 residues exchanged in the chimeric mutants contribute to targeting of RacH: the RacH-4Ala and the RacG-chim-4Ala mutants, although carrying a net positive charge of +6, were still substantially retained at endomembranes.

One more determinant of the subcellular localisation of RacH appears to be the insert region. Although this region does not change conformation upon activation, in combination with the effector domain it contributes to determine the specificity of interactions of Rho GTPases (Feltham et al., 1997). For example, although not required for binding to, it is required for activation of the NADPH oxidase complex by Rac (Freeman et al., 1996) or phospholipase D1 by Cdc42. The specificity of interactions of Rho GTPases with its effectors is also demonstrated by the severe cytokinesis defect of RacE null cells. Neither RacC overexpression, which is as RacE localised to the plasma membrane, nor RacE/RacC chimeras could correct the defect. This result strongly suggests that RacE must undergo highly specific protein interactions independent from its carboxyl terminus (Larochelle et al., 1997).

Altogether our results indicate that regions other than the hypervariable region are responsible for proper targeting of Rho GTPases, and this might be a more general principle applicable to lipid-modified GTPases of the Ras superfamily, as has been shown recently for Rab GTPases in an extensive study (Ali et al., 2004). GTPases lacking this targeting information might be retained at the ER and Golgi membranes as default localisation.

2.3 Proper targeting of RacH is required for function

The fact that RacG and RacH display radically different subcellular localisations and play different roles was exploited to investigate to which extent targeting of the GTPase to a particular region or compartment determines its biological functions. RacG regulates mainly processes that require actin remodeling at the cell cortex: overexpression of RacG elicits extension of filopods, stimulates particle uptake and impairs chemotaxis (Somesh, 2002). Targeting of RacH to the plasma membrane was accompanied by extension of filopods and impaired F-actin response to cAMP but fairly normal chemotactic response. By contrast, targeting of RacG to internal membranes impaired phagocytosis but had no effect on the rate of growth and pinocytosis or on

cytokinesis, which are severely affected in RacH-WT cells. This indicates that RacH is able to interact with effectors and/or regulatory elements of other Rho GTPases at the plasma membrane, but is prevented of doing so by retention at inner membrane compartments. Whereas the phenotype elicited by overexpression of RacH is strongly dependent on its subcellular localisation and its local effectors as the studies with the chimeras and RacH Δ ins revealed. The mutants do not recapitulate any of the phenotypes elicited by overexpression of RacH-WT. Reports that address the importance of membrane targeting of Rab GTPases also underscore our conclusion. Rab27a, a protein that associates specifically with melanosomes, did not rescue the coat color phenotype of a Rab27a null mouse when mistargeted to the ER (Gomes et al., 2003), and in yeast mistargeted lipid tail variants of two essential Rab proteins, Ypt1p and Sec4p, were not able to complement thermosensitive alleles of the respective gene (Calero et al., 2003).

Summary / Zusammenfassung

In this study, we investigated the functions of the two Rho GTPases RacA and RacH in *Dictyostelium discoideum*. Both genes are constitutively expressed and mRNA and protein are present throughout the complete developmental cycle of *Dictyostelium*. RacA belongs to the subfamily of Rho BTB proteins that are characterised by a modular organisation, consisting of a GTPase domain, a proline-rich region, a tandem of two BTB domains and a C-terminal region of unknown function. Thus RacA promises to be both, a highly specific adaptor molecule thanks to its BTB domains, and a regulator of signal transduction due to its GTPase domain. The particularity about RacH is that, in contrast to the other characterised Rho GTPases residing at the plasma membrane, RacH was targeted to the nuclear envelope, ER and Golgi apparatus. The pivotal process regulated by Rho GTPases is the rearrangement of the actin cytoskeleton. Therefore we investigated the role of RacA and RacH in cytoskeleton-dependent processes by analysing the performance of the respective knock out mutants in processes depending on the re-organisation of the cortical actin cytoskeleton.

RacA-KO cells show conditional defects when cultured in suspension: they are severely impaired in growth, cytokinesis and cell shape probably due to lowered cortical tension and F-actin distribution and reveal a slight chemotactical defect as well as reduced rates of pinocytosis and phagocytosis. Considering the correspondence in phenotypes of cells lacking either RacA, PAKa or myosin II and the PAKa-binding by RacA, a model in which RacA acts in concert with Rac1 GTPases as a regulator of PAKa activity working in parallel to the PI3-kinase/PKB pathway that elicits PAKa activity upon chemoattractant stimulation, is proposed. Moreover putative RacA binding partners have been identified.

Cells deficient in RacH have a decreased rate of fluid phase endocytosis and exocytosis and a divergent performance in the endocytosis process in comparison to the WT, but no other apparent defects. In a cell-free system RacH stimulated actin polymerisation, suggesting that it might be involved in actin-based trafficking of vesicular compartments, more specifically in the delivery of cargo to early endosomes. The lack of RacH causes defective early endocytosis leading to defects also observed at later stages of this process. By means of chimeric constructs and alanine exchange mutants it was also shown that several regions of the molecule, not only the hypervariable region, determine targeting of RacH and that targeting to the correct membrane compartment probably makes interactions with appropriate regulators and effectors possible, and is therefore essential for function.

In dieser Studie wurden die Funktionen der beiden Rho GTPasen RacA und RacH in *Dictyostelium discoideum* untersucht. Beide Proteine werden konstitutiv, auf Transkriptions- und Proteinebene, während des gesamten Entwicklungszyklus von *Dictyostelium* exprimiert. RacA gehört der RhoBTB Unterfamilie der Rho GTPasen an, die eine charakteristische modulare Organisation bestehend aus einer GTPase Domäne, einer Prolin-reichen Region, zwei aufeinanderfolgenden BTB-Domänen und einer C-terminalen Region unbekannter Funktion aufweist. Aufgrund dieser Organisation verspricht RacA mittels der BTB-Domäne sowohl ein hoch spezifisches Adapter-Molekül, als auch dank der GTPase-Domäne ein Regulator-Molekül eines Signaltransduktionsweges zu sein. RacH unterscheidet sich von den bisherigen charakterisierten Rho GTPasen in *Dictyostelium discoideum* durch seine Lokalisierung an Endomembranen des ER und des Golgi-Apparates. Die Hauptaufgabe der Rho GTPasen, die Regulierung des Actin-Zytoskeletts, wurde hier im Fall von RacA und RacH untersucht, indem man das Verhalten von Stämmen, denen die jeweilige GTPase fehlte (KO-Stämme), in zytoskelettabhängigen Prozessen untersuchte.

Kultiviert in Suspension wiesen RacA-KO Zellen konditionale Defekte auf: sie sind schwerwiegend an normalem Wachstum, Zytokinese, Zellform - wahrscheinlich bedingt durch verminderte kortikale Spannung - und F-Aktin Verteilung gehindert. Außerdem weisen sie leichte Defizite in Chemotaxis, Pino- und Phagozytose auf. Berücksichtigt man die Übereinstimmung der Phänotypen von RacA, PAKa und Myosin II defizienten Zellen und die Interaktion von PAKa und RacA, kann man ein Modell für die Regulierung des Zytoskeletts durch RacA aufstellen: RacA aktiviert wie die Rac1 GTPasen PAKa. Außerdem wird PAKa parallel noch durch einen cAMP-abhängigen Signaltransduktionweg über PI3K und PKB reguliert. Wenn also die RacA-bedingte Stimulation von PAKa aufgrund des Fehlens von RacA ausfällt, führt dies zu verminderter Myosin II Zusammenlagerung, die Abnormalitäten in Zytokinese, Chemotaxis und Zellform mit sich führt.

RacH-KO Zellen weisen verminderte Endo- und Exozytoseraten und ein vom WT abweichendes Endozytoseverhalten auf, jedoch keine weiteren Defekte. In einem Zell-freien System stimuliert Rac Aktin-Polymerisierung, was darauf hinweist, daß RacH am Aktin-vermittelten Vesikeltransport mitwirkt; genauer an der Belieferung früher Endosomen. Fehlt RacH führt das zu fehlerhafter früher Endozytose, die sich auf spätere Stadien auswirkt. Mit Hilfe von chimären Konstrukten und Alanin-Austausch Mutanten konnte nachgewiesen werden, daß neben der hypervariablen Region weitere Regionen die zelluläre Lokalisation von RacH bedingen. Außerdem konnte gezeigt werden, daß die korrekte zelluläre Lokalisation Interaktionen mit geeigneten Regulatoren und Effektoren ermöglicht und somit essentiell für die Funktion von RacH ist.

Appendix

Table 5: Oligonucleotides designed for the different applications of this work.

Group	Name	Sequence	
GFP-RacA overexpressors	RacA P fwdB	<u>GGATCCTCAAATCATCAGAGAAAGCAGTACCAATTCC</u>	
	RacAuni/BN	<u>GGATCCCATATGCAAGCAATTAATAGTAGTAGTAGG</u>	
	RacA rev/B	<u>GGATCCTTATTTTTAAACCAACCTTTTGAAGAAC</u>	
	RacA(V12) fwdB	<u>GGATCCATGCAAGCAATTAATAGTAGTAGTAGGGTATGTTG</u> CTG	
	RacAGTPase rev/R	<u>GAATTCAGATGCTGAGCATAATATAACACGATGTGC</u>	
	RacA-CAAX rev/B	<u>GGGATCCTTACATTATAATACATCCACCCTTTTTTTAGCTGA</u> TGC	
	RacA P fwdB	<u>GGATCCTCAAATCATCAGAGAAAGCAGTACCAATTCC</u>	
	RacA B1 fwd B	<u>GGATCCATGGATATTATTACAAGTTCTTATGATAAAGAGATG</u>	
	RacA B1 fwdN	<u>CCATGGATATTATTACAAGTTCTTATGATAAAGAGATG</u>	
	RacA B1 revB	<u>GGATCCTTAAAGTAAAGAATAGCTCTTTACTAGTTTC</u>	
	RacA-B2-fwdB	<u>GGATTCATGGGCACTTTCTTAAATGACCAA</u>	
	RacA B2 rev/B	<u>GGATCCTTACAACCTCCGATCTGAAAATACCAATTG</u>	
	RacA C fwdB	<u>GGATCCATGGGTATTTTCAGATCGGAGTTGG</u>	
	RacA-Ko screen	B1 fwd	<u>GGATCCATTATTACAAGTTCTTATGATAAAGAGATG</u>
		B1 rev	<u>GGATCCTTAAAGTAAAGAATAGCTCTTTACTAGTTTC</u>
	Cullin yeast-2-Hybrid	Cul A E fwd	<u>GAATTCAAAATGTCAATGATGACAAGTACACCAACC</u>
Cul A Xrev		<u>CTCGAGTTAATGAGCCAATTGTTTTCTCATTTCATG</u>	
Cul III N41 fwd Xmal		<u>CCCGGGAATTC AAGAAATCCAGCGTAAGAATAAC</u>	
Cul III Srev		<u>GAGCTCTTAAGCCATATAATTATAAATCTTCTG</u>	
Cul IV 1Nfwd		<u>CCATGGAACCATTAACGAATAGTTTAGCAGGTAC</u>	
Cul IV 1rev		<u>CCATGGAACCATTAACGAATAGTTTAGCAGGTAC</u>	
Cul IV 2fwd		<u>CGGTTAAATCAATTTGGGATTTAGG</u>	
Cul IV 2Xrev		<u>CTCGAGTTAAGCCATGTAATTATATATCATCATTGC</u>	
CulVN fwd		<u>CCATGGAAATGTCAGATCAAATAACAGTTGATGAG</u>	
Cul V1rev		<u>GGCGAATTGTTCTTGTAATTGC</u>	
Cul V2 fwd		<u>CCAATCGTGCAATCAATACATGCCG</u>	
CulVX rev		<u>CTCGAGTTAAGCCATATATTCATATTTTCTTGC</u>	
RT-PCR/Antibodies		RacA-B1-revP	<u>CTGCAGTTAAGTAAAGAATAGCTCTTTACTAGTTTCAC</u>
		RacA-B2-revP	<u>CTGCAGTTACAACCTCCGATCTGAAAATACCCTGCAG</u>
Cullin-N-terminal expression in Dd		RacA-revP	<u>CTGCAGTTATTTTTAAACCAACCTTTTGAAGAAC</u>
		CulAE fwd	<u>GAATTCAAAATGTCAATGATGACAAGTACACCAACC</u>
NTAP-vector	CulAshortErev	<u>AGATCTTTATGTGAGTTTTAATAATTGTGACATATG</u>	
	CulBshortE fwd	<u>GAATTCATGATGAATGGATTGGGTAGACAAGATATTGATTC</u>	
	CulBshortE rev	<u>AGATCTTTAACAACCAGAAAAGAATAATTTCCATTG</u>	
	Cul III E fwd	<u>GAATTCAAAATGATGGCAAAACCAAATGG</u>	
	Cul III Eshortrev	<u>AGATCTTTACATTGAAGTCTTGTGATTGATCC</u>	
	Cul IV Eshortfwd	<u>GAATTCATGCCATTAACGAATAGTTTAGCAGGTACACCA</u>	
	Cul IV Eshortrev	<u>AGATCTTTAACTTTGATTTGTATGATCTTTCCAAATTGAATTTAT</u> AG	
	Cul V Eshortfwd	<u>GAATTCAAAATGTCAGATCAAATAACAGTTGATGAG</u>	
	Cul V Eshortrev	<u>AGATCTTTAACTTGACATCTTCCACTCATTCCATTG</u>	
	RacAXb fwd	<u>TCTAGACATATGCAAGCAATTAATAGTAGTAGTAGG</u>	
	RacAXb rev	<u>TCTAGATTATTTTTAAACCAACCTTTTGAAGAAC</u>	
	RacH rev2 Ala	<u>CCTTTGAGTCTTTAGCACCTTTTTTAGAGGCTTTTTTTG</u>	
	RacH mutagenesis	RacH rev3 Ala	<u>GAATTCATTATTGTATTATACAAGCCTTTGAGGCTTTAGCACC</u>
		RacHΔins fwd	<u>TTAGATCTTCGTGGTGAAGTTACACCAGAAATGGGTG</u>
		RacHΔins rev	<u>GTAAC TTCACCACGAAGATCTAATTTAGTTCCAAC</u>
		PT7 fwd	<u>ATACGACTCACTATAGGGAG</u>
Sequencing/ orientation check	MB38 fwd	<u>GTGAAAGTCGAGCTCGGTACCC</u>	
	M13 reverse	<u>CAGGAAACAGCTATGAC</u>	
	SP6 universal	<u>ATTTAGGTGACACTATAG</u>	
	T7 universal	<u>TAATACGACTCACTATAGGG</u>	

*Sequence is shown from 5' to 3' end. Restriction enzyme sites are underlined, complementary sequences of a pair of primers used for deletion mutagenesis are shown in *italics*.

Table 5: cDNA-clones from the National Institute of Genetics, Japan used as PCR-templates for cullin vector construction. If two clones were available, the one used as template is highlighted in red. In the case of Cul IV and V the largest part of the proteins was covered by the cDNA. The missing N-termini were generated by RT-PCR. The obtained PCR-products were designed such that they overlapped and could be fused by PCR.

Cullin clones	cDNA clone(s)
CulA cDNA	ddv44g23
CullIII	ddc54b16 ddv63f07
CullIV	RT, ddv1f23
CuIV	RT, ddc21e07, ddv24b09

Bibliography

Ahmad, K. F., Engel, C. K., and Prive., G. G. (1998). Crystal structure of the BTB domain from PLZF. *Proc Natl Acad Sci USA*, *95*, 12123–12128.

Ali, B. R., Wasmeier, C. R., Lamoreux, L., Strom, M., and Seabra., M. C. (2004). Multiple regions contribute to membrane targeting of Rab GTPases. *Journal of Cell Science* *117*, 6401-6412.

Aniento, F., and Gruenberg, J. (1995). Membrane-transport from early to late endosomes. *Cold Spring Harb Symp Quant Biol* *60*, 205-209.

Aravind, L., and Koonin, E. V. (1999). Fold prediction and evolutionary analysis of the POZ domain: structural and evolutionary relationship with the potassium channel tetramerization domain. *J Mol Biochem J* *285*, 1353–1361.

Aubry, L., Klein, G., Martiel, J. L., and Satre., M. (1994). Kinetics of endosomal pH evolution in *Dictyostelium discoideum* amoebae. Study by fluorescence spectroscopy. *J Cell Sci* *105*, 861-866.

Blaauw, M. M., Linskens, H. K., and Haastert., P. J. M. v. (2000). Efficient control of gene expression by a tetracycline-dependent transactivator in single *Dictyostelium discoideum* cells. *Gene* *252*, 71-82.

Bourne, H. R., Sanders, D. A., and McCormick., F. (1991). The GTPase superfamily: conserved structure and molecular mechanism. *Nature* *349*, 117-127.

Brazill, D. T., Caprette, D. R., Myler, H. A., Hatton, R. D., Ammann, R. D., Lindsey, D. F., ABrock, D., and Gomer., R. H. (2000). A protein containing a serine-rich domain with vesicle-fusing properties mediates cell-cycle dependent cytosolic pH regulation. *J Biol Chem* *275*, 19231–19240.

Bretscher, M. S. (1996). Getting membrane flow and the cytoskeleton to cooperate in moving cells. *Cell* *87*, 601-606.

Buczynski, G., Grove, B., Nomura, A., Kleve, M., Bush, M., AFirtel, R., and Cardelli., J. (1997). Inactivation of Two *Dictyostelium discoideum* Genes, DdPIK1 and DdPIK2, Encoding Proteins Related to Mammalian Phosphatidylinositide-3-kinases, Results in Defects in Endocytosis, Lysosome to Postlysosome Transort, and Actin Cytoskeleton Oganization. *THE JOURNAL OF CELL BIOLOGY* *136*, 1271-1286.

Bush, J., Nolta, K., Rodriguez-Paris, J., Kaufmann, N., O'Halloran, T., Ruscetti, T., Temesvari, L., Steck, T., and Cardelli., J. (1994). A Rab4-like GTPase in *Dictyostelium discoideum* colocalizes with V-H(+)-ATPases in reticular membranes of the contractile vacuole complex and in lysosomes. *J Cell Sci* *107*, 2801-2812.

Calero, M. C., Chen, W., Zhu, N., Winand, K., Havas, P. M., Gilbert, C. G., Burd, G., and Collins., R. N. (2003). Dual prenylation is required for Rab protein localization and function. *Mol Biol Cell* *14*, 1852-1867.

-
- Chang, F., and Peter, M. (2002). Formins set the record straight. *Science* 297, 531-532.
- Chimini, G. a. C., P. (2000). Function of Rho family proteins in actin dynamics during phagocytosis and engulfment. *J Cell Biol*, 147, 559-575.
- Choy, E. V. K., Chiu, J., Silletti, M., Feoktsov, T., Morimoto, D., Michaelson, I. E., and Philips., M. R. (1999). Endomembrane trafficking of Ras: the CAAX motif targets proteins to the ER and Golgi. *Cell* 98, 69-80.
- Chung, C. Y., and Firtel, R. A. (1999). PAKa, a putative PAK family member, is required for cytokinesis and the regulation of the cytoskeleton in *Dictyostelium discoideum* cells during chemotaxis. *J Cell Biol*, 147, 559-575.
- Chung, C. Y., Lee, S., Briscoe, C., Ellsworth, C., and Firtel., R. A. (2000). Role of Rac in controlling the actin cytoskeleton and chemotaxis in motile cells. *Proc Natl Acad Sci USA*, 97, 5225-5230.
- Chung, C. Y., Potikyan, G., and Firtel., R. A. (2001). Control of cell polarity and chemotaxis by Akt/PKB and PI3 kinase through the regulation of PAKa. *Mol Cell* 7, 937-947.
- Clarke, M., Köler, J., Arana, Q., Liu, T., Heuser, J., and Gerisch., G. (2002). Dynamics of the vacuolar H⁺-ATPase in the contractile vacuole complex and the endosomal pathway of *Dictyostelium* cells. *Journal of Cell Science* 115, 2893-2905.
- Clow, P. A., and McNally, J. G. (1999). In vivo observations of myosin II dynamics support a role in rear retraction. *Mol Biol Cell* 10, 1309-1323.
- Cox, D., Chang, P., Zhang, Q., Reddy, P. G., Bokoch, G. M., and Greenberg., S. (1997). Requirement for both rac1 and cdc42 in membrane ruffling and phagocytosis in leukocytes. *JExp Med* 186, 1487-1494.
- Crean, E. V., and Rossomando, J. (1979). Effects of sugars on glycosidase secretion in *Dictyostelium discoideum*. 110, 315-322.
- Cunningham, C. C. (1995). Actin polymerization and intracellular solvent flow in cell surface blebbing. *J Cell Biol*, 129, :1589-1599.
- DelaRoche, Mahasneh, A., Lee, S., Rivero, F., and Cote., G. P. (2005). Cellular Distribution and Functions of Wild-Type and Constitutively Activated *Dictyostelium* PakB. *Molecular Biology of the Cell* 16.
- Deshaies, R. J. (1999). SCF and Cullin/Ring H2-based ubiquitin ligases. *Annu Rev Cell Dev Biol* 15, 435-467.
- Dimond, R. L., Burns, R. A., and Jordan., K. B. (1981). Secretion of lysosomal enzymes in the cellular slime mold, *Dictyostelium discoideum*. *J Biol Chem* 256, 6565-6572.

Drengk, A., Fritsch, J., Schmauch, C., Rühling, H., and Maniak., M. (2003). A coat of filamentous actin prevents clustering of late-endosomal vacuoles in vivo. *Curr Biol* 13, 1814-1819.

Du, W., Lebowitz, P. F., and Prendergast., G. C. (1999). Cell growth inhibition by farnesyltransferase inhibitors is mediated by gain of geranylgeranylated RhoB. *Mol Cell Biol* 33, 1831-1840.

Dumontier, M., Höcht, P., Mintert, U., and Faix., J. (2000). Rac1 GTPases control filopodia formation, cell motility, endocytosis, cytokinesis and development in *Dictyostelium*. *J Cell Sci* 113, 2253-2265.

Durrbach, A., Louvard, D., and Coudrier., E. (1996). Actin filaments facilitate two steps of endocytosis. *J Cell Science* 109, 457-465.

Eichinger, L., Pachebat, J. A., Glockner, G., and G, R. M., Suggang R, Berriman M, Song J, Olsen R, Szafranski K, Xu Q, Tunggal B, Kummerfeld S, Madera M, Konfortov BA, Rivero F, Bankier AT, Lehmann R, Hamlin N, Davies R, Gaudet P, Fey P, Pilcher K, Chen G, Saunders D, Sodergren E, Davis P, Kerhornou A, Nie X, Hall N, Anjard C, Hemphill L, Bason N, Farbrother P, Desany B, Just E, Morio T, Rost R, Churcher C, Cooper J, Haydock S, van Driessche N, Cronin A, Goodhead I, Muzny D, Mourier T, Pain A, Lu M, Harper D, Lindsay R, Hauser H, James K, Quiles M, Madan Babu M, Saito T, Buchrieser C, Wardroper A, Felder M, Thangavelu M, Johnson D, Knights A, Louseged H, Mungall K, Oliver K, Price C, Quail MA, Urushihara H, Hernandez J, Rabbinowitsch E, Steffen D, Sanders M, Ma J, Kohara Y, Sharp S, Simmonds M, Spiegler S, Tivey A, Sugano S, White B, Walker D, Woodward J, Winckler T, Tanaka Y, Shaulsky G, Schleicher M, Weinstock G, Rosenthal A, Cox EC, Chisholm RL, Gibbs R, Loomis WF, Platzer M, Kay RR, Williams J, Dear PH, Noegel AA, Barrell B, Kuspa A. (2005). The genome of the social amoeba *Dictyostelium discoideum*. *Nature* 435, 43-57.

Ellis, S., and Mellor, H. (2000). Regulation of endocytic traffic by Rho family GTPases. *Trends Cell Biol*, 10, 85-88.

Escalante, R., Wessels, W., Soll, D. R., and Loomis., W. F. (1997). Chemotaxis to cAMP and Slug Migration in *Dictyostelium* Both Depend on MigA, a BTB Protein. 8, 1763-1775.

Feltham, J. L., Dötsch, V., Raza, S., Manor, D., Cerione, R. A., Sutcliffe, M. J., Wagner, G., and Oswald., R. E. (1997). Definition of the switch surface in the solution structure of Cdc42Hs. *Biochemistry* 35, 8755-8766.

Freeman, J. L., Abo, A., and Lambeth., J. D. (1996). Rac "insert region" is a novel effector region that is implicated in the activation of NADPH oxidase, but not PAK65. *J Biol Chem* 271, 19794-19801.

Fukui, Y., Lozanne, A. D., and Spudich., J. A. (1990). Structure and function of the cytoskeleton of a *Dictyostelium* myosin-defective mutant. *J Biol Chem* 110, 367-378.

Funamoto, S. K., Milan, R., Meili, A., and Firtel., R. (2001). Role of PI3 kinase and a downstream PH domain-containing protein in controlling chemotaxis in *Dictyostelium*. *J Cell Biol*, 153, 795-809.

-
- Funamoto, S. R., Meili, S., Lee, L., Parry, L., and Firtel, R. (2002). Spatial and temporal regulation of 3-phosphoinositides by PI3-kinase and PTEN mediates chemotaxis. *Cell* 109, 611-623.
- Furukawa, M., He, Y. J., C, C. B., and Xiong., Y. (2003). Targeting of protein ubiquitination by BTB-Cullin 3-Roc1 ubiquitin ligases. *Nat Cell Biol* 5, 1001-1007.
- Gasman, S., Kalaidzidis, Y., and Zerial., M. (2003). RhoD regulates endosome dynamics through Diaphanous-related formin and Src tyrosine kinase. *Nature Cell Biol* 5, 195-204.
- Gerald, N., Dai, H. J., Ting-Beall, P., and Lozanne., A. D. (1998). A Role for Dictyostelium RacE in Cortical Tension and Cleavage Furrow Progression. *The Journal of Cell Biology* 141, 483-492.
- Gerisch, G., and Keller., H. U. (1981). Chemotactic reorientation of granulocytes stimulated with micropipettes containing fMet-Leu-Phe. *J Cell Sci* 52, 1-10.
- Geyer, R., Wee, S., Anderson, S., Yates, J., and Wolf., D. A. (2003). BTB/POZ domain proteins are putative substrate adaptors for cullin 3 ubiquitin ligases. *Mol Cell* 12, 783-790.
- Gomes, A. Q., Ali, J. S., Ramalho, R. F., Godfrey, F., Barral, D. C., Hume, A. N., and Seabra., M. C. (2003). membrane targeting of Rab GTPases is influenced by the prenylation motif. *Mol Biol Cell* 14, 1882-1899.
- Hacker, U., Albrecht, R., and Maniak., M. (1997). Fluid-phase uptake by macropinocytosis in Dictyostelium. *J Cell Sci* 110, 105-112.
- Hall, A. (1998). Rho GTPases and the actin cytoskeleton. *Science* 279, 509-514.
- Hanahan, D. (1983). Studies on transformation of Escherichia coli with plasmids. *J Mol Biol* 166, 557-580.
- Hancock, H. J., Paterson, J. H., and Marshall., C. J. (1990). A polybasic domain or palmytoilation is required in addition to the CAAX motif to localize p21ras to the plasma membrane. *Cell* 63, 133-139.
- Hancock, K., Cadwallade, J. F., Paterson, K., and Marshall., H. (1991). A CAAX or CAAL motif and a second signal are sufficient for plasma membrane targeting of ras proteins. *EMBO J* 10, 4033-4039.
- Hohman, T. C., and Bowers., B. (1986). Vacuolar pH is one factor that regulates hydrolase secretion. *Eur J Cell Biol*, 475-480.
- Insall, R., Muller-Taubenberger, A., Machesky, L., Kohler, J., Simmeth, E., Atkinson, S. J., Weber, I., and Gerisch., G. (2001). Dynamics of the Dictyostelium Arp2/3 complex in endocytosis, cytokinesis, and chemotaxis. *Cell Motil Cytoskeleton* 50, 115-128.
- Jay, P. Y., Pham, P. A., Wong, S. A., and Elson., E. L. (1995). A mechanical function of myosin II in cell motility. *J Cell Science* 108, 387-393.

-
- Jenne, H. R., Rauchenberger, R., Hacker, U., Kast, T., and Maniak., M. (1998). Targeted gene disruption reveals a role for vacuolin B in the late endocytic pathway and exocytosis. *J Cell Sci* 111, 61-70.
- Jung, G., Wu, X., and Hammer., J. A. (1996). Dictyostelium mutants lacking multiple classic myosin I isoforms reveal combinations of shared and distinct functions. *J Cell Biol* 133, 305-323.
- Kipreos, E. T., Lander, L. E., Wing, J. P., He, W. W., and Hedgecock., E. M. (1996). Cul-1 is required for cell cycle exit in *C.elegans* and BPOZ and EGR2, two genes involved in the PTEN signaling pathway identifies a novel gene family. *Cell* 85, 829-839.
- Knecht, D., and Loomis, W. F. (1988). Developmental consequences of the lack of myosin heavy chain in Dictyostelium discoideum. *Dev Biol* 128, 178-184.
- Kominami, E., and Ueno., T. (1996). Lysosomal proteinosis based on decreased degradation of a specific protein, mitochondrial ATP synthase subunit C: Batten disease. *Adv Exp Med Biol* 389, 121-128.
- Kurz, T., Pintard, J., Willis, J. H., RHamill, D., Gonczy, P., Peter, M., and Bowerman., B. (2002). Cytoskeletal regulation by the Nedd8 ubiquitin-like protein modification pathway. *Science* 295, 1294-1298.
- Kuspa, A., and Loomis, W. F. (1996). Ordered yeast artificial chromosome clones representing the Dictyostelium discoideum genome. *Proc Natl Acad Sci USA*, 93, 5562-5566.
- Lamaze, C. (1997). The actin cytoskeleton is required for receptor-mediated endocytosis in mammalian cells. *J Biol Chem* 272, 20332–20335.
- Larochelle, A., Vithalani, A. D., and Lozanne., K. K. D. (1997). Role of the *Dictyostelium racE* in cytokinesis: Mutational analysis and localization studies by use of green fluorescent protein. *Mol Biol Cell* 8, 935-944.
- Larochelle, D. A., AVithalani, and Lozanne., K. K. D. (1996). A novel member of the rho family of small GTP-binding proteins is specifically required for cytokinesis. *Mol Biol Cell* 133, 1321-1329.
- Lebowitz, L. D., Du, W., and Prendergast., G. C. (1997). Prenylation of RhoB is required for its cell transforming function but not its ability to activate serum response element-dependent transcription. *J Biol Chem* 272, 16093-16095.
- Lee, E., David, J. S., Harris, E., Cardelli, J. A., and Knecht., D. A. (2003). RacB Regulates Cytoskeletal Function in Dictyostelium spp. *EUKARYOTIC CELL*, June 2003, 474–485.
- Lee, S., Rivero, R., Park, K. C., Huang, E., Funamoto, S., and Firtel., R. A. (2004). Dictyostelium PAKc is required for proper chemotaxis. *Mol Biol Cell* 15, 5456-5469.
- Li, G. D., and D´Souza-Schorey, M. A. (1995). Evidence for phosphatidy-3-kinase as a regulator of endocytosis via activation of Rab5. *Proc Natl Acad Sci USA*, 92, 10207-10211.
- Lozanne, A. D., and Spudich, J. A. (1987). Disruption of the Dictyostelium myosin heavy chain gene by homologous recombination. *Science* 236.

-
- Luna, A. O., Matas, O. B., Martínez-Menárguez, J. A., Mato, E., Durán, J. M., Way, M., and Egea, G. (2002). Regulation of protein transport from the Golgi complex to the endoplasmic reticulum by Cdc42 and N-WASP. *Mol Biol Cell* 13, 866-897.
- Maeda, I., Koizumi, T., and Fukuda, M. (2001). In vitro ubiquitination of cyclin D1 by ROC1-CUL1 and ROC1-CUL3. *FEBS Lett* 494, 181-185.
- Maniak, M. (1999). Green fluorescent protein in the visualization of particle uptake and fluid-phase endocytosis. *Meth Enzymol* 302, 43-50.
- Maniak, M. (2001). Fluid-phase uptake and transit in axenic *Dictyostelium* cells. *Biochim Biophys Acta* 1525, 197-204.
- Maniak, M. (2003). Fusion and Fission in the Endocytic pathway of *Dictyostelium*. *Traffic* 4.
- McCallum, S. J., Erickson, J. W., and Cerione, R. A. (1998). Characterization of the association of the actin-binding protein IQGAP and activated Cdc42 with Golgi membranes. *J Biol Chem* 273, 22537-22544.
- Michaelson, D., Silletti, J., Murphy, G., D'Eustachio, P., Rush, M., and Philips, M. R. (2001). Differential localization of Rho GTPases in live cells: regulation by hypervariable regions and RhoGDI binding. *J Cell Biol* 152, 111-126.
- Michel, J. J., McCarville, J.F., and Xiong, Y. (2003). A role for *Saccharomyces cerevisiae* CUL8 ubiquitin ligase in proper anaphase progression. *J Biol Chem* 278, 22828-22837.
- Michel, J. J., and Xiong, Y. (1998). Human CUL-1, but not other cullin family members, selectively interacts with SKP1 to form a complex with SKP2 and cyclin A. *Cell Growth Differ* 9, 435-449.
- Monita, Y. S., Jung, G., Hammer, J. A., and Fukui, Y. (1996). Localization of *Dictyostelium* myoB and myoD to filopodia and cell-cell contact sites using isoform-specific antibodies. *Eur J Cell Biol*.
- Moores, S. L., Sabry, J. H., and Spudich, J. A. (1996). Myosin dynamics in live *Dictyostelium* cells.
- Morrow, I. C., and Parton, R. G. (2005). Flotillins and the PHB domain protein family: rafts, worms and anaesthetics. *Traffic* 6, 725-740.
- Myers, S. A., Ji, W., Han, J., Yoonsung, L., Firtel, R. A., and Chung, C. Y. (2005). A *Dictyostelium* homologue of WASP is required for polarized F-actin assembly during chemotaxis. *Mol Biol Cell* 16, 2191-2206.
- Neujahr, R., Heizer, C., Albrecht, R., Ecke, M., Schwartz, J. M., Weber, I., and Gerisch, G. (1997b). Three-dimensional patterns and redistribution of myosin II and actin in mitotic *Dictyostelium* cells. *J Cell Biol*, 139, 1793-1804.
- Noegel, A. A., and Schleicher, M. (2000). The actin cytoskeleton of *Dictyostelium*: a story told by mutants. *J Cell Sci* 113.

-
- Nolta, K. V., Rodriguez-Paris, J. M., and Steck., T. L. (1994). Analysis of successive endocytic compartments isolated from *Dictyostelium discoideum* by magnetic fractionation. *Biochim Biophys Acta* 1224, 237-246.
- Novak, K. D., Peterson, M. D., Reedy, M. C., and Titus., M. A. (1995). *Dictyostelium* myosin I double mutants exhibit conditional defects in pinocytosis. *J Cell Biol*, 131, 1205-1221.
- Novak, K. D., and Titus, M. A. (1998). The myosin I SH3 domain and TEDS rule phosphorylation site are required for in vivo function. *Mol Biol Cell* 9, 75-88.
- Ou, C. Y., CHEN, Y. F., Lin, Y. J., and Chien., C. T. (2002). Distinct protein degradation mechanisms mediated by Cul1 and Cul3 controlling Ci stability in *Drosophila* eye development. *Genes Dev* 16, 2403-2414.
- Palmieri, S. T., Nebl, R. K., Pope, R., Seastone, D. J., Lee, E., Hinchcliffe, E. H., Sludder, G., Knecht, D., Cardelli, J., and Luna., E. J. (2000). Mutant Rac1b expression in *Dictyostelium*: effects on morphology, growth, endocytosis, development, and the actin cytoskeleton. *Cell Motil Cytoskel* 46, 285-304.
- Park, K. C., Rivero, F., Meili, R., Lee, S., Apone, F., and Firtel., R. A. (2004). Rac regulation of chemotaxis and morphogenesis in *Dictyostelium*. *EMBO J* 23, 4177-4189.
- Pasternak, C., Spudich, J. A., and Elson., E. L. (1989). Capping of surface receptors and concomitant cortical tension are generated by conventional myosin. *NATURE* 341, 549-551.
- Peracino, B., Borleis, J., Jin, T., Westphal, M., Schwartz, J. M., L, L. W., Bracco, E., Gerisch, G., Devreotes, P., and Bozzaro., S. (1998). G protein b subunit-null mutants are impaired in phagocytosis and chemotaxis due to inappropriate regulation of the actin cytoskeleton. *J Cell Biol* 141.
- Petroski, M. D., and Deshaies., R. J. (2005). Function and regulation of cullin ubiquitin ligases. *Nature Reviews| Molecular cell biology* 6, 9-20.
- Pintard, L., Willis, J. J., and Willems., J. (2003). The BTB protein MEL-26 functions as a substrate-specific adaptor of the CUL-3 ubiquitin-ligase. *Nature* 425, 311-316.
- Prokopenko, S. N., Saint, S., and Bellen., H. J. (2000). Untying the gordian knot of cytokinesis: role of small G proteins and their regulators. *J Cell Biol* 148, 843-848.
- Qualmann, H., and Mellor, H. (2003). Regulation of endocytic traffic by Rho GTPases. *Biochem J* 371, 233-241.
- Raftopoulou, M., and Hall, A. (2004). Cell migration: Rho GTPases lead the way. *Dev Biol* 265, 23-32.
- Ramos, S., Khademi, F., Somesh, B. P., and Rivero., F. (2002). Genomic organization and expression profile of the small GTPases of the RhoBTB family in human and mouse. *Gene* 298, 147-157.

Randazzo, P. A. (2003). RhoD, Src, and hDia2C in Endosome Motility. *Developmental Cell*, 4, 287–293.

Rauchenberger, R. U., Hacker, J., Murphy, J., Niewöhner, J., and Maniak., M. (1997). Coronin and vacuolin identify consecutive stages of a late, actin-coated endocytic compartment in *Dictyostelium*. *Curr Biol* 7, 215-218.

Rivero, F., Dislich, H., Glöckner, G., and Noegel., A. A. (2001). The *Dictyostelium* family of Rho-related proteins. *Nucleic Acids Res* 29, 1068-1079.

Rivero, F., Illenberger, F., Somesh, B. P., Dislich, H., Adam, N., and Meyer., A.-K. (2002). Defects in cytokinesis, actin reorganization and the contractile vacuole system in cells deficient in RhoGDI. *EMBO J* 21, 4539-4549.

Rivero, F., Richard, A., Dislich, H., Bracco, E., Graciotti, L., Bozzaro, S., and Noegel., A. A. (1998). RacF1, a novel member of the Rho protein family in *Dictyostelium discoideum*, associates transiently with cell contact areas, macropinosomes and phagosomes. *Mol Biol Cell* 10, 1205-1219.

Rivero, F., and Somesh, B. P. (2002). Signal transduction pathways regulated by Rho GTPases in *Dictyostelium*. *J Muscle Res Cell Motil* 23, 737-749.

Rodriguez-Paris, J. M., Nolta, K. V., and Steck., T. L. (1993). Characterization of lysosomes isolated from *Dictyostelium discoideum* by magnetic fractionation. *J Biol Chem* 268, 9110-9116.

Rupper, A., and Cardelli, J. (2001). Regulation of phagocytosis and endo-phagosomal trafficking pathways in *Dictyostelium discoideum*. *Biochim Biophys Acta* 1525, 205-216.

Rupper, A., Rodriguez-Paris, S., and J.Cardelli. (2001). p110-related PI3-kinases regulate phagosome-phagosome fusion and phagosomal pH through a PKB/Akt dependent pathway in *Dictyostelium discoideum*. *Journal of Cell Science* 114, 1283-1295.

Rybin, V., Ullrich, O., Rubino, M., Alexandrow, K., and Zerial, M. (1996). GTPase activity of Rab5 acts as a timer for endocytic membrane fusion. *NATURE* 383, 266-269.

Sambrook, J., David, J., and Russell., W. (2001). *Molecular Cloning: A Laboratory Manual*. 3rd ed. (Cold Spring Harbor, New York, Cold Spring Harbor Laboratory Press).

Seastone, D., Lee, E., Bush, J., Knecht, D., and Cardelli., J. (1998). Overexpression of a novel Rho family GTPase, RacC, induces unusual actin-based structures and positively affects phagocytosis in *Dictyostelium discoideum*. *Mol Biol Cell* 9, 2891-2904.

Seastone, D. J., Harris, E., Temesvari, L. A., BeaR, J. E., Saxe, C. L., and Cardelli., J. (2001). The WASP-like protein Scar regulates macropinocytosis, phagocytosis and endosomal membrane flow in *Dictyostelium*. *J Cell Sci* 114, 2673-2683.

Senadheera, D., Haataja, L., Groffen, J., and Heisterkamp., N. (2001). The small GTPase Rac interacts with ubiquitination complex proteins Cullin-1 and CDC23. *Int J Mol Med* 8, 127-133.

Singer, J. D. G.-W., M, Clurman, B., and Roberts., J. M. (1999). Cullin-3 targets cyclin E for ubiquitination and controls S phase in mammalian cells. *Genes Dev* 13, 2375–2387.

Soll, D. R., Wessels, D., Voss, E., and Johnson, O. (2001). Computer-assisted systems for the analysis of amoeboid cell motility. *Methods Mol Biol* 161, 45-58.

Somesh, B. P. (2002). Functional Analysis of *Dictyostelium discoideum* Rho-related Proteins RacG and RacH. Phd thesis.

Souza, G. M., Metha, D. P., Lammertz, M., Rodriguez-Paris, J., Wu, R., Cardelli, J. A., and Freeze, H. H. (1997). *Dictyostelium* lysosomal proteins with different sugar modifications sort to functionally distinct compartments. *J Cell Sci* 110, 2239-2248.

Sultana, H., Rivero, F., Blau-Wasser, R., Schwager, S., Balbo, A., Bozzaro, S., Schleicher, M., and ANoegel, A. (2005). Cyclase-associated protein is essential for the functioning of the endo-lysosomal system and provides a link to the actin cytoskeleton. *Traffic* 6, 930-946.

Symons, M., and Rusk, N. (2003). Control of Vesicular Trafficking by rho GTPases. *Current Biology* 13, R409-R418.

Takai, R., and Ono, M. (2001). Activating and inhibitory nature of the murine paired immunoglobulin-like receptor family. *Immunol Rev* 181, 215-222.

Taunton, T. B., Rowning, B. A., Coughlin, M. L., Wu, M., Moon, R. T., Mitchinson, J., and Larabell, C. A. (2000). Actin-dependent propulsion of endosomes and lysosomes by recruitment of N-WASP. *J Cell Biol* 148, 519-530.

Temesvari, L., Bush, J., Peterson, M. D., Novk, K. D., Titus, M. A., and Cardelli, J. (1996). Examination of the endosomal and lysosomal pathways in *Dictyostelium discoideum*. *Journal of Cell Science* 109, 663-673.

Valderrama, F., Babia, T., Martinez-Merarguez, J. A., Ballesta, J., Barth, B., Champonier, C., Renau-Piqueras, J., and Egea, G. (2000). The golgi-associated COPI-coated buds and vesicles contain beta/gamma -actin. *Proc Natl Acad Sci USA*, 97, 1560-1565.

VanAelst, L., and D'Souza-Schorey, C. (1997). Rho GTPases and signaling networks. *Genes Dev* 11, 2295-2322.

vanDeurs, B., Holm, P. K., Kayser, L., and Sandvig, K. (1995). Delivery to lysosomes in the human carcinoma cell line HEp-2 involves an actin filament-facilitated fusion between mature endosomes and preexisting lysosomes. *Eur J Cell Biol* 66, 309-323.

Weeks, G., Gaudet, G., and Insall, R. H. (2004). The Small GTPase Superfamily.

Westphal, M., Jungbluth, A., Heidecker, M., Mühlbauer, B., Heizer, C., Schwarz, J.-M., Marriot, G., and Gerisch, G. (1997). Microfilament dynamics during cell movement and chemotaxis monitored using a GFP-actin fusion. *Curr Biol* 7, 176-183.

Wilkins, A., Ping, Q., and Carpenter, C. L. (2004). RhoBTB2 is a substrate of the mammalian Cul3 ubiquitin ligase complex. *Genes Dev* 18, 856-861.

Williams, K. L., and Newell, P. C. (1976). A genetic study in the cellular slime mold *Dictyostelium discoideum* using complementation analysis. *Genetics* 82, 287-307.

Wu, W. J., Erickson, J. W., Lin, R., and Cerione., R. (2000). The gamma-subunit of the coatmer complex binds Cdc42 to mediate transformation. *NATURE* 10, 758-765.

Xu, L., Wei, Y., Reboul, J., Vaglio, P., Shin, T., Vidal, M., Elledge, S., and Harper:, J. W. (2003). BTB proteins are substrate-specific adaptors in an SCF-like modular ubiquitin ligase containing CUL-3. *NATURE* 425, 316-321.

Zhang, A. P., and Casey, J. (1996). Protein prenylation: molecular mechanisms and functional consequences. *Annu Rev Biochem* 65, 241-269.

Erklärung

Ich versichere, dass ich die von mir vorgelegte Dissertation selbstständig angefertigt, die benutzten Quellen und Hilfsmittel vollständig angegeben und die Stellen der Arbeit - einschließlich Tabellen und Abbildungen -, die anderen Werken im Wortlaut oder dem Sinn nach entnommen sind, in jedem Einzelfall als Entlehnung kenntlich gemacht habe; dass diese Dissertation noch keiner anderen Fakultät oder Universität zur Prüfung vorgelegen hat; dass sie - abgesehen von unten angegebenen beantragten Teilpublikationen- noch nicht veröffentlicht ist, sowie, dass ich eine Veröffentlichung vor Abschluss des Promotionsverfahrens nicht vornehmen werde. Die Bestimmungen dieser Promotionsordnung sind mir bekannt. Die von mir vorgelegte Dissertation ist von Frau Prof. Dr. A. A. Noegel betreut worden.

Köln, im November 2005

Carola Neffgen

Curriculum vitae

Name Carola Christine Neffgen

Date of birth 13.06.1978

Place of birth Germany, Cologne

Nationality German

School Education

1984-1988 Attendance of the primary school in Cologne

1988-1997 Attendance of the secondary school in Cologne concluded with a bilingual (German/-French) Abitur

University Studies

1997-2002 Studies of Biology at the Department of Mathematics and Sciences at the University of Cologne with main emphasis on Genetics and Biochemistry

October 1999 First Diploma passed

September 2000 - January 2001 one semester of studies in the School of Biological Sciences at the University of Manchester

August 2001 Diploma examinations (theoretical part)

09. 2001- 08.2002 Practical part of the Diploma at the GBF (Gesellschaft für Biotechnologische Forschung, Braunschweig), department of "Experimental Immunology". Title of the Diploma thesis: Mutagenese der zytoplasmatischen Domäne des β_7 -Integrin Gens in embryonalen Stammzellen der Maus

09.2002-01.2003 Tutor at the University of Cologne

Doctoral Studies

01.2003 -12.2005 Advisor: Prof. Dr. Angelika A. Noegel, Institute of Biochemistry I, Medical Faculty, University of Cologne, Cologne, Germany. Title of the Ph.D. thesis: Functional Analysis of the *Dictyostelium discoideum* Rho GTPases RacH and RacA

Lebenslauf

Name Carola Christine Neffgen

Geburtsdatum 13.06.1978

Geburtsort Köln

Staatsangehörigkeit deutsch

Schulbildung

1984-1988 Besuch der Grundschule

1988-1997 Besuch des Gymnasiums mit dem Abschluß des bilingualen (deutsch-französisch) Abiturs

Studium

1997-2002 Biologiestudium an der Universität zu Köln

October 1999 Vordiplom

September 2000 - Januar 2001 Austauschsemester (ERASMUS-Programm) an der Universität von Manchester

August 2001 Diplomprüfungen (theoretischer Teil)

09. 2001- 08. 2002 Praktischer Teil der Diplomprüfung an der GBF (Gesellschaft für Biotechnologische Forschung, Braunschweig), in der Abteilung "Experimentelle Immunologie".
Zum Thema: Mutagenese der zytoplasmatischen Domäne des β_7 -Integrin Gens in embryonalen Stammzellen der Maus

09.2002-01.2003 Tätigkeit als Tutor an der Universität zu Köln

Promotionsstudium

01. 2003 -12. 2005 Betreuerin: Prof. Dr. Angelika A. Noegel, Institut für Biochemie I, Medizinische Fakultät der Universität zu Köln. Thema: Functional Analysis of the *Dictyostelium discoideum* Rho GTPases RacH and RacA